

INAUGURAL-DISSERTATION

zur

Erlangung der Doktorwürde

der

Naturwissenschaftlich-Mathematischen Gesamtfakultät

der

Ruprecht-Karls-Universität

Heidelberg

vorgelegt von

Rui Yan, M.Eng.

aus Shandong, China

Tag der mündlichen Prüfung: 04. 11. 2016

DISSERTATION

Submitted to the
Combined Faculties of Natural Sciences and Mathematics
Ruprecht-Karls-University Heidelberg, Germany
for the degree of
Doctor of Natural Sciences (Dr. rer. nat.)

Presented by

Rui Yan, M.Eng.

Born in Shandong, China

Oral examination: 04. 11. 2016

Modification of Self-Assembled Monolayers and Hydrogel Nanomembranes by Ultraviolet Light

This dissertation was carried out at the
Department of Applied Physical Chemistry
of the Heidelberg University

Referees

Prof. (apl.) Dr. Michael Zharnikov

Prof. (apl.) Dr. Reiner Dahint

Zusammenfassung

Maßgeschneiderte organische und biologische Oberflächen und „soft matter lithography“ sind wichtige Aspekte der modernen Nanotechnologie, sowie der physikalischen Chemie der Grenzflächen. Ein wichtiges Hilfsmittel diesbezüglich ist Ultraviolettes-(UV)-Licht, dieses kann zur Erstellung von Mustern und für kontrollierte Modifikation von organischen und biologischen Oberflächen dienen. In diesem Zusammenhang wurden die Auswirkungen von UV-Licht auf Alkanthiolen (AT), insbesondere deren selbst aggregierten Monolagen (SAMs) auf Gold, untersucht. Der Fokus lag hierbei auf die Abhängigkeit von der verwendeten Wellenlänge. Die durchgeführten Experimente wurden zuerst an den fundamentalen Systemen der nicht substituierten AT-SAMs getestet. Diese zeigten eine qualitativ vergleichbare Photooxidation bei der Verwendung der Wellenlängen von 254-375 nm, jedoch eine Verminderung der Photooxidation im Querschnitt bei höheren Wellenlängen. Gestützt auf diesen Ergebnissen wurde die Möglichkeit der UV-gestützten Austauschreaktion (UVPER) mit der Verwendung von nicht substituierten AT-SAMs als primärer Matrix erfolgreich getestet und weiterführend die Verwendung von Azid-substituierten ATs realisiert. Auf Grund dessen war eine Herstellung von gemischten SAMs möglich, welche eine variable Endgruppenfunktionalisierungsdichte von Aziden besaßen. Die Azid-Endgruppenfunktionalisierungen ermöglichen nachträgliche Modifikation via click-Reaktion mit verschiedensten Arten von Molekülen und Alkynyl-Gruppen. Die Durchführung solcher Click-Reaktionen verschiedenster repräsentativer Substituenten wurde hier demonstriert. Ferner wurde die oben erwähnte Herangehensweise erweitert auf Oligoethylenglycol-substituierte AT-SAMs, welche als proteinabweisende primäre Matrix dienen. Bei der Kombination aus UVPER und der folgenden Click-Reaktion mit einem Biotin-tragenden Substituenten, konnten biorepulsive Schablonen mit kontrollierter Dichte der Ankopplungsstellen hergestellt werden. Diese Ankopplungsstellen können für die spezifische Adsorption von Biotin-komplementären Proteinen, wie Avidin und Streptavidin, verwendet werden und wurden erfolgreich auf ihre spezifische und nicht-spezifische Proteinaffinität getestet. Diese Vorgehensweise wurde auf UV-Lithographie erweitert und resultierte in anwendungsspezifischen, graduell haftenden Mustern. Schlussendlich wurde basierend auf den Resultaten der OEG-AT SAMs der Effekt von UV-Licht auf proteinabweisende Polyethylenglycol-(PEG)-Membranen untersucht. Es konnte hierbei gezeigt werden, dass Bestrahlung mit UV-Licht eine umfassende Desorption des PEG-Materials ohne Photooxidation oder auffällige Veränderung in chemischer Zusammensetzung, Bioabweisendem Verhalten und

Hydrogeleigenschaften der verbleibenden Membran verursacht. Dies eröffnet eine völlig neue Herangehensweise an das 3D-Strukturieren von allen PEG-Materialien, welche für die Herstellung von Nanomaterialien und in der Biotechnologie eine wichtige Rolle spielen könnten.

Abstract

Custom design of organic and biological surfaces and soft matter lithography are important issues of modern nanotechnology and physical chemistry of interfaces. An important tool in this regard is ultraviolet (UV) light which can be used for controlled modification and patterning of organic and biological surfaces. In this context, the effect of UV light on alkanethiolate (AT) self-assembled monolayers (SAMs) on gold substrates was studied, with a particular emphasis on its wavelength dependence. The experiments were first performed for the most basic system of non-substituted AT SAMs which exhibited qualitatively similar photooxidation behavior at UV wavelength variation from 254 to 375 nm but a strong decrease of the photooxidation cross-section with increasing wavelength. Based on these results, the possibility of UV-promoted exchange reaction (UVPER) with non-substituted AT SAMs as the primary matrix and azide-substituted ATs as substituents was tested and successfully realized, resulting in the fabrication of mixed SAMs with variable density of the azide tail groups, capable of the subsequent click reaction with various kinds of molecules and functional moieties with alkynyl group. Such a click reaction with several representative substituents was demonstrated. Further, the above approach was extended to oligo(ethylen glycole) substituted AT SAMs serving as protein repelling primary matrix. Combining UVPER and the subsequent click reaction with a biotin-bearing substituent, biorepulsive templates with controlled density of the docking sites for the specific adsorption of biotin-complementary proteins such as avidin and streptavidin were prepared and successfully tested regarding their non-specific and specific protein affinity. This approach was extended to UV lithography, resulting in preparation of custom-designed, gradient protein-adhesion patterns. Finally, based on the results for the OEG-AT SAMs, the effect of UV light on protein-repelling poly(ethylen glycole) (PEG) nanomembranes was studied. It was demonstrated that UV irradiation induces extensive desorption of the PEG material, without photooxidation or other noticeable changes in the chemical composition, biorepelling behavior and hydrogel properties of the residual membrane. This opens a new way of 3D patterning of all-PEG materials, potentially useful for nanofabrication and biotechnology.

Contents

List of abbreviations	VII
1. Introduction	1
2. Theoretical background.....	5
2.1 Self-assembled monolayers.....	5
2.2 Ultraviolet light	6
2.3 Click reactions	7
2.4 X-ray photoelectron spectroscopy	7
2.5 Near edge X-ray absorption fine structure spectroscopy	11
2.6 Ellipsometry.....	13
2.7 Scanning electron microscopy.....	14
2.8 Contact angle goniometry.....	15
3. Materials, Preparation procedures and Characterization	17
3.1 Chemicals and Compounds.....	17
3.1.1 Gold substrates.....	17
3.1.2 Chemicals.....	17
3.2 Preparation procedures	19
3.2.1 Modification of non-substituted AT SAMs by UV light.....	19
3.2.1.1 Preparation of the DDT SAMs.....	19
3.2.1.2 UV irradiation of DDT SAMs	19
3.2.1.3 Exchange reaction with MUDA	19
3.2.2 UV promoted exchange reaction: DDT	19
3.2.2.1 Preparation of the mixed DDT/C12N3 SAMs.....	19
3.2.2.2 Click reaction for the mixed DDT/C12N3 SAMs	20
3.2.3 UV promoted exchange reaction: EGn.....	20
3.2.3.1 Preparation of the mixed EGn/C12N3 SAMs	20
3.2.3.2 Click reaction for the mixed EGn/C12N3 SAMs.....	20
3.2.3.3 Preparation of UV patterns	20
3.2.3.4 Protein adsorption.....	21
3.2.4 PEG nanomembranes	21
3.2.4.1 Preparation of PEG nanomembranes	21
3.2.4.2 Modification of PEG nanomembranes by UV light	22
3.3 Characterization experiments.....	22
4. Results and discussion	25
4.1 Modification of non-substituted AT SAMs by UV light.....	25
4.1.1 UV light modified SAMs: XPS.....	25
4.1.2 UV promoted exchange reaction with MUDA: water contact angle.....	28
4.2 UV promoted exchange reaction: DDT	31
4.2.1 Mixed DDT/C12N3 SAMs.....	31
4.2.1.1 Mixed DDT/C12N3 SAMs: Water contact angle	31
4.2.1.2 Mixed DDT/C12N3 SAMs: XPS	32
4.2.1.3 Mixed DDT/C12N3 SAMs: NEXAFS Spectroscopy.....	34

4.2.2 Click reactions of the mixed DDT/C12N3 SAMs.....	37
4.2.2.1 Mixed SAMs after the click reaction: XPS	37
4.2.2.2 Effect of exchange time: XPS	38
4.2.2.3 Thickness measurements: Ellipsometry	39
4.3 UV promoted exchange reaction: EGn SAMs	41
4.3.1 Mixed EGn/C12N3 SAMs.....	41
4.3.1.1 Mixed SAMs: XPS.....	41
4.3.1.2 Mixed SAMs: water contact angle	42
4.3.1.3 Mixed SAMs: NEXAFS spectroscopy	43
4.3.2 Click reaction of mixed EGn/C12N3 SAMs.....	45
4.3.2.1 Free-catalyst click reaction of mixed SAMs: XPS	45
4.3.2.2 Catalyst click reaction of mixed SAMs: XPS	46
4.3.3 Specific protein adsorption.....	47
4.3.3.1 Protein adsorption on free-catalyst clicked SAMs: XPS	47
4.3.3.2 Protein adsorption on free-catalyst clicked SAMs: NEXAFS spectroscopy.....	49
4.3.3.3 Protein adsorption on free-catalyst clicked SAMs: lithography	49
4.3.3.4 Protein adsorption on catalyst clicked SAMs: XPS	51
4.3.3.5 Protein adsorption on catalyst clicked SAMs: lithography	52
4.4 Modification of PEG nanomembranes by UV light	55
4.4.1 UV irradiated membranes: XPS.....	56
4.4.2 Swelling properties of UV irradiated membranes: Ellipsometry.....	60
4.4.2.1 Swelling properties at humidity variation.....	60
4.4.2.2 Swelling properties at temperature variation.....	61
4.4.3 UV patterning of PEG membrane	63
5. Conclusions and outlook.....	65
Bibliography	67
Acknowledgements.....	79

List of abbreviations

AFM Atomic force microscopy

AT Alkanethiolate

BE Binding energy

BPA Biotin-PEG4-alkyne

BSA Bovine serum albumin

C12N3 12-Azido-1-dodecanethiol

DBPB Dibenzocyclooctyne-PEG4-biotin conjugate

DDT 1-Dodecanethiol

EBL Electron beam lithography

EFB 1-Ethynyl-3,5-bis(trifluoromethyl) benzene

EG Ethylene glycol

EG_n HS-(CH₂)₁₁(OCH₂CH₂)_n-OH

EtOH Ethanol

HOMO Highest occupied molecular orbital

KE Kinetic energy

LUMO Lowest unoccupied molecular orbital

MUDA 11-Mercaptoundecanoic acid

NEXAFS Near edge X-ray absorption fine structure

OEG Oligo(ethylene glycol)

PBS Phosphate buffered saline

PEG Poly(ethylene glycol)

rpm Rotation per minute

RT Room temperature

SAM Self-assembled monolayer

SEM Scanning electron microscopy

STAR2k-EPX Epoxy-terminated, four-arm polyethylene glycols, $M_n = 2000$ g/mol

STAR2k-NH₂ Amino-terminated, four-arm polyethylene glycols, $M_n = 2000$ g/mol

UHV Ultra high vacuum

UV Ultraviolet

UVPER UV promoted exchange reaction

XPS X-ray photoelectron spectroscopy

1. Introduction

Self-assembled monolayers (SAMs) have since long become a valuable part of modern nanotechnology.^{1,2,3} One of the major advantages of these systems is the possibility of precise control of chemical composition of surfaces and interfaces. This is generally achieved by selection of a proper terminal tail group which, provided a contamination-free character and a dense molecular packing of the monolayer, comprises the SAM-ambient interface, redefining the chemical properties of the entire system. The family of potential tail groups is very broad, ranging from small moieties such as methyl or hydroxyl to larger species of electrochemical (e.g., ferrocene), nanotechnological (e.g., azobenzene) or biological (e.g., biotin) significance.³

Along with one-component SAMs bearing a specific tail group, mixed monolayers comprising of molecules with different tail groups can be formed. Such monolayers have several advantages as compared to the single-component films. First, the variety of possible chemistries can be significantly extended. Second, chemical composition of the SAM-ambient interface can be precisely tuned to achieve a particular property or serve a particular application. Third, the surface density of a particular tail group can be precisely varied, with the second tail group serving as a passive matrix.

The most popular way to prepare mixed monolayer is coadsorption, starting from a mixed solution of both SAM precursors within the standard immersion procedure. The resulting surface composition can, however, differ noticeably or even drastically from the solution composition. An even more important constraint is a possible phase separation in the mixed SAMs, following a thermodynamical drive for assembly of similar species. Such a phase separation can affect properties of the mixed films, especially at the nanoscale, resulting in failing performance. An alternative approach is a backfilling procedure, starting from a low-density film of one component and filling the residual space with the second component, until a dense molecular film is formed. This procedure can, however, be only applied to certain molecular precursors, differing significantly in their SAM building ability. Finally, there is a substitution procedure, relying on the substitution reaction between the primary, single-component monolayer and a second SAM precursor bearing a different tail group. Such a procedure works, however, for certain combinations of molecules only. In addition, the substitution reaction can take very long and occur to a certain extent only.

Recently, our group has suggested a way to avoid the limitations of the standard substitution reaction promoting it by electron irradiation of the primary, single-component SAM or by its exposure to ultraviolet (UV) light.⁴⁻⁸ Such a

Introduction

pretreatment creates defects in the primary monolayer, which, subsequently, enables effective exchange reaction between the defect-affected molecules in the primary film and potential substituents in solution. As a result, the kinetics of the substitution process can be significantly accelerated and the composition of the resulting mixed SAMs can be varied in a broad range by adjusting either irradiation dose or duration of the exchange reaction.⁵ Limitations related to the specific SAM precursors can be released as well, so that a broad variety of different molecules can be mixed, starting, most frequently, from a primary SAM of non-substituted or specifically substituted alkanethiolate (AT) monolayers on gold. Finally, the promoted exchange reaction can be applied lithographically, resulting in quite sophisticated chemical and biological patterns.^{8,9}

A valuable extension of the above approach can be a use of a substituent bearing a tail group capable of further modification of subsequent attachment chemistry. A perspective group in this regard is azide (-N=N=N) which is capable of a click reaction with ethynyl, enabling attachment of a broad variety of species having the respective substitution.¹³⁻¹⁶ Accordingly, in the given thesis I looked at the possibility to use azide-substituted ATs as substituents in promoted exchange reaction. As primary matrix I used either non-substituted or oligo(ethylene glycole) (OEG) substituted ATs, targeting mixed SAMs of chemical and biological significance. It is well-known that properly designed OEG substituted monolayers exhibit pronounced protein-repelling properties, building therefore an ideal, biologically-inert matrix for specific biological receptors.¹⁷⁻²² As a promoting tool for the substitution reaction I used UV light which has essential advantages over electron irradiation since the exposure to UV light does not require vacuum and can be performed under standard laboratory conditions^{6,10,11} and even in solution.¹²

Before starting the substituted experiments, I performed the basic studies of the effect of UV light on non-substituted ATs, looking in particular, for the effect of the wavelength. In this context, I compared the results of UV light irradiation at three different wavelengths, viz. 254 nm, 312 nm and 375 nm. I demonstrated that UV light can be applied in a given wavelength range for the modification of SAMs but the efficiency of the modification decreases significantly with increasing wavelength of UV light. Cross-sections of the major UV-induced processes in AT SAMs were determined. Based on these results, I performed extensive experiments on UV light promoted exchange reaction (UVPER) with the non-substituted and OEG-substituted AT SAMs as the primary matrix and with an azide-bearing AT as substituent. The experiments were performed at wavelength of 254 nm and 375 nm, respectively. The

advantage of UVPER at 254 nm is its high efficiency while UV light with a longer wavelength has more potential for lithography, in particular because of the availability of respective, commercial lithographic setups. Note, however, that UV lithography with SAM-like resists and templates can be performed at shorter wavelengths as well but requires quite expensive, custom-designed experimental setups.^{23,24,26}

The above experiments as well as previous results of our and other groups suggested that UV light can be considered as a simple and efficient method to modify the OEG/PEG based compounds for the bio-technology. In this context, along with the SAM studies, I applied UV light to the modification of novel, protein-repelling hydrogel PEG nanomembranes, the fabrication of which has been recently developed in our group. Note that, nowadays, specifically designed macromolecular membranes have significant potential for biomedical and biological research as well as for various practical applications such as medical diagnostics, sensor fabrication, and therapy.²⁷⁻²⁹ Previously our group have modified the PEG membranes by electron irradiation and the wetting properties, chemical composition, swelling behavior, and protein-repelling properties of the irradiated PEG films were analyzed in detail, exhibiting a specific behavior. Within this thesis, instead of electron irradiation, UV light with a wavelength of 254 nm was used as a modification tool, with monitoring of chemical composition and swelling behavior. Surprisingly, the modification of the PEG membranes by UV light was found to be different than by electrons, resulting in new possibilities for applications.

In summary, the contents of the thesis are presented as follows:

Chapter 1 is the introduction of the thesis.

Chapter 2 provides basic information regarding SAMs, ultraviolet light, click reaction, and the relevant characterization techniques.

Chapter 3 is a general overview of materials for the experiments, the details of the preparation procedures, and the characterization experiments.

Chapter 4 presents the experimental results. In the first part, UV light induced modification of non-substituted AT SAMs is described, taking dodecanethiolate monolayers as a representative system and with a particular emphasis on the effect of the wavelength. The second part is devoted to the result of the UVPER experiments on non-substituted and PEG-substituted AT SAMs with an azide-bearing AT as substituent. In the last part, modification of the PEG membranes by UV light is described, with a particular emphasis on UV-induced desorption processes and persistence of the swelling properties.

Introduction

Chapter 5 presents the final conclusions and an outlook for further research in the given area.

2. Theoretical background

2.1 Self-assembled monolayers

Self-assembled monolayers (SAMs), which are densely packed and well-ordered monolayers adsorbing on suitable substrates, represent a convenient way to control properties of the surfaces, such as adhesion, wetting, lubrication, biocompatibility and corrosion.^{30,31} Generally, every molecule in the SAMs is made of a headgroup attaching to the substrate, a chain-like spacer connecting the other two parts and a tail group to identify the interface between the SAM and the environment.³² But the assembly molecules can just exhibit low structural quality, which should be owed to the unperfect balance of the structure forces in the SAMs. These procedures suffer from several limitations so that usually can do not form the desired films. For this reason, people developed a novel approach to fabricate desired mixed SAMs, this method is called the irradiation-promoted exchange reaction (IPER).^{33,34} This method means using preliminary electron irradiation to promote exchange reactions between potential molecular substituents and a target SAM. The applicability of this approach for mixed SAMs consists of similar molecules, such as alkanethiols (ATs).

Not only the chemical stability of thiolate SAMs, the thiolate group also have an excellent bonding strength. On one hand, this strength can guarantee a very strong attachment between the SAM-constituents and the substrate; on the other hand, it allows the dynamical movement of these moieties.^{35,36,38,39} The last one is specially importance for the good quality of most thiolate SAMs, that is because the high mobility of headgroups can make molecular packing to form the SAM efficiently, it is the main reason why the thiolate-derived SAMs have a more superior quality than the SAMs with covalently bound headgroups, such as trichlorsilanes.³⁷

Controlling the surface properties is an very important challenge and it can lead to a broad relevance of different areas, which ranges from just protection issues to the fabrication of biochips and medical implants.^{40,41} A approach in this aspect is to functionalize the target surface by a chemi-sorbed monomolecular, SAM can offer the interface or surface a new chemical identity. About this normal architecture, the properties of the functionalized surface are predominantly defined by the chemical identity of the tail group as far as the SAM remains intact. For this reason, people can design a molecular with a required tail group to get a required property.⁴²

2.2 Ultraviolet light

Ultraviolet (UV) light is a kind of electromagnetic radiation with a wavelength range from 10 nm to 380 nm, which is longer than X-rays but shorter than visible light. There is much UV radiation in sunlight. It can also be produced by specialized lights such as tanning lights, mercury-vapor lights, and black lights and also by electric arcs. Long-wavelength ultraviolet radiation lacks the energy to ionize atoms, but it can also cause chemical reactions and many substances to fluoresce or glow. Consequently, effects of UV on biological are much greater than just heating effects, and many UV practical applications are due to the interactions with organic molecules.⁴³

The electromagnetic spectrum of ultraviolet radiation (UVR) can be divided into a series of ranges shown below:⁴⁴

Table 2.1 Classification of UV light according to the wavelengths.

Name	Abbreviation	Wavelength (nm)	Photon energy (eV, aJ)
Ultraviolet A	UVA	315-400	3.10-3.94, 0.497-0.631
Ultraviolet B	UVB	280-315	3.94-4.43, 0.631-0.710
Ultraviolet C	UVC	100-280	4.43-12.4, 0.710-1.987
Near ultraviolet	NUV	300-400	3.10-4.13, 0.497-0.662
Middle ultraviolet	MUV	300-400	4.13-6.20, 0.662-0.993
Far ultraviolet	FUV	200-300	6.20-12.4, 0.993-1.987
Hydrogen Lyman-alpha	H Lyman- α	122-200	10.16-10.25, 1.628-1.642
Vacuum ultraviolet	VUV	10-200	6.20-124, 0.993-19.867
Extreme ultraviolet	EUV	10-121	12.4-124, 1.99-19.87

Various of vacuum devices and solid-state have been used for different parts of the UV spectrum. UV can be measured by suitable photocathodes and photodiodes, which tailored to be sensitive to different kinds of the UV spectrum. Spectrometers and radiometers are made to measure UV radiation. Sensitive ultraviolet photomultipliers are available. Silicon detectors are used for the whole spectrum.⁴⁵

2.3 Click reactions

Sharpless' "click chemistry" is attracting more and more attention in surface chemistry, especially about the functionalization of SAMs on gold surface. Click chemistry is a kind of selective chemical reactions which has high yields, can tolerate various solvents (including water), air, and functional groups.⁴⁶ Click reaction is reported to fabricate many biosensors, such as immunosensor, enzyme-based biosensor and aptamer-based biosensor.

As we know, the previous copper-catalyzed cycloaddition of azides and alkynes is particularly useful for facile and rapid construction of arrays for drug discovery. The reaction is conducted in the presence of aqueous solvents and air to get stable 1,2,3-triazoles.⁴⁸ Click reaction can be used for facile and rapid modification of surfaces. It shows a group of bimolecular reactions which allows the quick formation of a covalent link between a substrate and a surface or between two substrates. Most of click reactions are based on Diels–Alder cycloadditions or 1,3-dipolar addition to carbon–carbon multiple bonds, and imine formation.

However, the azide–alkyne cycloaddition above needed Cu^+ as catalyst, which can strongly reduce biocompatibility. But Bertozzi and co-workers have overcome this limitation by using ring-strained alkynes as substrate to readily proceed. Since then the strain-promoted azide–alkyne cycloaddition (SPAAC) has long development of applications in labeling, such as, nucleotides, carbohydrates, and lipids. To expand the potential of this method, Ting and co-workers designed a lipolic acid ligase, which can ligate a small encoded recognition peptide onto a cyclooctyne-containing substrate. In the next step, the incorporated cyclooctyne moiety then functioned as a specific site for labeling in cells.⁴⁹

Because alkyne and azide moieties are very rare in nature, i.e., 'bioorthogonal', strain promoted azide–alkyne cycloadditions and the copper-catalyzed have found many applications in labeling protein modification, biomolecules, developing biotech tools, and synthesis of bioconjugates. These strategies give pretty good selectivity but also require derivatization of substrates with a lot of different functionalities.^{50,51}

2.4 X-ray photoelectron spectroscopy

X-ray photoelectron spectroscopy (XPS), which is also named electron spectroscopy for chemical analysis (ESCA) is a widely used method for surface characterization. It uses the photoelectric effect to analyze the surfaces chemical composition. The sample is irradiated by low-energy (~1.5 keV) X-rays to excite the photoelectric effect.

Theoretical background

The energy spectrum of the emitted photoelectrons is determined by means of a high-resolution electron spectrometer. The concentration of the sample's emitting atom decides the amount of photoelectrons emitted. The analysis chamber is ultrahigh vacuum (UHV) ($p < 10^{-8}$ bar). Only the top layer of only several nanometers can be measured. There is an interesting fact that chemical environment also has an effect on the energy of the photoelectrons. There will be a chemical shift depending on the hybridization, oxidation state or inductively acting substituents on the atom.⁶⁴⁻⁶⁶

Basic physics

X-ray photoelectron spectroscopy works by irradiating a sample material with monoenergetic soft X-rays causing electrons to be ejected. Identification of the elements in the sample can be made directly from the kinetic energies of these ejected photoelectrons. The relative concentrations of elements can be determined from the photoelectron intensities. An important advantage of XPS is its ability to obtain information on chemical states from the variations in binding energies, or chemical shifts, of the photoelectron lines. To characterize the thickness and type of corrosion layers to investigate passivation phenomena, solid catalysts, adsorption effects and processes in the surface treatment. An electron of a certain binding energy BE absorbs a photon of the energy $h\nu$ and is emitted with the kinetic energy KE.⁶⁷⁻⁶⁹

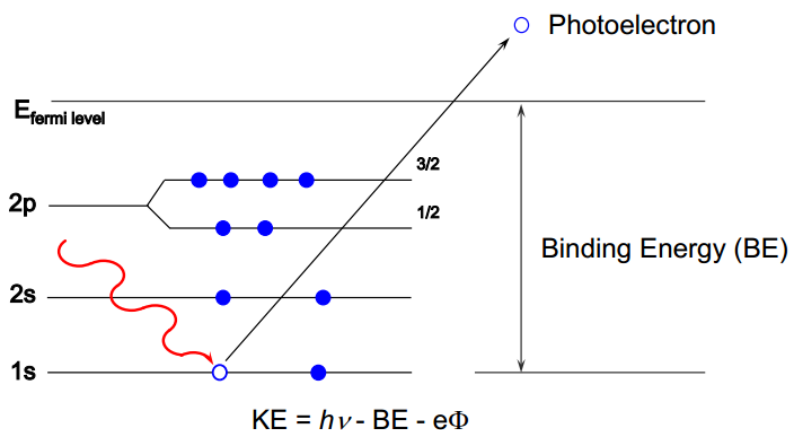


Figure 2.1 Sketch of the energy diagram of the photoexcitation process.

The relationship governing the interaction of a photon with a core level is:

$$KE = h\nu - BE - e\phi$$

KE: Kinetic Energy of ejected photoelectron,

$h\nu$: characteristic energy of X-ray photon,

BE: Binding Energy of the atomic orbital from which the electron originates.

$e\phi$: spectrometer work function

Construction of apparatus

The schematic diagram of XPS is shown in Figure 2.2. The measurement condition must be ultra vacuum because when photoelectrons are transferred from sample to the detector without colliding with any gas molecules. Usually XPS is made of three elements: the X-ray source, the detector and the energy analyzer. As discussed in last part, kinetic energy of the photoelectron according to the X-rays' wavelength, so using X-ray irradiation at low energy defined as the line width is important. Mostly Mg and Al are used as anode material, Mg has emission K alpha line at 1253.6 eV with a FWHM of 0.7 eV and Al has emission K alpha line at 1486.6eV with a FWHM of 0.85 eV (Table 3.1).⁷⁰

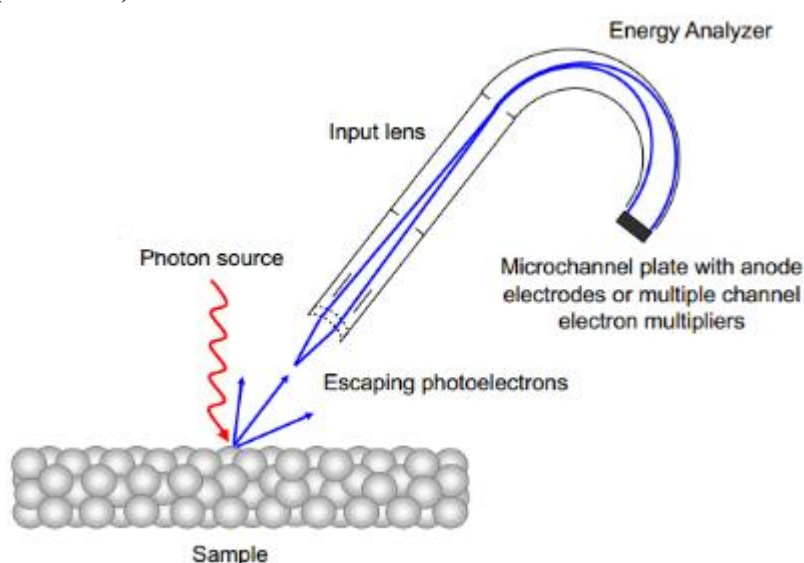


Figure 2.2 Basic components of a monochromatic XPS system.

Table 2.2 General properties of Mg K α and Al K α X-ray radiation source.

X-ray source	Energy (eV)	Width (eV)
Mg K α	1253.6	0.70
Al K α	1486.6	0.85

Attenuation length and film thickness

For estimating the thickness of layer A on substrate B, the influence of the layer thickness, the energy dependent attenuation length, or the photoelectrons emission angle on their photoemission intensities are used. In simple case, the thickness d of a homogeneous layer, the layer intensities I_A and the substrate intensities I_B are given by:

Theoretical background

$$I_A = I_{A\infty} \left[1 - \exp\left(-\frac{d}{\lambda_{A,A} \cos\theta}\right) \right] \quad (1)$$

$$I_B = I_{B\infty} \exp\left(-\frac{d}{\lambda_{B,A} \cos\theta}\right) \quad (2)$$

$I_{A\infty}$ and $I_{B\infty}$ are the intensities of the pure bulk elements A and B. $\lambda_{A,A}$ and $\lambda_{B,A}$ are the inelastic mean free paths (better: the attenuation lengths AL considering the elastic scattering of the photoelectrons) of the electrons in A (second index letter) emitted by the element A or B (first index letter). The emission angle θ of the electrons is given regarding the surface normal (polar angle).⁷¹

Equations. 1 and 2 are reasonable by the following assumptions:

- Samples are flat and homogeneous.
- Interfaces are abrupt.
- Samples are amorphous or fine-grained, for which photoelectrons don't show interference effects.

To reduce the thickness estimation's uncertainties, using the intensity ratios as evaluation methods, e.g. I_A/I_B . Most commonly used method to measure thickness of thin films, the intensity ratio I_A/I_B of photoelectron peaks of the layer A and the substrate B is applied (Method 1):

$$\frac{I_A}{I_B} = \frac{I_{A\infty} \{1 - \exp[-d/(\lambda_{A,A} \cos\theta)]\}}{I_{B\infty} \exp[-d/(\lambda_{B,A} \cos\theta)]} \quad (3)$$

the intensity ratio of the bulk elements is

$$\frac{I_{A\infty}}{I_{B\infty}} = \frac{N_A \sigma_A \lambda_{A,A} T_A}{N_B \sigma_B \lambda_{B,B} T_B} \quad (4)$$

In this equation, N is so-called atomic density, σ is the ionization cross-section of the observed photoelectron line and T is the spectrometer's transmission function. With the corrected intensity

$$I' = \frac{I}{\sigma \lambda T} \quad (5)$$

the ratio is given by

$$\frac{I'_A}{I'_B} = \frac{N_A \{1 - \exp[-d/(\lambda_{A,A} \cos\theta)]\}}{N_B \exp[-d/(\lambda_{B,A} \cos\theta)]} \quad (6)$$

Because of the approximation $\lambda_{A,A} \approx \lambda_{B,A} = \lambda$, we can get the layer thickness d:

$$d = \lambda \cos\theta \ln\left(\frac{I'_A N_B}{I'_B N_A} + 1\right) = \lambda \cos\theta \ln\left(\frac{I_A N_{B\infty}}{I_B N_{A\infty}} + 1\right) \quad (7)$$

2.5 Near edge X-ray absorption fine structure spectroscopy

NEXAFS spectroscopy, short of Near Edge X-Ray Absorption Fine Structure, means the absorption fine structure near to the absorption edge, almost the first 30 eV begin with the actual edge.^{72,73} In this section there is usually the largest variations in the X-ray absorption coefficient and often dominated by narrow, intense resonances. NEXAFS is also named XANES (X-Ray Absorption Near Edge Structure). Now, NEXAFS is especially used for soft X-ray absorption spectra and XANES for hard X-ray spectra.⁷⁴ In NEXAFS the X-ray energy is scanned and the absorbed X-ray intensity is measured. And it is different from XPS, in which the photon energy is fixed and the electron intensity is measured as a function of electron kinetic energy. Electron yield and transmission measurements are the most common methods. Note that the absorption coefficient μ is obtained either as the logarithm or the direct ratio of the detected intensities I_t and I_e and incident intensity I_0 , as indicated in the Figure 2.3.

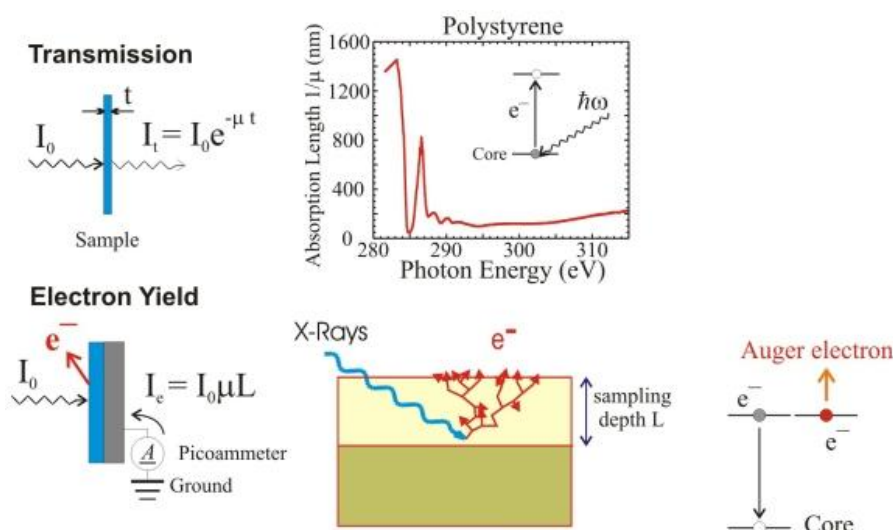


Figure 2.3 Two most popular methods of recording x-ray absorption spectra.

The transmission technique needs thin foils but electron yield technique, often called total electron yield (TEY) detection, and used for normal samples. The absorbed X-ray intensity is not measured directly in TEY measurements, but the photoelectrons created by the absorbed X-rays.⁷¹ X-rays are absorbed through excitations to empty states of core electrons above Fermi level or the vacuum. Then the holes are filled with Auger decay. The intensity of emitted primary Auger electrons is used in Auger electron yield (AEY) measurements and is a direct measurement of the x-ray absorption process. AEY is very highly surface-sensitive, which is similar to XPS.

Theoretical background

When they leave the sample, the primary Auger electrons can create scattered secondary electrons (see Figure 2.4) which dominate the total electron yield (TEY) intensity. The TEY cascade involves several scattering events and originates from an average depth, the electron sampling depth L . Electrons created in the deeper sample lose much more energy to overcome the workfunction of the sample and can not contribute to the TEY. The sampling depth L in TEY measurements is typically a few nanometers, on the other hand for AEY measurements it is usually less than 1 nm.

Why NEXAFS is called element specific is that different elements have different energies of X-ray absorption edges. Figure 2.4 compares XPS and NEXAFS spectra of the same polymer.⁷² The XPS spectra was recorded at a photon energy of 750 eV. Both of the two spectra have pronounced peaks related to C, N, O, and F atoms in the sample. For example, in the NEXAFS spectra the C K-edge threshold peak lies at about 285 eV (photon energy). But in the XPS spectra it corresponds to a peak at $750 \text{ eV} - 285 \text{ eV} = 465 \text{ eV}$ (kinetic energy).

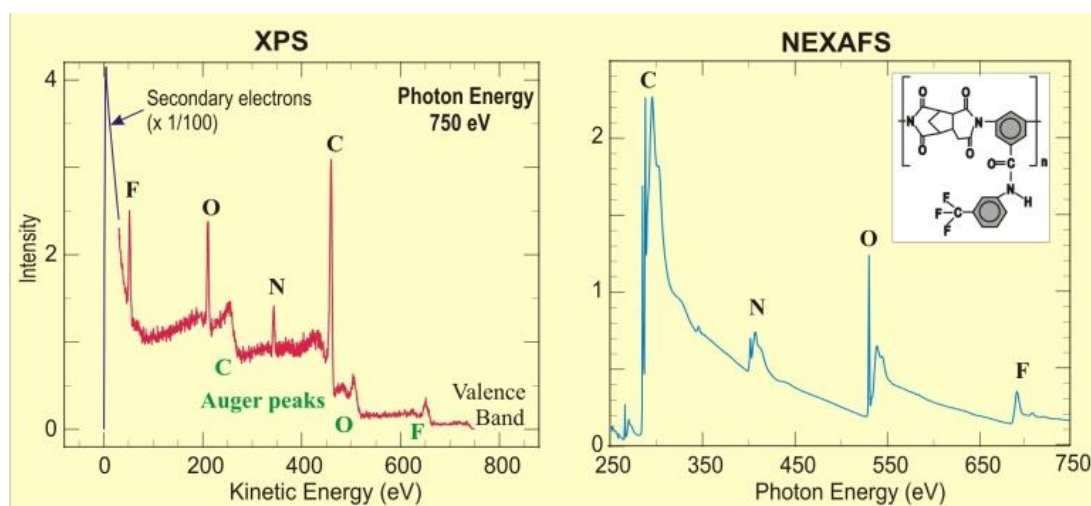


Figure 2.4 Comparison of XPS and NEXAFS spectra for a polyimide polymer, whose structural formula is shown in the inset.

Like XPS, NEXAFS is also sensitive to the environment of absorbing atom which is already shown in Figure 2.4. The NEXAFS spectra shows considerable fine structures above elemental absorption edges. These fine structures arise from excitations to unoccupied molecular orbitals. In a corresponding picture one can think of the resonances which is arising from scattering of the excited low-energy photoelectron by the molecular potential. People always use a spectral "fingerprint" technique to character the local bonding environment.

2.6 Ellipsometry

Ellipsometry is a method which can measure changes in polarization as light reflects from a material structure.⁷⁵ The polarization change can be represented as an amplitude ratio, Ψ , and the phase difference, Δ . The response measured depends on thickness of individual materials and optical properties. For this reason, ellipsometry is mostly used to measure film thickness and optical constants. What's more, it can also be used to characterize composition, doping concentration, roughness, crystallinity, and other material properties associated with a change in optical response.

From 1960s, as ellipsometry became to provide enough sensitivity of measure nanometer-scale layers used in microelectronics, more and more people pay attention to it. Nowadays, Its applications consists of the basic research in physical sciences, data storage solutions and semiconductor, flat panel display, biosensor, communication, and optical coating industries.⁷⁶ This is also because that it has increasing dependence on thin films in many areas and the flexibility to measure most material types: semiconductors, dielectrics, metals, organics, superconductors, composites of materials, and biological coatings.

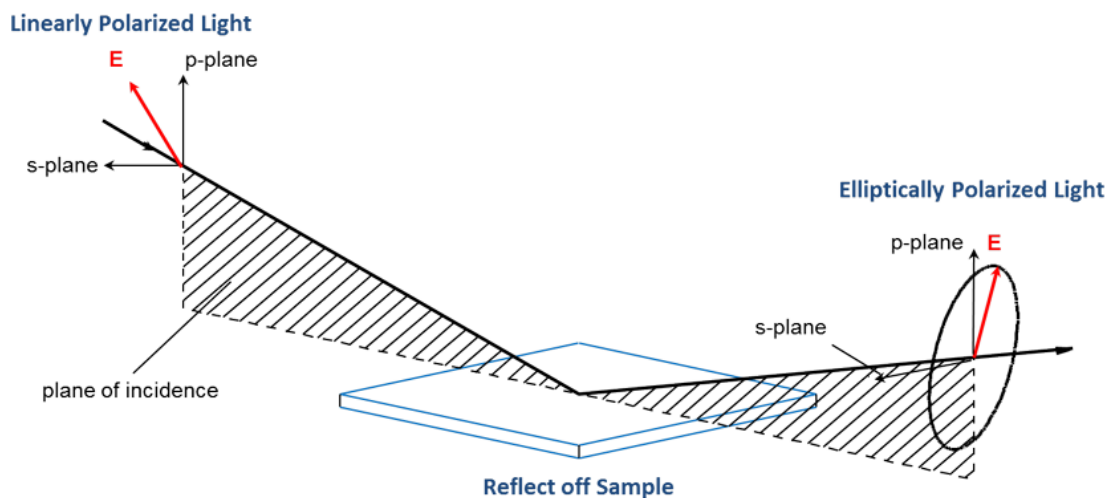


Figure 2.5 Schematic setup of an ellipsometry experiment.

Ellipsometry is very sensitive to the surface layers' presence on the order of just a fraction of a nanometer. However, the interaction between light and these ultra-thin layers can not provide good enough sensitivity to determine both refractive and index thickness. For this case, it is better to assume an approximate refractive index and only get the film thickness. The preferred upper thickness limit for most visible-to-near infrared measurements is less than 5 microns. Even for films of 1 to 5

Theoretical background

microns thick, it is better to measure with multiple incidence angles to make sure that you have a unique thickness solution.⁷⁷

Ellipsometry is used to measure various of thin films, which has no restriction on the material's type, just need light reflects from the surface. But if the coating is too rough, it can prevent ellipsometry measurements because it scatters the probe beam away from the detector. Ellipsometry is commonly applied to dielectrics, semiconductors, organics, and even metal layers.⁷⁸ The coatings can be homogenous or graded, isotropic or anisotropic. Ellipsometry is also applied to multilayer structures, with films of different materials. The only restriction for thickness measurements is whether light can pass through to the underlying substrate and back.

2.7 Scanning electron microscopy

Basic description

Scanning electron microscope (SEM) uses a focused high-energy electron beam to generate various signals from the surface of solid samples. The signals carry information of the sample including chemical composition, external morphology (texture), crystalline structure and orientation of materials which are making up the sample.^{79,80} Areas range from about 1 cm to 5 microns in width and it can be imaged in a scanning mode when using conventional SEM techniques (magnification ranging from 20X to approximately 30,000X, spatial resolution of 50 to 100 nm). The SEM has good analysis performance of selected points on the sample.

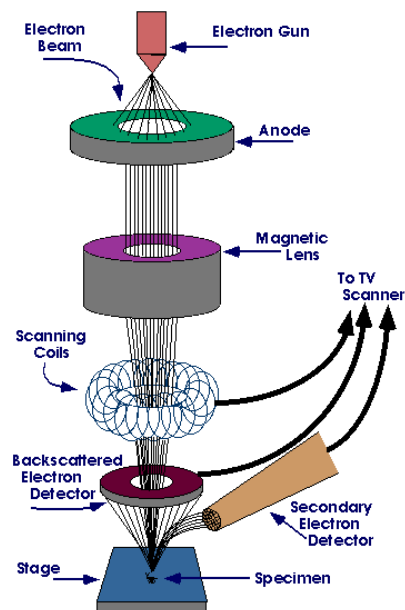


Figure 2.6 Schematic of the electron and X-ray optics of a combined SEM-EPMA.

In SEM, Accelerated electrons can carry significant amounts of kinetic energy, and this energy is scattered as various of signals which are produced by interactions of electron-sample when the incident electrons are decelerated in the sample.⁸¹ These signals consists of secondary electrons (produce SEM images), diffracted backscattered electrons (EBSD used to determine crystal structures and orientations of minerals), backscattered electrons (BSE), photons (continuum X-rays and characteristic X-rays used for elemental analysis), heat and visible light (cathodoluminescence–CL).

Applications

SEM is usually used to generate high-resolution images of objects' shapes (SEI) and to indicate spatial variations of chemical compositions.⁸² SEM is widely used to identify phases based on crystalline structure and qualitative chemical analysis. Accurate measurement of very small objects and detail features down to 50 nm is also accomplished. Backscattered electron images (BSE) can be used for quick distinguish of phases in multiphase samples. SEMs with diffracted backscattered electron detectors (EBSD) can be used to measure crystallographic orientation and microfabric in many materials.

2.8 Contact angle goniometry

When there is an interface between a solid and a liquid, the angle between the contact surface's outline and the liquid's surface is named the contact angle θ . The contact angle can indicate the wettability of a solid by a liquid.⁸³ When a liquid is dropped on a smooth homogeneous horizontal surface, it may spread all over the substrate and if complete wetting takes place the contact angle will be almost zero. On the other hand, if wetting is partial, the contact angle reaches equilibrium in the range of surface energy of the material. The smaller the contact angle, the better the wettability of the substrate is. Contact angle is a good method for surface wettability.

When complete wetting, the contact angle is 0° . Between 0° and 90° , the surface is good wetting and above 90° it is bad wetting. When the materials is ultrahydrophobic, which means it has the so-called lotus effect, θ will approach 180° which is the theoretical limit. According to Young's equation, there is a relationship between the surface tension of the liquid σ_l , the contact angle θ , free energy σ_s of solid and the surface and the interfacial tension σ_{sl} between liquid.⁸⁴

$$\sigma_s = \sigma_{sl} + \sigma_l \cos\theta$$

Theoretical background

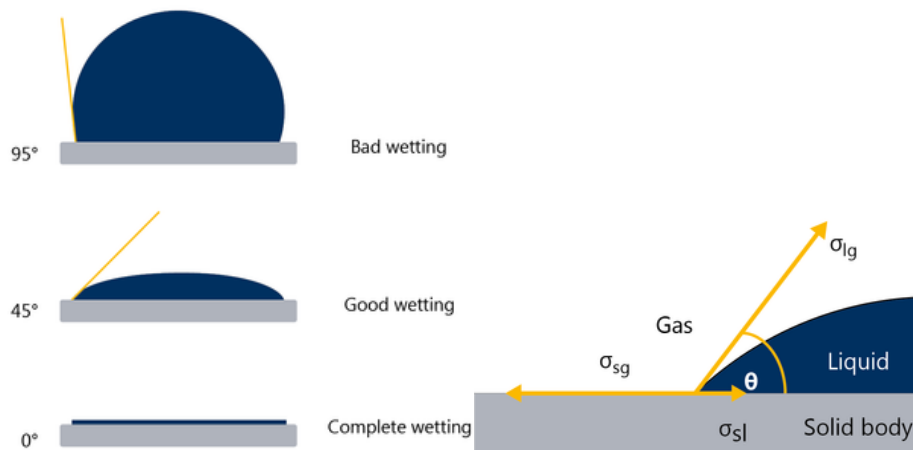


Figure 2.7 Schematic of contact angle (CA) for a water drop placed on surfaces of different hydrophobicities.

Contact Angle Measurement is a better and very accurate method for characterizing the interactions between a solid and a liquid.⁸⁵ Contact Angle Meter is an ideal academic or industrial tool for R & D engineers, product development engineers who need repeatability and precision. Contact Angle Measurement combines a non-destructive testing method with high technology test instrumentation to make an objective, accurate and repeatable analysis. With this method, you can learn about the effects of a series of surface treatments and get data that related to various surface conditions, such as wettability, lubricity, surface energy etc.

3. Materials, Preparation procedures and Characterization

3.1 Chemicals and Compounds

3.1.1 Gold substrates

The gold substrates were purchased from Georg Albert PVD-Beschichtungen and used as received. They were prepared by thermal evaporation of gold (30-100 nm thickness, 99.99% purity) onto polished single-crystal silicon (100) wafers (Silicon Sense) that had been precoated with a 5 nm titanium adhesion layer. The films were polycrystalline, exposing preferably (111) orientated surfaces of individual crystallites.

3.1.2 Chemicals

Solvents

All solvents were purchased from Sigma-Aldrich and used as received.

Precursors of SAMs

The SAM precursors used in this study, viz. dodecanethiol (DDT), 11-mercaptoundecanoic acid (MUDA), HS-(CH₂)₁₁(OCH₂CH₂)_n-OH (EG_n; n=3 and 6), and 12-Azido-1-dodecanethiol (C12N3) are shown in Schema 3.1.⁵²⁻⁵⁶ The DDT and EG_n compounds were purchased from Sigma-Aldrich and ProChimia Surfaces, respectively, and used as received. The C12N3 compound was custom-synthesized by our partners.

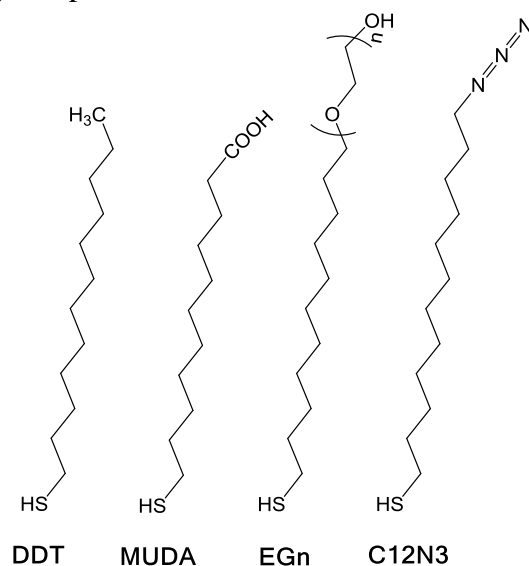


Figure 3.1 SAM precursors of this study, along with the respective abbreviations.

Chemicals used for the click reaction

The compounds for the click reaction included 1-Ethynyl-3,5-bis(trifluoromethyl) benzene (EFB, 630241), Dibenzocyclooctyne-PEG4-biotin conjugate (DBPB), and Biotin-PEG4-alkyne (BPA).^{57, 58} These compounds were purchased from Sigma-Aldrich and are shown in Figure 3.2. Further compounds and biomolecules used in this study include (+)-Sodium L-ascorbate (A7631) and Copper(II) sulfate pentahydrate (209198), avidin (A9275) and bovine serum albumin (BSA, A7638). All these compounds were purchased from Sigma-Aldrich.

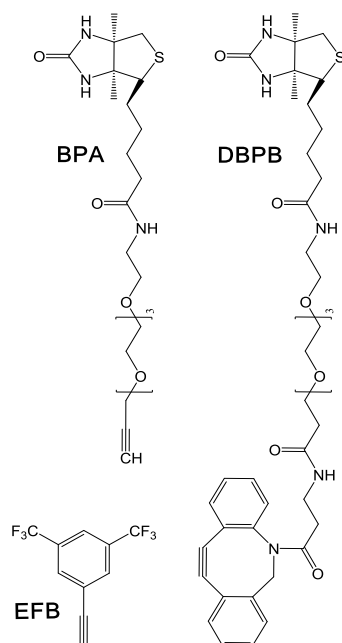


Figure 3.2 Compounds for the click reaction with the azide group, along with the respective abbreviations.

Proteins

Our experiment used these two kinds of protein to conduct specific and non-specific adsorption, avidin (A9275) and bovine serum albumin (BSA, A7638).^{59, 60} Both of these two compounds were purchased from Sigma-Aldrich.

Precursors of the PEG membranes

Epoxy- and amino-terminated, four-arm polyethylene glycols with $M_n = 2000$ g/mol (abbreviated as STAR2k-EPX and STAR2k-NH₂, respectively)⁶¹ used as precursors of the PEG membranes were purchased from Creative PEGWorks USA.

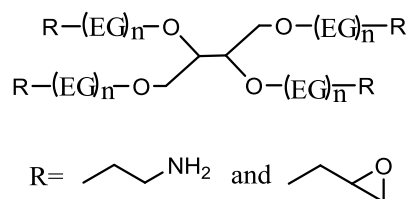


Figure 3.3 Epoxy- and amino-terminated, fourarm poly (ethylene glycols).

3.2 Preparation procedures

3.2.1 Modification of non-substituted AT SAMs by UV light

3.2.1.1 Preparation of the DDT SAMs

For this study I used dodecanethiol (DDT) SAM as a representative example of non-substituted ATs. In this sub-project, I chose to use Au wafer as substrate, this wafer consist of 100 nm Au, 5 nm Ti and 1 mm Si. It was reported as a nice substrate to form SAMs because of strong energy of Au-s bond. I immersed Au substrate into 1 mmol/L DDT (ethanol) solution for 24 h, which is long enough to form well-ordered SAMs.^{62,63}

3.2.1.2 UV irradiation of DDT SAMs

I aimed to monitor the effect of UV wavelengths on DDT SAMs, for this reason, I used 254 nm (ultraviolet C), 312 nm (ultraviolet B) and 375 nm (ultraviolet A) UV light to irradiate DDT SAMs. The intensity of 254 nm UV light was 2 mW/cm², the distance between the UV sources and samples was 1.5 cm; the intensity of 312 nm UV light was 2 mW/cm², the distance between the UV sources and samples was 3 cm; The intensity of 375 nm UV light was 37 mW/cm², the distance between the UV sources and samples was 15 cm. After irradiation, the samples were avoided washing with ethanol or water, they were measured directly to avoid removal of weakly-bound species.

3.2.1.3 Exchange reaction with MUDA

I used irradiated SAMs to exchange with 11-mercaptoundecanoic acid (MUDA) and then performed the contact angle measurement. Through this process, I could easily get the portion of DDT in mixed SAMs, and I could also find out how much Au-S bond was destroyed by UV light irradiation.

3.2.2 UV promoted exchange reaction: DDT

3.2.2.1 Preparation of the mixed DDT/C12N3 SAMs

I immersed Au substrate into 1 mmol/L DDT(ethanol) solution for 24 h, which is long enough to form well-ordered SAMs. I used 254 nm UV light to irradiate DDT SAMs because it is more effective and will take less time and get good result. The intensity of 254 nm UV light is 2 mW/cm², the distance between light and samples is 1.5 cm. Then I put irradiated DDT SAMs into 1 mmol/L C12N3 solution for 2 h to get mixed DDT/C12N3 SAMs.

3.2.2.2 Click reaction for the mixed DDT/C12N3 SAMs

Click reaction was performed in either catalyst-mediated or catalyst-free fashion. CuSO₄ was reduced by sodium ascorbate at RT to get Cu⁺ as catalyst. Subsequently, the DDT/C12N3 films were immersed into mixed solution of Cu⁺ and EFB at RT for 72 h.

3.2.3 UV promoted exchange reaction: EGn

3.2.3.1 Preparation of the mixed EGn/C12N3 SAMs

100 nm gold substrates were immersed into 1mmol EGn solution for 24 h to form EGn SAMs, and UV LED Optical Module was used to irradiate the pristine EGn SAM (375 nm UV, 38 mW/cm²) and then immersed into C12N3 solution to get mixed SAMs, the UV sources can be controlled to transfer various kinds of pattern to the substrate surface.

3.2.3.2 Click reaction for the mixed EGn/C12N3 SAMs

Click reaction was performed in either catalyst-mediated or catalyst-free fashion. CuSO₄ was reduced by sodium ascorbate at RT to get Cu⁺ as catalyst. Subsequently, the EGn/C12N3 films were immersed into mixed solution of Cu⁺ and BPA at RT for 72 h (catalyst-mediated click reaction). In addition, catalyst-free click reaction was performed, by immersing the EGn/C12N3 films into solution of DBPB at RT for 72 h.

3.2.3.3 Preparation of UV patterns

There are two main parts of lithographic setup, the V4100 - DLP DiscoveryTM Production Bundles and the High-power UV LED Optical Module for DLP DiscoveryTM 0.7 XGA DMD purchased from Texas Instruments Inc. Via ViALUX GmbH, Germany. This setup is shown in Figure 3.4. Especially, the V4100 Bundles are made of ALP-4.2 "high speed" Controller Suite and the V4100 board with 0.7" XGA 2x LVDS (UV) DMD for UV light.⁶³

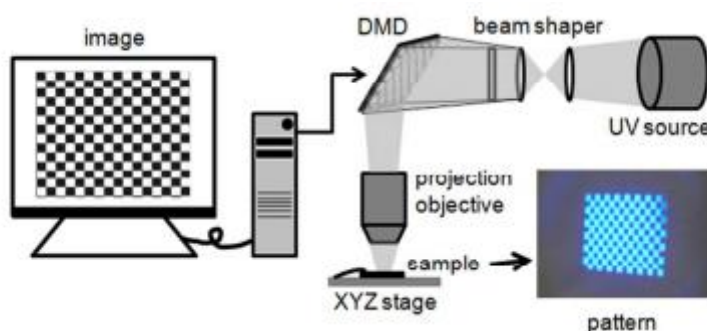


Figure 3.4 Schematic representation of a projection-based, maskless UV lithographic setup. The major elements are marked. A pattern designed in the computer serves as the input for the DMD chip which projects the pre-shaped UV beam to the sample, mimicking the original pattern.⁶³

There are 1024×768 individually controlled micromirrors in the DMD chip, with a pitch of 13.6 μm. The high-power UV LED Optical Module is made of a UV LED source (10 W, 375 nm) and projection optics. I can design the patterns in a computer with some commercial graphical softwares and transfer a picture file to the DMD controller. One can control each micromirror in the chip independently (just ON or OFF). The high-speed controller software can maximize the switching rates of the mirrors under gray value patterns, full-array global shutter operation, LED control, and precise triggering. The flux density onto the sample is measured with a multichannel energy meter which is equipped with a PD300-UV sensor. The flux is estimated at ~38 mW/cm² homogeneous illumination, which is about 80% of LED power and the normal adjustment of optical elements. Several performance and resolution tests are made by using a CMOS monochrome board camera (5 mega pixel resolution at 2.2 μm pixel size) and a commercial photo-sensitive resist.

3.2.3.4 Protein adsorption

Put clicked SAMs into 1 mg/ml BSA and avidin (dissolved in PBS solution) for 0.5 h, rinsed it with PBS solution and water. BSA and avidin were used for the DW and IPER process, respectively. The protein adsorption was performed from a 0.1 mg/ml solution of the respective protein in a PBS (P4417TAB, pH=7.4 at 25 °C Sigma-Aldrich) solution prepared using Millipore water. The incubation time was 30 min. After protein adsorption, the samples were rinsed thoroughly in PBS solution, washed in Millipore water, and dried under argon flow.

3.2.4 PEG nanomembranes

3.2.4.1 Preparation of PEG nanomembranes

PHMs were prepared by the previously established technique (Figure 7.1), from the epoxy/amine-terminated four-arm STARPEGs with $M_n = 2000$ g/mol (Creative PEGWorks), abbreviated as STAR2k-EPX and STAR2k-NH₂, respectively. According to the molecular weight, the PEG arms include monomers, corresponding to an arm length of 3.5–3.9 nm. The PEG compounds were separately dissolved in chloroform, mixed together with the joint concentration of 5 mg/mL, spin-coated onto an Au (111) substrate (Georg-Albert-PVD, Germany), the rotating speed is 4000 rpm, cross-linked by prolonged thermal annealing (6 h, 80 °C), and ultrasonicated to remove the weakly bound material. The thickness of membrane is 30-40 nm. In contrast to the previous work where the complementary PEG compounds, serving as precursors for the membrane fabrication, were exclusively mixed in the equilibrium 1:1 ratio. The joint concentration of the STAR2k materials was, however, kept constant, as mentioned above.

3.2.4.2 Modification of PEG nanomembranes by UV light

In this experiment, UV light of 254 nm was used to irradiate the PEG membrane to modify the properties of it. I changed the distance between UV light and the samples. By doing this, the flux was changed. So if you need to reach the same dose, the irradiation time will be increasing. When the distance was ~1.5 cm, the flux was 3 mW/cm²; when the distance was ~4 cm, the flux was 2 mW/cm²; when the distance was ~8.5 cm, the flux was 0.5 mW/cm².

3.3 Characterization experiments

Contact Angle Goniometry

The single-component and mixed monolayers were characterized by contact angle goniometry. Advancing contact angles of Millipore water were measured on freshly prepared samples with a Kruss goniometer Model G1. The measurements were performed under ambient conditions with the needle tip in contact with the drop. The drop volume was about 2 μ L. At least three measurements at different locations on each sample were made. The averaged values are reported. Deviations from the average were less than 2 °.

XPS

For the XPS characterization, a dedicated spectrometer (MAX200, Leybold-Heraeus) equipped with an Mg K α X-ray source (1253.6 eV; 200 W) and a hemispherical analyser was used. The X-ray source was positioned ~1.5 cm away from the sample. The spectra were recorded in normal emission geometry with an energy resolution of

~0.9 eV. The recorded spectra were divided by the spectrometer transmission function and the binding energy (BE) scale was referenced to the Au 4f_{7/2} peak of clean gold at 84.0 eV.⁶⁶ Apart from the characterization of the SAMs, XPS was also used to monitor the protein adsorption, which was performed on the basis of the characteristic N 1s signal following the methodology of our previous publications.^{6,7,10}

NEXAFS spectroscopy

NEXAFS spectroscopy measurements were performed at the bending magnet HE-SGM beamline of the synchrotron storage ring BESSY II (Helmloltz-Zentrum-Berlin). A dedicated experimental station was used.¹²⁶ The spectra acquisition was carried out at the carbon and nitrogen K-edges in the partial electron yield (PEY) mode with retarding voltages of 150 V and 300 V, respectively. As the primary X-ray source, linearly polarized synchrotron light with a polarization factor of ~91% was used. The incidence angle of the X-rays was varied in some cases following the standard approach.¹⁰⁰ The energy resolution was ~0.3 eV at the C K-edge and ~0.5 eV at the N K-edge. The photon energy (PE) scale was referenced to the pronounced π^* resonance of highly oriented pyrolytic graphite at 285.38 eV.¹²⁷ Raw NEXAFS spectra were normalized to the incident photon flux by division through a spectrum of a clean, freshly sputtered gold sample. Subsequently, the spectra were reduced to the standard form by subtracting a linear pre-edge background and normalizing to the unity edge jump (determined by a nearly horizontal plateau 40-50 eV above the respective absorption edges).

SEM

The fabricated protein patterns were imaged using a Leo 1530 Gemini SEM device (Zeiss, Germany). The images were recorded at an acceleration voltage of 5 kV. The residual gas pressure was ca. 5×10^{-6} mbar.

AFM

The lithographically created topographic patterns were characterized by atomic force microscopy (AFM) using a Dimension 3100 microscope (Digital Instruments) with a Nanoscope IIIa controller (Veeco Instruments). The measurements were performed under ambient conditions, in the tapping mode.

4. Results and discussion

4.1 Modification of non-substituted AT SAMs by UV light

4.1.1 UV light modified SAMs: XPS

To analyse the change of DDT molecular on gold surface, I used XPS spectra to see what would happen on the molecular chain. In figure 4.1a, I can see that the main C 1s peak (284.6 eV) has a small intensity reduction with the dose increasing accompanied by a shift of the major emission to lower BE and there is a weak signal increasing at higher BE (286.8 eV) which represents C-O bond. When laid under the UV light, the alkyl chains have a partial damage and oxidation of the alkyl chains which is less than the analogous processes at the SAM-substrate interface and the Au-S bond is oxidized by the oxygen in the air.¹⁰

In Figure 4.1a, in DDT spectra there is a characteristic doublet (S 2p_{3/2,1/2}) at a BE position of ~162.0 eV (S 2p_{3/2}) which corresponds to the thiolate binding to the noble metal surfaces and no other sulfur-derived species exhibits. When irradiated, the intensity of S 2p_{3/2} doublet decreases, and at the same time a new doublet at a BE ~168.0 eV ((R-SO₃⁻), which associated with photooxidized sulphur group, appears and increases in intensity with progressive UV exposure. This is typically peak in the case of thiol-derived SAMs on noble metal substrates. Besides R-SO₃⁻, other sulfur-derived moieties such as sulfenates (R-SO⁻), sulfinates (R-SO₂⁻), and sulfates (SO₄⁻) were observed as well. The emerging doublets at BEs of 165.6, 166.7, 167.9, and 168.5 eV (S 2p_{3/2}) can be assigned to the sulfenate (SO), sulfinates (SO₂), sulfonate (SO₃), and sulfate (SO₄) species, respectively. They will have more or less changes according to the intensity of UV sources or irradiation time. The progressive and controlled photooxidation of the thiolate headgroup at this interface builds a basis for a variety of lithographic applications both in the framework of conventional lithography and versatile chemical lithography. The latter relies on significant weakening of the adsorbate-substrate bond for the sulfonate headgroups as compared to the one of the original thiolate anchors.^{86,90}

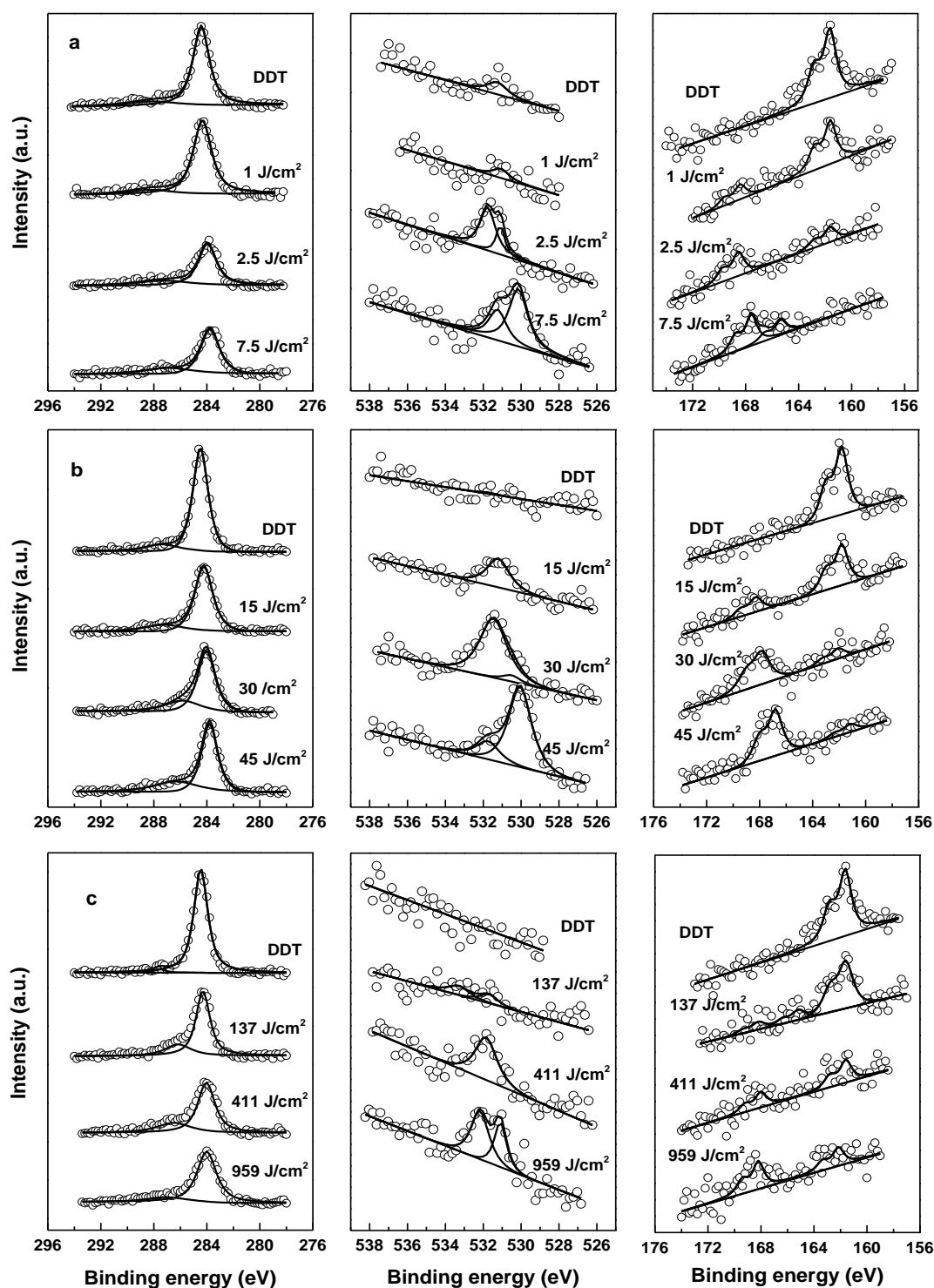


Figure 4.1 XPS spectra of the irradiated DDT monolayers irradiated by (a) 254 nm, (b) 312 nm, and (c) 375 nm UV light.

Comparing the three different wavelength, I got similar tendency about intensity against binding energy. For this reason, according to the intensity, I calculate the percentage of undamaged DDT in the irradiated SAMs and plot them in the Figure 4.2 below:

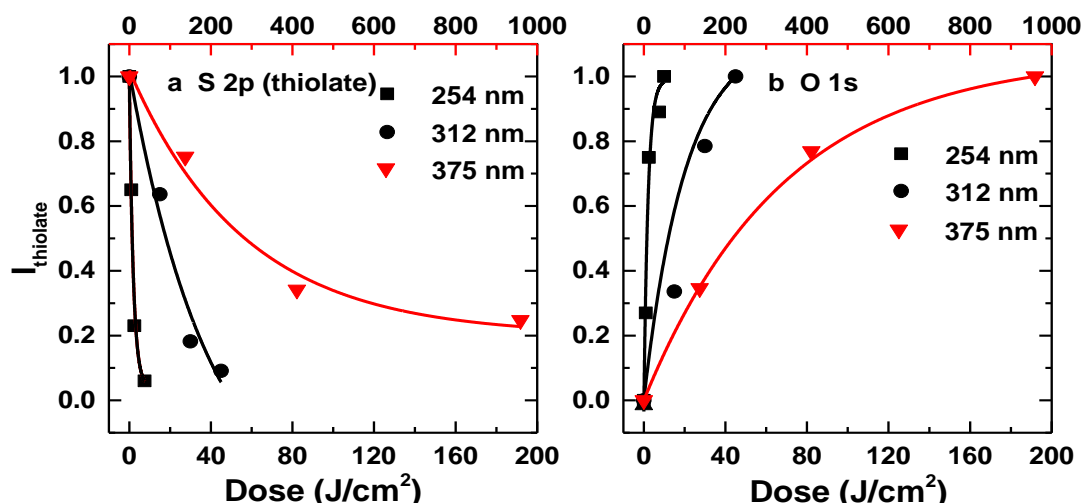


Figure 4.2 The relative intensities of the a) S 2p thiolate component and b) O 1s signals for the in the DDT monolayers irradiated by 254 nm (squares), 312 nm (circles), and 375 nm (triangles) plotted as functions of UV dose; the intensities are normalized to the values for the pristine film.

In the Figure 4.2a, the tendency of the main doublet S 2p at 162 eV is shown. The dose needed of different wavelengths are rather different, in 254 nm the dose ranges from 0 J/cm² to 10 J/cm², and this figure in 312 nm and 375 nm are 0-45 J/cm² and 0-1000 J/cm², respectively. This is a similar change of O 1s peak shown in Figure 4.2b, it is also represented as an exponential curve. It means when the irradiation time increases, more and more Au-S bond are oxidized to -SO_x group.

The cross sections of the UV induced photooxidation of the SAM–substrate interface were evaluated from the variation of the relative intensity of the thiolate component in the S 2p spectra as a function of irradiation dose as shown in Figure 4.2. The relative intensity of the thiolate component decreased exponentially with progressive exposure of the DDT SAMs to UV light, which could be fitted with a similar first-order exponential decay function to calculate the cross section values that are presented in Table 4.1. The cross section values could be calculated following the formalism:^{10,88,89}

$$I = I_{sat} + (I_{prist} - I_{sat}) \times \exp(-\sigma \Phi_{UV}) \quad (8)$$

where I is the characteristic intensity value as a function of UV exposure, Φ_{UV} is the UV exposure per area (in J/cm²), I_{prist} and I_{sat} are the intensity values for the pristine and strongly irradiated (a leveling off behavior) DDT monolayers, respectively, and the cross section σ (expressed here in cm²/J) is a measure of the rate at which a process occurs and saturation is achieved. To avoid the unusual unit of the cross section, I referred it to the number of photons, N , using a formula for N per joule, $N =$

Results and discussion

$\lambda \times 5.03 \cdot 10^{15}$, where λ is the wavelength of UV light in nanometers. This formula can be easily obtained from the basic equation $E = hc/\lambda$, where h is the Planck's constant, and c is the speed of light. The calculated cross section values for the degradation of the DDT chains are given in Table 4.1. The cross sections for decomposition of the DDT part were found to increase with decreasing length of the DDT chain.

Table 4.1 Cross section of the UV induced modification of the DDT monolayers (SAM-ambient interface) according to the intensity of the S 2p doublet(162 eV for S 2p_{3/2}).

Wavelength of UV light	254 nm	312 nm	375 nm
Cross section (in the Units of 10^{-21} cm^2)	450 ± 85.3	35.3 ± 13.5	2.1 ± 0.57

The most relevant cross section for the decomposition of the DDT molecular is presented in Figure 4.3 as a function of the wavelength. The observed dependence can be fitted well by an exponential function.

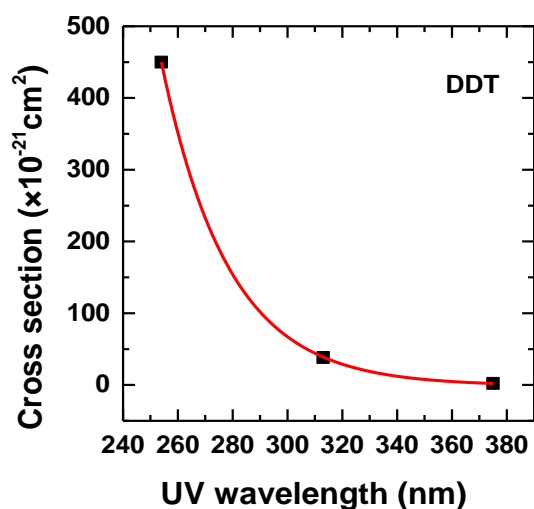


Figure 4.3 Cross section of the UV induced modification of the DDT monolayers (SAM-ambient interface) according to the intensity of the S 2p doublet(162 eV for S 2p_{3/2}) as a function of the wavelength. The solid line is an exponential fit to the experimental data.

4.1.2 UV promoted exchange reaction with MUDA: water contact angle

In order to characterize the portion of oxidized SAMs, I use MUDA (11-mercaptoundecanoic acid) as a substituent to exchange with oxidized DDT SAM, the procedure is shown in Figure 4.4.

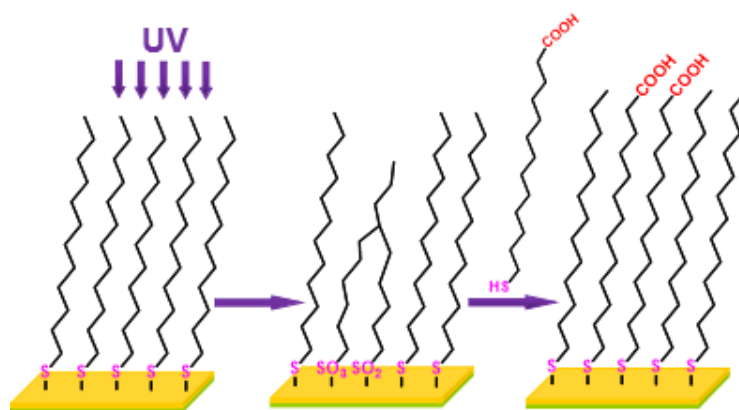


Figure 4.4 Schematic of UVPER between the DDT SAM and MUDA.

That is because that MUDA has a much lower contact angle and after exchange there is a obvious decrease. The contact angle of MUDA (in our laboratory conditions) is 54° and the contact angle of DDT is 110° . There is a relationship of contact angle between mixed SAMs and two pristine SAMs as shown below:⁹⁵

$$\cos\alpha = f\theta_1 + (1-f)\cos\theta_2 \quad (9)$$

In this equation, α is contact angle of mixed SAMs, θ_1 is contact angle of one composition and f is its portion, θ_2 is contact angle of the other composition. According to this function, I can get portion of MUDA in mixed SAMs as shown in Figure 4.5.

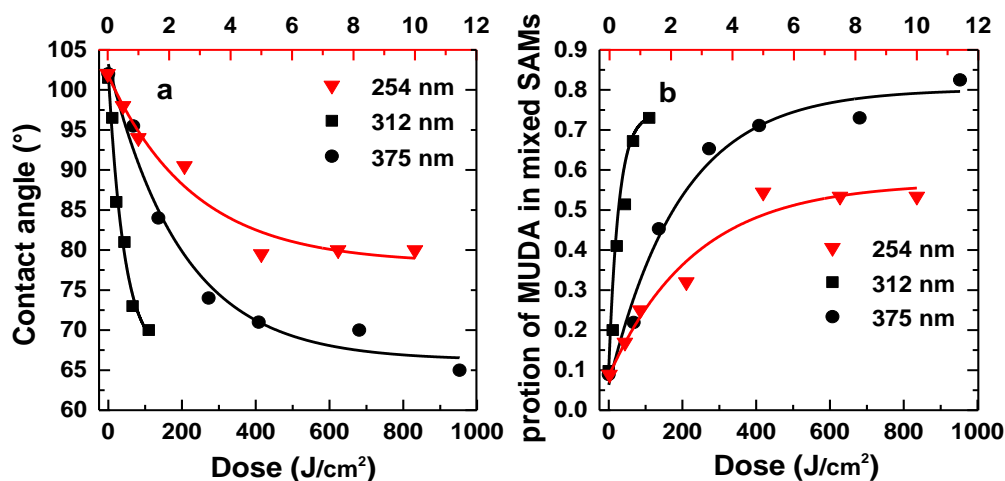


Figure 4.5 a) Advanced water contact angle for the DDT monolayers irradiated by 254 nm (triangles), 312 nm (squares), and 375 nm (circles) and subsequently exchanged with MUDA plotted as functions of UV dose; b) The portions of MUDA in the mixed SAMs plotted as functions of UV dose according to the water contact angle data.

Results and discussion

As it is shown in Figure 4.5, all of three kinds of wavelength have same trend of contact angle: decrease with dose increasing which is also same to XPS intensity trend. Comparing the portion of MUDA in mixed SAMs and the I_{thiolate} portion in SAMs, there is also a rather good match.

The cross section values for the degradation of the DDT chains calculated by the contact angle of mixed DDT/MUDA SAMs are given in Table 4.2. The cross sections for decomposition of the DDT part were found to increase with decreasing length of the DDT chain.^{91,92}

Table 4.2 Cross section of the UV induced modification of the DDT monolayers (general effect) according to the water contact angle for the mixed DDT/MUDA SAMs.

Wavelength of UV light	254 nm	312 nm	375 nm
Cross section (in the Units of 10^{-21} cm^2)	322 ± 68.9	16.9 ± 5.8	2.1 ± 0.58

The most relevant cross section for the general effect of UV light on the DDT molecular is presented in Figure 4.6 as a function of the wavelength. The observed dependence can fit well by an exponential function which is quite similar to the results from S 2p thiolate decomposition.^{93,94}

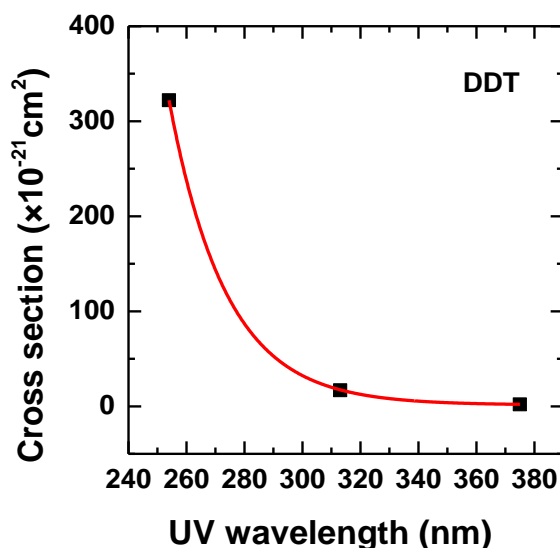


Figure 4.6 Cross section of the UV induced modification of the DDT monolayers (general effect) according to the water contact angle for the mixed DDT/MUDA SAMs as a function of the wavelength. The solid line is an exponential fit to the experimental data.

4.2 UV promoted exchange reaction: DDT

4.2.1 Mixed DDT/C12N3 SAMs

The results of the UV light promoted exchange reaction (UVPER) for the DDT templates were monitored by contact angle goniometry, XPS, and NEXAFS spectroscopy. The procedure is shown in Figure 4.7 below:

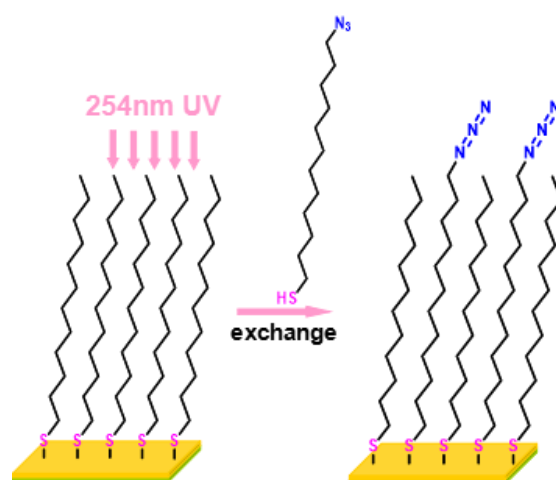


Figure 4.7 Schematic of UVPER between the DDT matrix and C12N3 substitute.

4.2.1.1 Mixed DDT/C12N3 SAMs: Water contact angle

Advancing water contact angle and derived portion of C12N3 for the DDT/C12N3 SAMs fabricated by UVPER are presented as functions of UV dose. The portion of C12N3 was calculated according to the Cassie law, viz. $\cos\alpha = f\theta_1 + (1-f)\cos\theta_2$, where α is the contact angle of the DDT/C12N3 monolayer and θ are the contact angles of the reference, single-component C12N3 and DDT SAMs, respectively. The latter values were estimated at 71 ° (C12N3) and 110 ° (DDT). The results are shown below in Table 4.3.

Table 4.3 The water contact angle for the mixed DDT/C12N3 SAMs and fraction of C12N3 in these SAMs.

Dose (J/cm ²)	0	0.25	0.5	1	2.5	5	10
Water contact angle (°)	101	95	90.5	86.5	81	77.5	74.5
Fraction of C12N3 in mixed SAMs	0.226	0.382	0.499	0.603	0.746	0.836	0.912

Results and discussion

According to Figure 4.8, the contact angle decreases gradually with the increasing UV dose, manifesting the efficient exchange reaction with the extent controlled by the dose. According to the evaluation, the portion of C12N3 in the DDT/C12N3 monolayers can be varied from ~20% to ~90% upon the dose variation from 0 to 10 J/cm². Significantly, the exchange reaction occurs to some extent even without UV irradiation (at the given conditions), which limits to some extent the dynamical range of UVPER and diminishes contrast of potential chemical patterns prepared by UVPER based lithography.

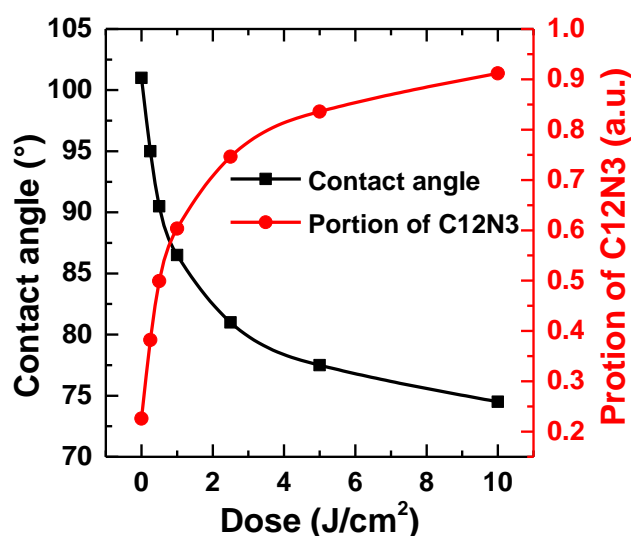


Figure 4.8 Advancing water contact angle (black squares and solid line) and portion of C12N3 (blue circles and solid line) for the DDT/C12N3 SAMs fabricated by UV-promoted exchange reaction. The UV dose was varied.

4.2.1.2 Mixed DDT/C12N3 SAMs: XPS

The above results were supported by the XPS data. The N 1s XPS spectra of the DDT SAMs after the non-promoted and promoted exchange reaction with C12N3 are shown in Figure 4.10 for several selected doses, along with the spectrum of the single-component C12N3 monolayer taken as a reference.

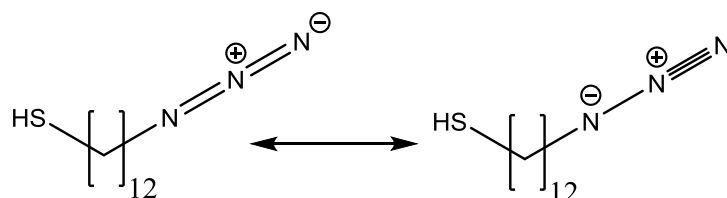


Figure 4.9 Possible molecular structures of azido group.⁵⁶

The spectrum of C12N3 exhibit characteristic emissions of the azide group at BEs of 400.7 and 404.1 eV, corresponding to the nitrogen atoms richer and poorer in electrons within the azide group.⁹⁶⁻⁹⁸ The azido group has two kinds of possible forms exist at the same time and they always convert to each other, shown in Figure 4.9.

The spectrum agrees well with the literature data,⁹⁹ including the intensity relation between the both components, and exhibits no trace of X-ray induced damage, which is in particular important for azide-containing systems because of their sensitivity to ionizing radiation.⁹⁹ The spectra of the films prepared by UVPER exhibit the same structure, establishing the formation of mixed DDT/C12N3 monolayers and intact character of the azide groups in these films. The intensity of the characteristic emissions increases with increasing dose, in accordance with the data in Figure 4.8, establishing once more that the portion of C12N3 in the mixed DDT/C12N3 SAMs can be precisely controlled by UV dose. The spectra of the films prepared by non-promoted exchange reaction (0 J/cm^2) exhibit no characteristic features of the azide group. This can be, however, related to the noisy character of these spectra associated with the comparably low photoionization cross-section of nitrogen and the limited time for the spectra acquisition. Consequently, a certain extent of non-promoted exchange reaction cannot be excluded, also in view of the contact angle data (Figure 4.8).

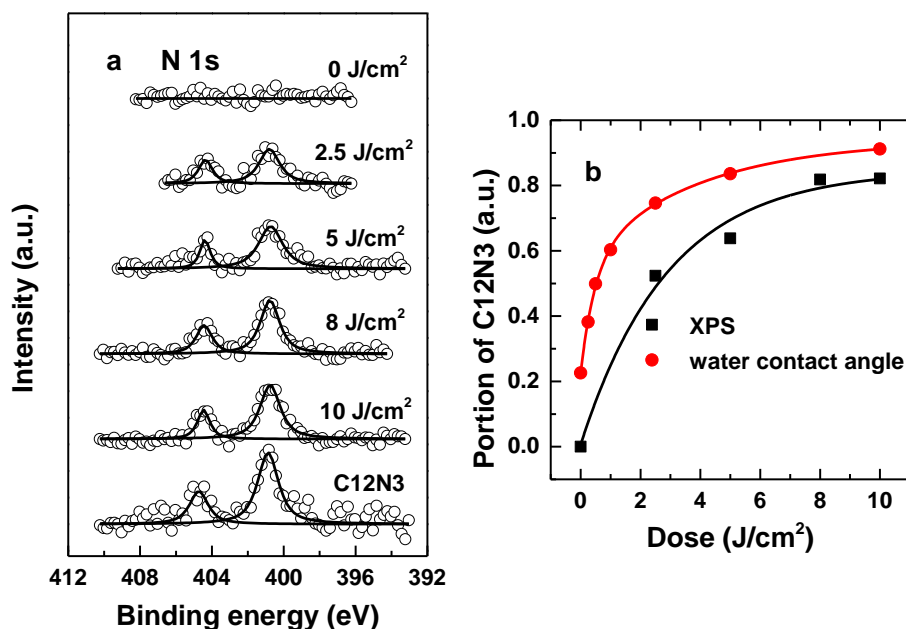


Figure 4.10 a) The N 1s spectra of the C12N3 in the mixed DDT/C12N3 monolayers irradiated by 254 nm UV light with different doses; b) the fractions of C12N3 in the mixed SAMs calculated from the N1s XPS peak intensity and water contact angle.

4.2.1.3 Mixed DDT/C12N3 SAMs: NEXAFS Spectroscopy

The NEXAFS data for the DDT SAMs after promoted (variable dose) exchange reaction with C12N3 are presented in Figure 4.11, along with the spectra of the single-component C12N3 and DDT monolayers taken as references. Two kinds of spectra are presented, viz. the spectra acquired at an X-ray incident angle of 55° which are exclusively representative of the electronic structure of the films and the difference between the spectra collected under the normal (90°) and grazing (20°) incidence geometry which is representative of the molecular orientation in the films.¹⁰⁰ The C K-edge spectra of the single-component DDT SAM in Figure 4.11a exhibit the characteristic absorption resonances of alkyl chain, viz. a most prominent feature at 287.7 eV (1) associated frequently with predominantly Rydberg states¹⁰¹ as well as two broader resonances at 293.4 eV (2) and 301.6 eV (3) related to valence, antibonding C-C* and C-C'* orbitals, respectively. These resonances exhibit pronounced linear dichroism, i.e. intensity dependence on X-ray incidence angle, as evidenced by the appearance of the intense peaks at the positions of these resonances in the difference spectra in Figure 4.11c. This suggests, as expected, a high orientational order in the DDT monolayers, with an upright orientation of the molecular chains as follows from the specific signs of the difference peaks in the 90° - 20° spectra.⁵ The C K-edge spectra of the single-component C12N3 SAMs and the monolayers prepared by UVPER exhibit the same absorption structure (Figure 4.11a), corresponding to the aliphatic backbone. The 90° - 20° spectra of these films exhibit pronounced linear dichroism, with the similar signs of the difference peaks as for DDT/Au (Figure 4.11c). This suggests that (i) azide substitution does not result in significant disordering of the resulting AT monolayers and (ii) the molecular order is persistent upon the mixture of DDT and C12N3. Note, however, that the lower intensities of the difference peaks in the spectra of C12N3 and DDT/C12N3 SAMs suggest a low extent of the orientational order in these systems as compared to DDT/Au. This is expectable since an ω -substitution usually has such an effect (C12N3/Au) and the mixing can be associated with a certain degree of disorder (DDT/C12N3 SAMs).⁵ Quantitative evaluation of the C K-edge NEXAFS data within the standard procedure,^{100,102} relying on the intensity of the R* resonance, gives average tilt angles of the alkyl backbones of 34° , 37° , 40° , and 37° for DDT/Au, C12N3/Au and DDT/C12N3 SAMs prepared at 5 and 10 J/cm², respectively (with a standard accuracy of such an evaluation, $\pm 3^\circ$). The former value is very close to the literature one^{103,104} while the latter values are only slightly higher supporting the

above conclusion regarding a minor effect of the azide substitution on the molecular orientation and establishing that the orientational order of the DDT/C12N3 SAMs is close to that of C12N3/Au.

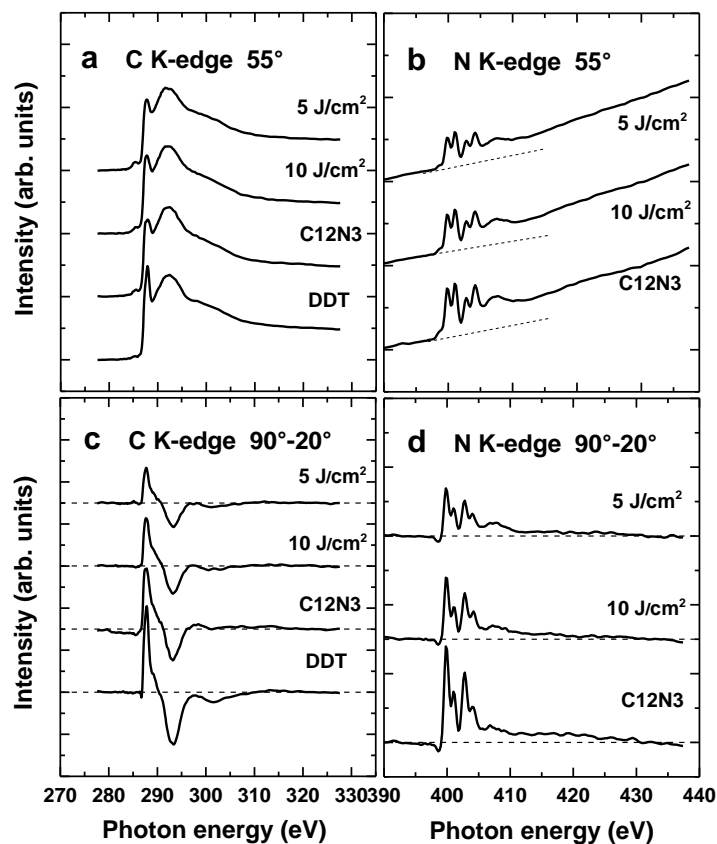


Figure 4.11 C (a,c) and N (b,d) K-edge NEXAFS spectra of the DDT SAMs after promoted (variable dose) exchange reaction with C12N3 (Figure 4.4), along with the spectra of the single-component C12N3 and DDT monolayers taken as references (bottom curves). The doses are marked at the spectra. Two kinds of spectra are presented, viz. the spectra acquired at an X-ray incident angle of 55° (a,b), and the difference between the spectra collected under the normal (90°) and grazing (20°) incidence geometry (c,d). Individual absorption resonances are marked by numbers (see text for the assignments).

The N K-edge spectra of the single-component C12N3 SAM in Figure 4.11c exhibit the characteristic absorption resonances of the azide group at photon energies of 399.7 eV (**1**), 400.9 eV (**2**), 402.6 eV (**3**) and 404.0 eV (**4**). Both the positions of these resonances and their relative intensities agree well with the previous work. The two former resonances (**1** and **2**) are associated with the terminal nitrogen atoms of the azide group and correspond to electron transition from the N 1s state to two different π^* orbitals.¹⁰⁵ The two latter resonances (**3** and **4**) are related to the positively

Results and discussion

charged, middle nitrogen atom of the azide group and correspond to electron transition from the respective N 1s state to two different π^* orbitals.¹⁰⁵ Similar to the C K-edge case, the N K-edge spectra of C12N3/Au exhibit pronounced linear dichroism (Figure 4.11d), suggesting that the azide groups at the SAM-ambient interface are well ordered. The positive sign of the π^* difference peaks in the 90° - 20° spectrum of C12N3/Au suggests an upright orientation of the azide groups, in view of the perpendicular orientation of the π^* orbitals with respect to the group backbone.

The N K-edge spectra of the films prepared by UVPER in Figure 4.11b mimic the absorption structure of the C12N3/Au case, establishing, in agreement with the contact angle and XPS data, the formation of mixed DDT/C12N3 monolayers and intact character of the azide groups in these films. The intensity of the characteristic absorption features increases with increasing dose, in accordance with the contact angle and XPS data, establishing once more that the portion of C12N3 in the mixed DDT/C12N3 SAMs can be precisely controlled by UV dose. The 90° - 20° N K-edge spectra of these films exhibit pronounced linear dichroism, with the similar signs of the difference peaks as for C12N3/Au (Figure 4.11d). This suggests, in agreement with the C-Kedge data that (i) azide substitution does not result in disordering of the resulting AT monolayers and (ii) the molecular order is persistent upon the mixture of DDT and C12N3. Note that in the given case, the lower intensities of the difference peaks in the 90° - 20° spectra of the DDT/C12N3 SAMs do not necessary suggest a lower extent of the orientational order in these systems as compared to DDT/Au, since these intensities should be "normalized" to those in the 55° spectra (Figure 4.11b). Consequently, the orientational order of the azide groups in the single-component C12N3 SAMs and mixed DDT/C12N3 monolayers is presumably similar. Quantitative evaluation of the N K-edge NEXAFS data within the standard procedure, relying on the intensity of the π^* resonances, gives average tilt angles of the azide backbones of 22° , 24° , and 24° for C12N3/Au and DDT/C12N3 SAMs prepared at 5 and $10\text{J}/\text{cm}^2$, respectively (with a standard accuracy of such an evaluation, $\pm 3^\circ$). So, it seems the azide groups are only slightly inclined and well-ordered. Also, the values support the conclusion that the orientational order of the DDT/C12N3 SAMs is close to that of C12N3/Au.

Note that the results of the numerical evaluation of the N 1s XPS and N K-edge NEXAFS spectra of the mixed DDT/C12N3 monolayers prepared by UVPER in terms of the signal intensity, taking the spectra of C12N3/Au as the references, agree well with the results of the contact angle measurements (Figure 4.8). In particular, the

portion of C12N3 in the DDT/C12N3 films were estimated at 80% by XPS and 93% by the NEXAFS spectroscopy at a dose of 10 J/cm².

4.2.2 Click reactions of the mixed DDT/C12N3 SAMs

4.2.2.1 Mixed SAMs after the click reaction: XPS

Compared with pristine DDT, after exchange and click reaction, the clicked SAMs have obvious differences in components, which can be seen easily from XPS spectra. From Figure 4.12a we can see, at binding energy is ~285.3 eV, the peak corresponding to C atom in the benzene increases gradually, and because DDT and C12N3 have almost same amount of alkyl-C, so the C peak at 284.5 eV doesn't decrease too much. According to the area of two peaks, I got the ratio of I(C=C/C-C). These ratios can fit exponential curve very well and they approach to the ratio 0.89, which is the ratio of C12N3 clicked SAMs.

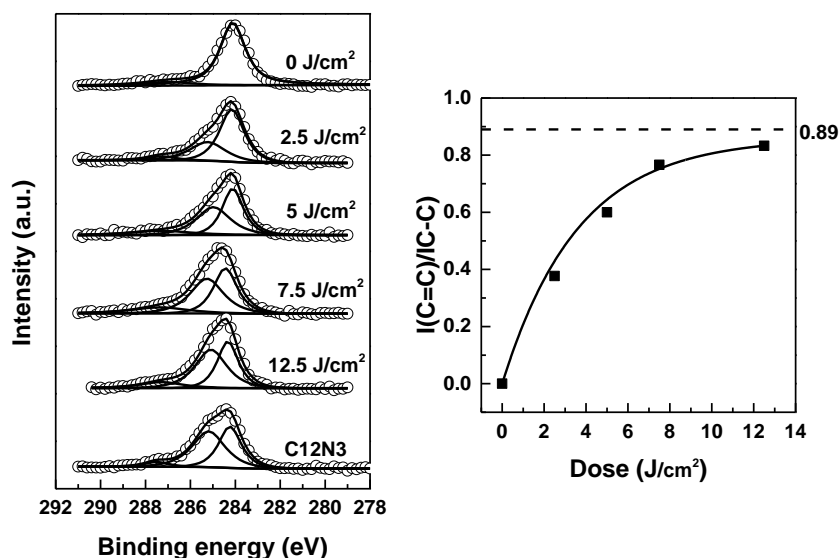


Figure 4.12 a) C 1s XPS spectra acquired after the click reaction between EFB and the mixed DDT/C12N3 SAMs irradiated by 254 nm UV of different doses; b) the normalized I(C=C)/I(C-C) ratio plotted as a function of UV dose.

The next step of the experimental procedure for the DDT template was the click reaction with EFB. The results of this step were monitored by XPS. The N 1s (a) and F 1s (b) XPS spectra acquired after this step are presented in Figures 4.13a and 4.13b, respectively, including the data for both DDT/C12N3 SAMs and reference C12N3 monolayers.⁵⁵ The presence of the EFB-characteristic F 1s emission in the spectra of all samples (Figure 4.13b) establishes an efficient click reaction. Significantly, the character of the N 1s spectra changed completely as compared to the situation before the click reaction: instead of two emissions at BEs of 400.7 and 404.1 eV (Figure

Results and discussion

4.10a), there is only one emission at a BE of 400.1 eV (Figure 4.13a). Consequently, the yield of the click reaction should be close to 100%. According to this assumption, the dependence intensities of the N 1s and F 1s intensities on UV dose after the click reaction in Figure 4.13c mimics the curve for the portion of C12N3 before the click reaction in Figure 4.8. The data in Figure 4.13c are one more evidence that the mixed DDT/C12N3 SAMs can be prepared successfully by UVPER, in a broad range of compositions precisely controlled by UV dose, along with the finding that these mixed SAMs are highly efficient with respect to the click reaction, similar to the one-component C12N3 monolayer.

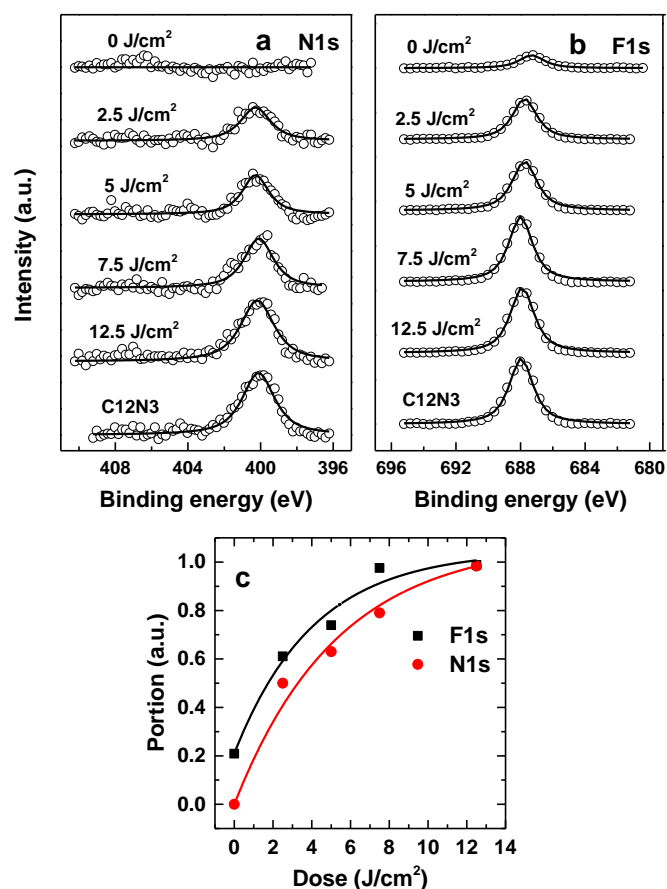


Figure 4.13 N 1s (a) and F 1s (b) XPS spectra of the DDT SAMs after the click reaction with EFB following the exchange reaction with C12N3 (variable dose), along with the analogous spectra for the single-component C12N3 monolayer taken as references (bottom curves). The doses applied upon UVPER are marked at the spectra. (c) Portion of EFB derived from the N 1s data (blue circles and solid line) and the F 1s data (red squares and solid line) as function of UV dose.

4.2.2.2 Effect of exchange time: XPS

To study the relationship between exchange time and extent of exchange, I put pristine DDT SAMs into 1mmol C12N3 solution for various time, then do the click reaction to get a relationship curve in Figure 4.14a.

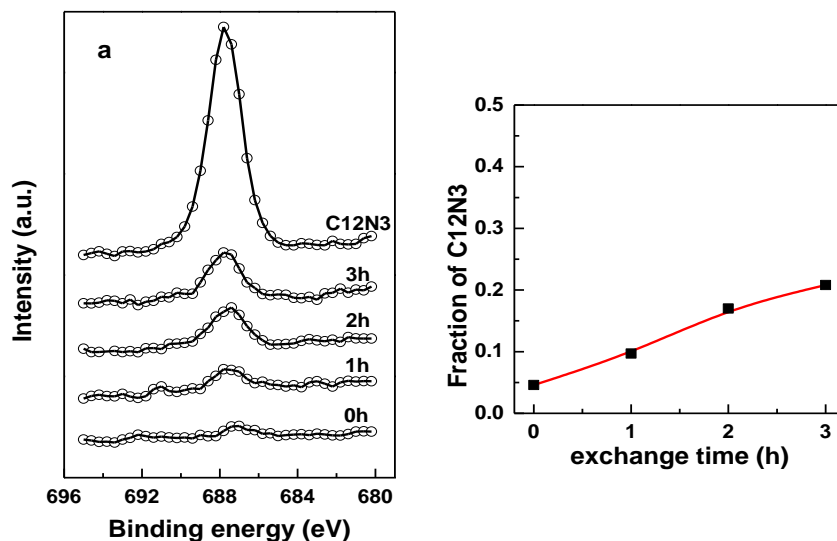


Figure 4.14 a) F 1s XPS spectra of the DDT/C12N3 SAMs after the click reaction with EFB; (b) Fraction of C12N3 derived from the F 1s XPS data as a function of exchange time.

We can see that when $t=0$ h, which means with no irradiation and no exchange but put it in click solution, there is still a little F 1s signal. It can be explained that the substrate absorb some click solution, because XPS is very sensitive to fluorine, the amount of fluorine on the substrate is very little. The sensitive is also the reason why I use F 1s as a characterization. From 0 h to 3 h, the portion of clicked C12N3 in mixed SAMs increase from ~ 0.05 to ~ 0.21 . At 2h, the portion is 0.17, similar to our rest results, such as XPS and contact angle. That is why I choose 2 h as exchange time.

4.2.2.3 Thickness measurements: Ellipsometry

The thickness of the mixed SAMs is just several nanometers and it is hard to measure, so I use ellipsometry to character the slight changes. In Figure 4.15, I can see that from 0 J/cm^2 to 12.5 J/cm^2 , the thickness increases from 1.8 nm to 2.4 nm. When the dose is lower, less molecular with a big tail group are formed. Upon the development step, each local dose was transformed in the respective density of the C12N3-clicked moieties. This density, in its turn, was transformed in the local height of the SAMs, that means this is a good method to get a a complex gradient-like pattern.

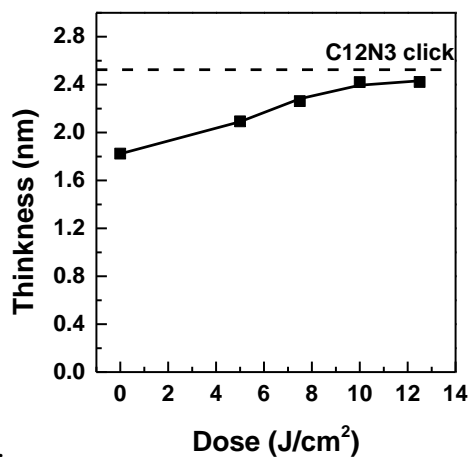


Figure 4.15 Thickness of the mixed DDT/C12N3 SAMs after the click reaction with EFB plotted as a function of UV dose.

As it is shown in Figure 4.16, more density can make SAMs better-ordered, which can result in higher SAMs.

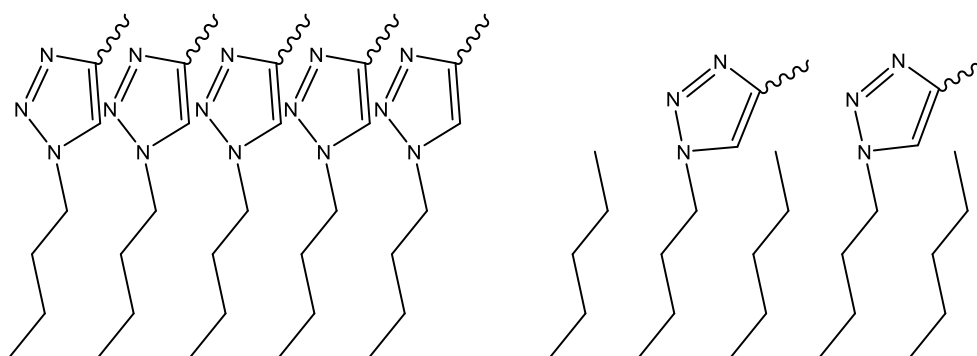


Figure 4.16 A schematic cartoon of well-ordered and strongly disordered SAMs after the click reaction.

4.3 UV promoted exchange reaction: EGn SAMs

As I studied in the previous part, UV is a convenient and reasonable method to form mixed SAMs with specific function. For this reason, I explored another kinds of mixed SAMs to satisfy the requirements in different fields.

4.3.1 Mixed EGn/C12N3 SAMs

4.3.1.1 Mixed SAMs: XPS

As shown in Figure 4.17, compare pristine EG3 and EG6, peak at 284.6 eV (C-C) and peak at 286.3 eV (C-O) have big differences at intensity. Because there are just 3 -(CH₂CH₂O)- groups in in EG3 molecular and in EG6 there are six -(CH₂CH₂O)- groups but the alkyl-chain part are almost same. So the ratio of I(C-O/C-C) are very different at the beginning. We can see from Figure 4.17c, I(C-O/C-C) of EG3 and EG6 are 1.88 and 0.76, respectively. With the dose increasing, the ratio decreases, which means part of EGn molecular C-O bond was damaged.

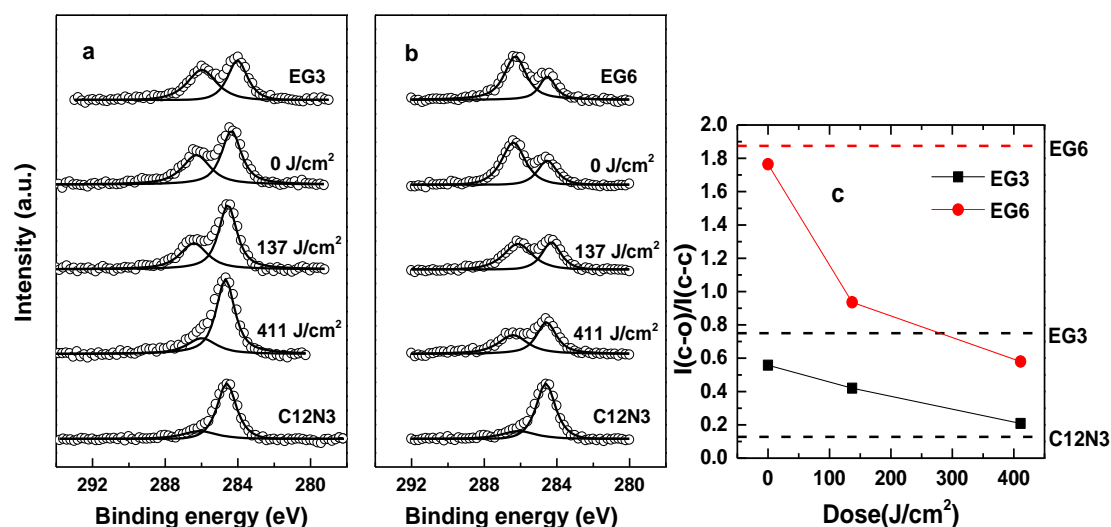


Figure 4.17 a,b) C 1s XPS spectra of the mixed EG3/C12N3 and EG6/C12N3 SAMs prepared by UVPER with different UV doses. The spectra of homogeneous EG3, EG6 and C12N3 SAMs are given as references, c) the I(C-O)/I(C-C) ratios in the mixed EGn/C12N3 SAMs plotted as functions of UV dose.

In Figure 4.18, O 1s and N 1s XPS spectra are shown, according to the change of the intensity, I got a graph that portion of EGn molecular in the mixed SAMs. According to the N 1s spectra, I can conclude that C12N3 are more hardly to

exchange with EG6 rather than EG3; according to the O 1s spectra, we can see that EG group in EG6 are easier to damage than EG3.

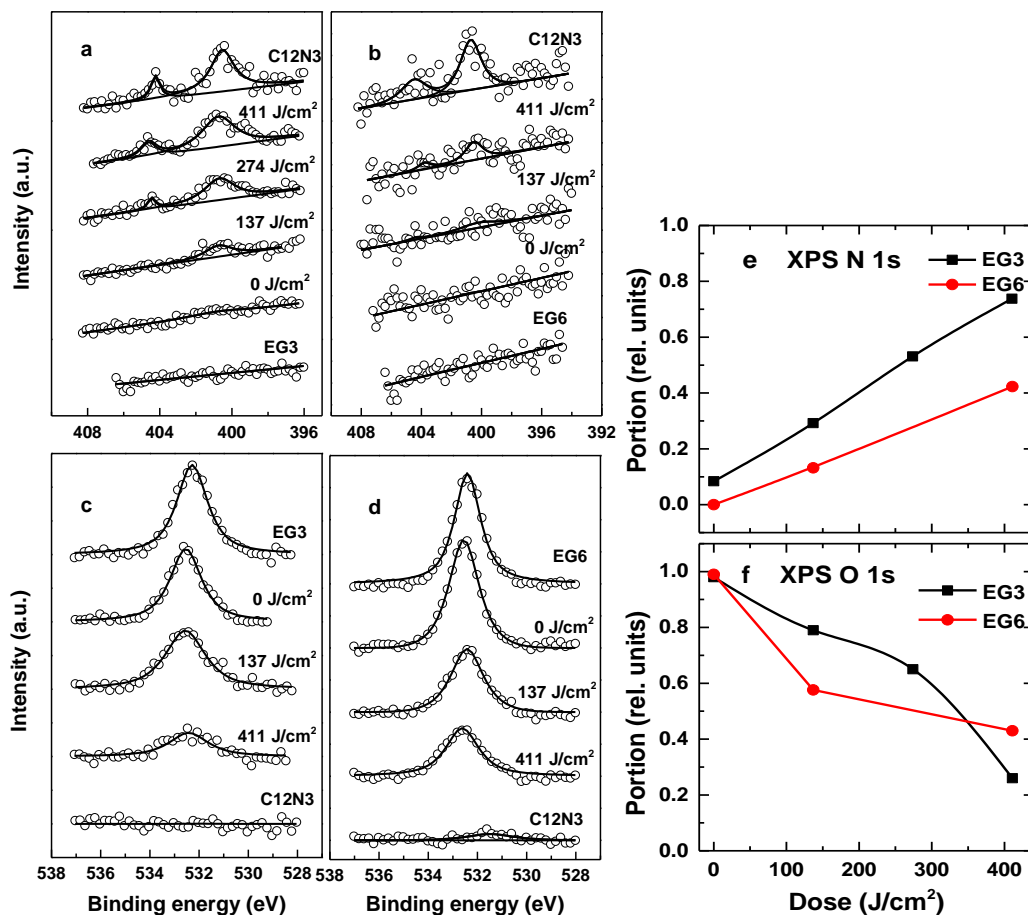


Figure 4.18 N 1s (a,b) and O 1s (c,d) spectra of the mixed EG3/C12N3 and EG6/C12N3 SAMs prepared by UVPER with different UV doses. The spectra of homogeneous EG3, EG6 and C12N3 SAMs are given as references. Portion of C12N3 in the mixed EGN/C12N3 SAMs derived from the (e) N 1s and (f) O 1s data as functions of UV dose.

4.3.1.2 Mixed SAMs: water contact angle

I measured water contact angle of mixed SAMs (C12N3 and EGN). The contact angle of pristine EG3 and EG6 are 38 ° and 34 °, respectively.¹⁰⁶⁻¹⁰⁸ The contact angle of C12N3 is 71 °. Due to the equation:

$$\cos\alpha = f\theta_1 + (1-f)\cos\theta_2$$

In this function, α is contact angle of mixed SAMs, θ_1 is contact angle of C12N3, θ_2 is contact angle of EGN, f is portion of C12N3 in mixed SAMs. According to this function, I can get portion of C12N3 in mixed SAMs as shown in Figure 4.19a. In this Figure 4.19b, we can see C12N3 is easier to exchange with EG3 than EG6. The

portion of C12N3 in C12N3/EG3 is from 0.15 to 0.61, which is very similar with the results of N 1s (from 0.1 to 0.7). The portion of C12N3 in C12N3/EG6 is from 0.09 to 0.41 and the results of N 1s is from 0 to 0.4 which maybe because that the N 1s is not very sensitive in XPS spectra.

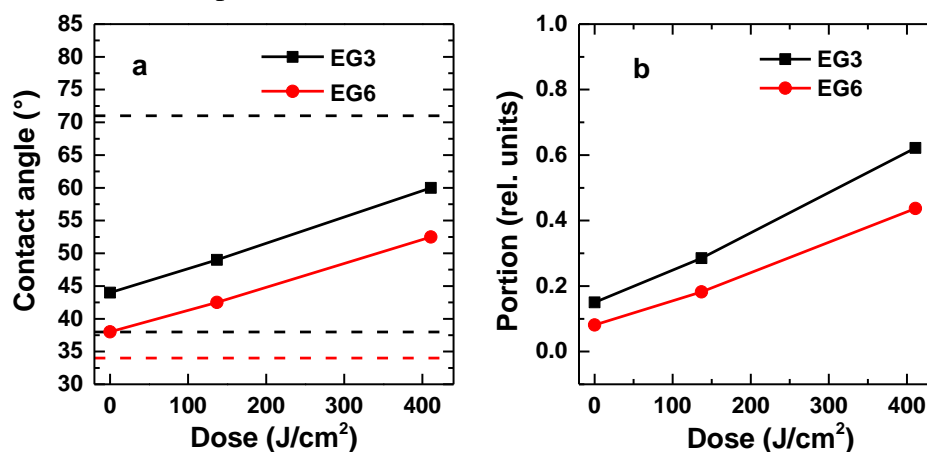


Figure 4.19 a) Water contact angles for the mixed EGn/C12N3 monolayers prepared by UVPER as functions of UV dose; b) The portions of C12N3 in the mixed SAMs plotted as functions of UV dose according to the water contact angle data.

4.3.1.3 Mixed SAMs: NEXAFS spectroscopy

Complementary information about the mixed C12N3/EG6 SAMs was obtained by NEXAFS spectroscopy. This technique samples the electronic structure of the unoccupied molecular orbitals and, in this regard, is especially sensitive to the chemical composition of the samples. In addition, NEXAFS spectra acquired in the partial electron yield (PEY) acquisition mode are much less affected by the self-attenuation of the electron signal than the analogous XPS spectra, since the PEY signal is comprised not only of the elastic Auger electrons but from the inelastic secondary electrons as well.

These spectra were acquired at so-called “magic angle” of X-ray incidence (55 °) and are therefore exclusively representative of the electronic structure of the samples, without admixture of any effects related to molecular orientation. N K-edge spectra (55 °) of the one-component C12N3 and EG6 monolayers as well as mixed C12N3/EG6 films prepared by UVPER (375 nm) are presented in Figure 4.20. The spectrum of the EG6 SAMs does not exhibit any features, in accordance with the chemical composition of this compound. As I said before, the two distinct π^* bonds at higher energy are related to electron transitions from the N 1s orbital of the positively charged nitrogen atom into two different π^* orbitals (402.5 eV and 403.9 eV). The

Results and discussion

two distinct π^* bonds at lower energy are related to the two nitrogen atoms (N1 and N3) adjacent to N2.

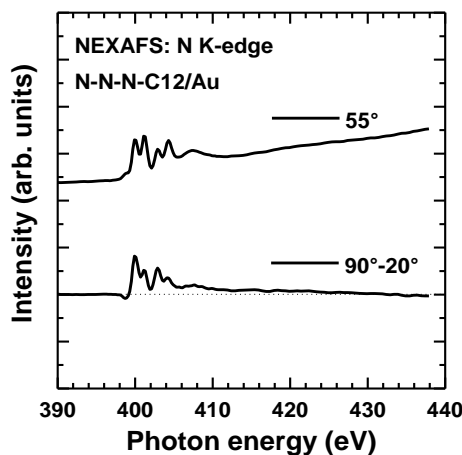


Figure 4.20 N K-edge NEXAFS spectra of the C12N3 SAMs. Two kinds of spectra are presented, viz. the spectra acquired at X-ray incident angles of 55° and the difference between the spectra collected under the normal (90°) and grazing (20°) incidence geometry.

These resonances exhibit characteristic intensity relation, with the former feature being significantly stronger. The spectra of the mixed C12N3/EG6 SAMs mimic that of the C12N3 monolayer exhibiting the same pattern of the absorption resonances.

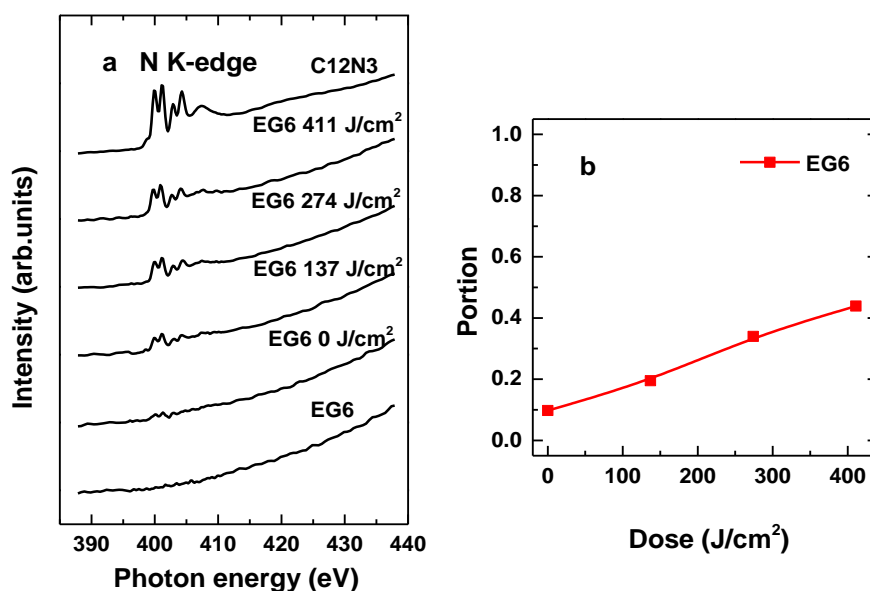


Figure 4.21 a) 55° N K-edge NEXAFS spectra of the pristine EG6 and C12N3 films, EG6 monolayers after the non-promoted (0 J/cm^2) and promoted ($137, 274, 411 \text{ J/cm}^2$) exchange reaction with C12N3, b) the portion of C12N3 in the mixed C12N3/EG6 SAMs plotted as a function of UV dose.

This is additional evidence that the electronic structure of the C12N3 moieties was not disturbed upon their imbedding into the EG6 matrix. Also, the spectral weight of C12N3 decreases with decreased UV dose in accordance with the expectations and all the above data. When the dose is 411 J/cm^2 , we can see from Figure 4.21, the portion of C12N3 in mixed SAMs is about 43%, which is also accordance with the results before.

4.3.2 Click reaction of mixed EGn/C12N3 SAMs

4.3.2.1 Free-catalyst click reaction of mixed SAMs: XPS

According to the study in previous experiment, we can see the XPS of N 1s, after click reaction, two typical N 1s peak at 400.8 eV and 404.4 eV which belong to azido group disappear and there is a new N 1s peak at $\sim 400.0 \text{ eV}$ which is related to aromatic nitrogen. So I use this single peak to characterize whether the click reaction happen totally and how much EGn molecular was exchanged by C12N3.¹¹¹ From Figure 4.22, we can see that there is just one single peak, which means the click reaction happened totally.

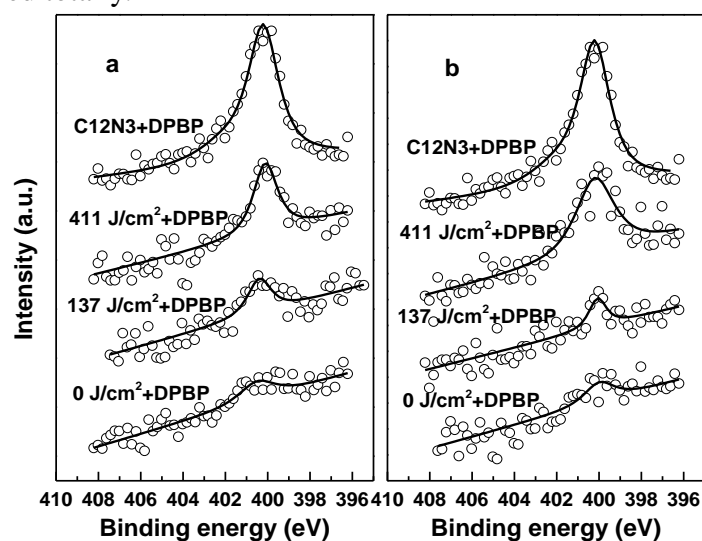


Figure 4.22 N 1s XPS spectra of the mixed EG3/C12N3 (a) and EG6/C12N3 (b) SAMs prepared by UVPER, after the free-catalyst click reaction with BPA. Irradiation doses are given at the respective spectra.

According to the intensity, I plot a curve shown in Figure 4.23 that portion of EGn click SAMs in the mixed SAMs against irradiation dose. Same to previous research, percentage of EG3 clicked molecular in mixed SAMs is still larger than EG6. The range of EG3 is around 13%~55%, and the range of EG6 is 6%~50%. This result has similar tendency to results before and can be regard as a reference.

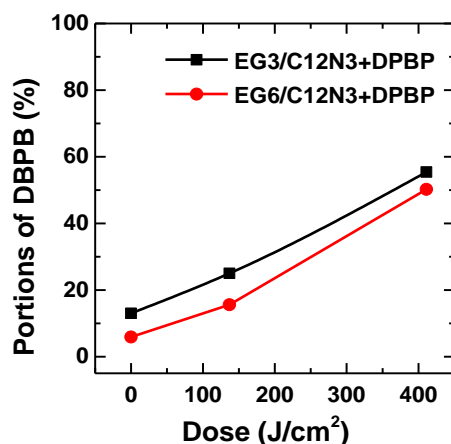


Figure 4.23 Portions of C12N3 in the mixed EG3/C12N3 (black curve) and EG6/C12N3 (red curve) SAMs prepared by UVPER and clicked with DBPB according to the N1s XPS data plotted as functions of UV dose.

4.3.2.2 Catalyst click reaction of mixed SAMs: XPS

As I studied in the previous experiment, we can see there is also the N 1s peak, after click reaction, at ~ 400.0 eV which is related to aromatic nitrogen appearing. So I use this single peak to characterize whether the click reaction happen totally and how much EGN molecular was exchanged by C12N3. From Figure 4.24, we can see there is just one single peak, which means the click reaction happened totally.

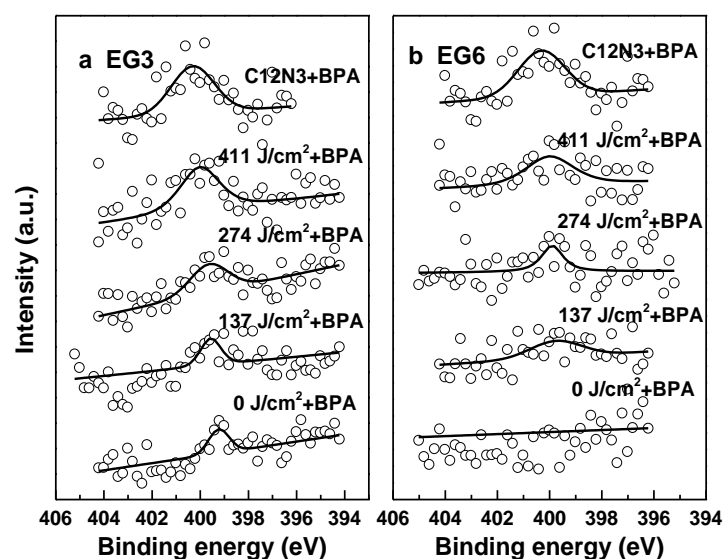


Figure 4.24 N 1s XPS spectra of a) EG3/C12N3 and b) EG6/C12N3 mixed SAMs prepared by UVPER after the catalyst-mediated click reaction with DPBP. UV doses are marked at the respective spectra.

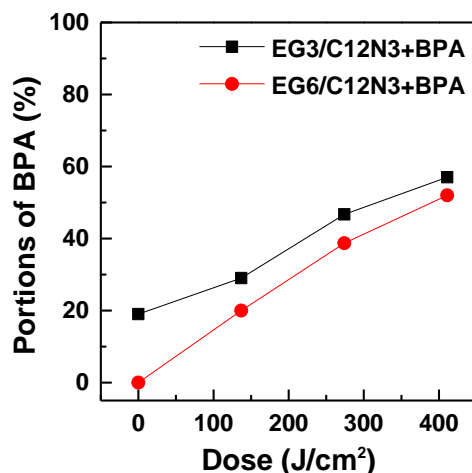


Figure 4.25 Portions of C12N3 in the mixed EG3/C12N3 (black curve) and EG6/C12N3 (red curve) SAMs prepared by UVPER and clicked with BPA according to the N1s XPS data plotted as functions of UV dose.

According to the intensity, I plotted a curve shown in Figure 4.25 that portion of EGn click SAMs in the mixed SAMs against irradiation dose. Same to before, percentage of EG3 clicked molecular in mixed SAMs is still larger than EG6. The range of EG3 is around 20%~57%, and the range of EG6 is 0~52%. This result is just an estimation but can not be regard as a accurate reference.

4.3.3 Specific protein adsorption

4.3.3.1 Protein adsorption on free-catalyst clicked SAMs: XPS

In our experiment, avidin and BSA are used as specific and non-specific, respectively.^{112,113} Because avidin and BSA have similar N content, I compared the N 1s of different situations, which shown in Figure 4.26. Firstly, DDT SAMs were immersed substrate into BSA and avidin of same concentration. We can see that when same amount protein absorbed on DDT surface, the content of N 1s in the avidin molecular is a little more than BSA.^{110,114} Secondly I compared pure C12N3 clicked molecular and after putting it into BSA and avidin. I can see that after putting into BSA, the N 1s peak intensity don't have a obvious increase, but after putting into avidin, the N 1s peak have a significant increase. That shows a very obvious specific.

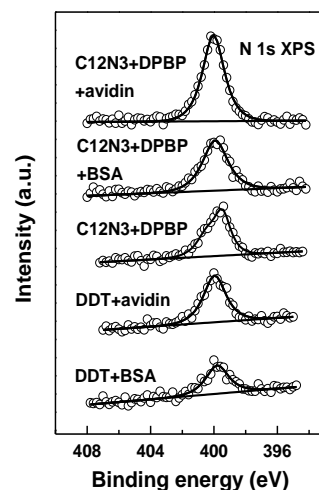


Figure 4.26 N 1s XPS spectra of pristine (DDT) and DPBP-functionalized SAMs before and after their immersion into avidin and BSA solutions. The spectrum of the pristine C12N3 SAM after the click reaction with DPBP is given as well.

Following this reaction, I did a series of experiments to compare EG3 and EG6 immersing into BSA and avidin. The results are shown in Figure 4.27.

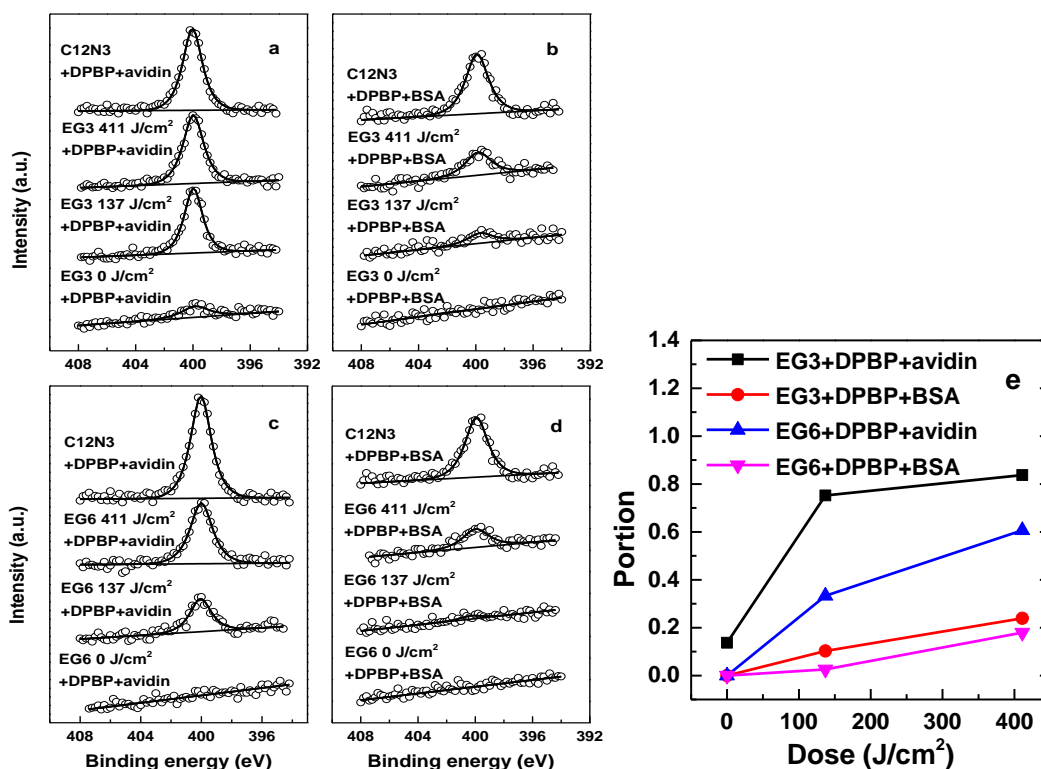


Figure 4.27 N 1s XPS spectra of DPBP functionalized a) EG3/C12N3 SAMs after immersion into avidin, b) EG3/C12N3 SAMs after immersion into BSA, c) EG6/C12N3 SAMs after immersion into avidin, d) EG6/C12N3 SAMs after immersion into BSA, e) relative intensity normalized to C12N3 that for the DPBP-functionalized, one-component SAMs immersed into avidin plotted as a function of UV dose.

Using C12N3 clicked SAMs immersed avidin as a reference, I plotted the ratio of the different samples intensity to C12N3 clicked SAMs into avidin. We can see that the intensity of these samples immersing to avidin are much larger than BSA, both EG3 and EG6 can resist protein well; the peak intensity of EG3 immersing into avidin are a little larger than EG6, which is also very correspond to the results before. But when the dose is 0 J/cm^2 , there is about 10% protein adsorption on the EG3 SAM, but EG6 SAM do not absorb obvious protein.

4.3.3.2 Protein adsorption on free-catalyst clicked SAMs: NEXAFS spectroscopy

The procedure of EG6 SAMs irradiated and exchange with C12N3 and click reaction and immerse into protein is shown in Figure 4.28. In Figure 4.28, I can calculate the percentage of C12N3 in mixed SAMs after exchange reaction according to the intensity of typical N K-edge 55° peak. We can also see the N K-edge photon energy changed after click reaction, the peak become to one single peak and after put into BSA, there is no obvious increase at intensity, but after immersing in avidin, the intensity increases significantly.

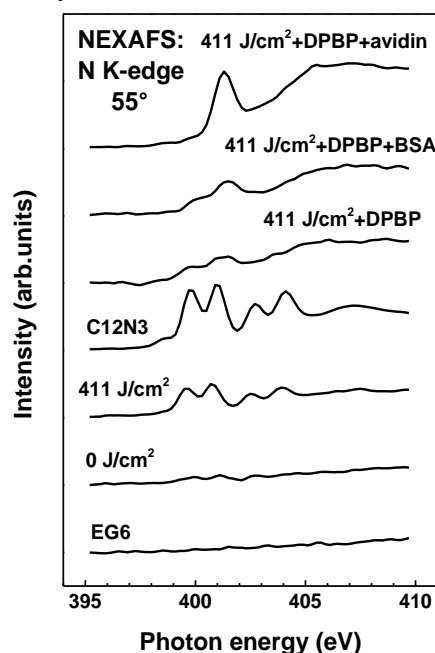


Figure 4.28 N K-edge 55° NEXAFS spectra of the EG6 SAMs before and after UV irradiation, free-catalyst click reaction with DPBP, and exposure to BSA and avidin.

4.3.3.3 Protein adsorption on free-catalyst clicked SAMs: lithography

In this part, I design a series of pattern to study the protein adsorption application.¹¹³
The pattern is shown below:

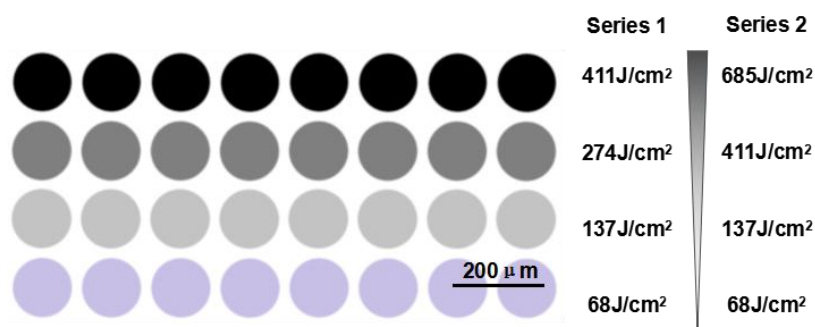


Figure 4.29 General design of the protein adsorption patterns.

Firstly, I use series 1 to do the research. Comparing a and b, we can see that avidin is much clearer than BSA, that is a good proof of specific protein adsorption; comparing a and c, we can see that EG6 is clearer than EG3, this is because EG3 at 0 J/cm² have more adsorption, which is maybe the main reason for clear pattern.

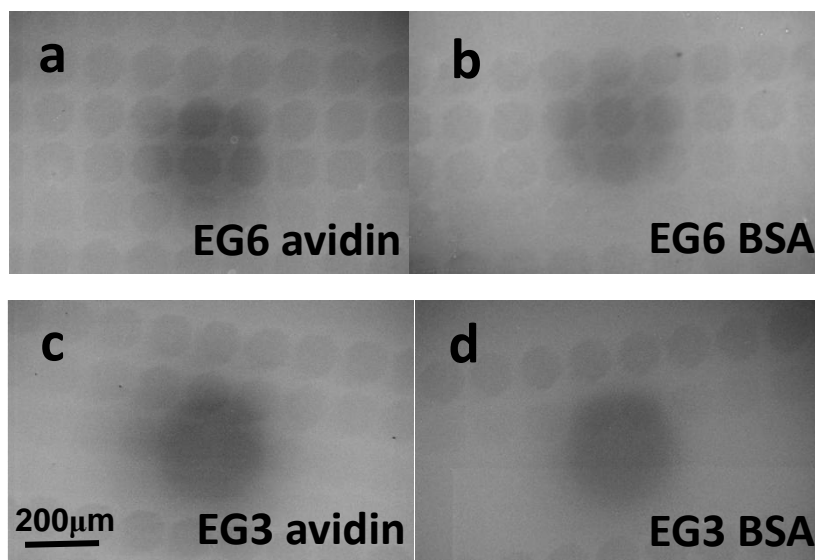


Figure 4.30 Protein patterns prepared by a combination of UVPER lithography and free-catalyst click reaction (series 1), a) EG6/C12N3-biotin template, exposure to avidin, b) EG6/C12N3-biotin template, exposure to BSA, c) EG3/C12N3-biotin template, exposure to avidin, d) EG3/C12N3-biotin template, exposure to BSA.

Because the pattern is not clear enough, I use larger dose (series 2) to get new pattern. In series 2, with higher dose, pattern are much more clearer but BSA also have much adsorption. Comparing 4.31a and 4.31c, we can see that EG6 is also clearer than EG3, this is because of the same reason that EG3 at 0 J/cm² have more adsorption.

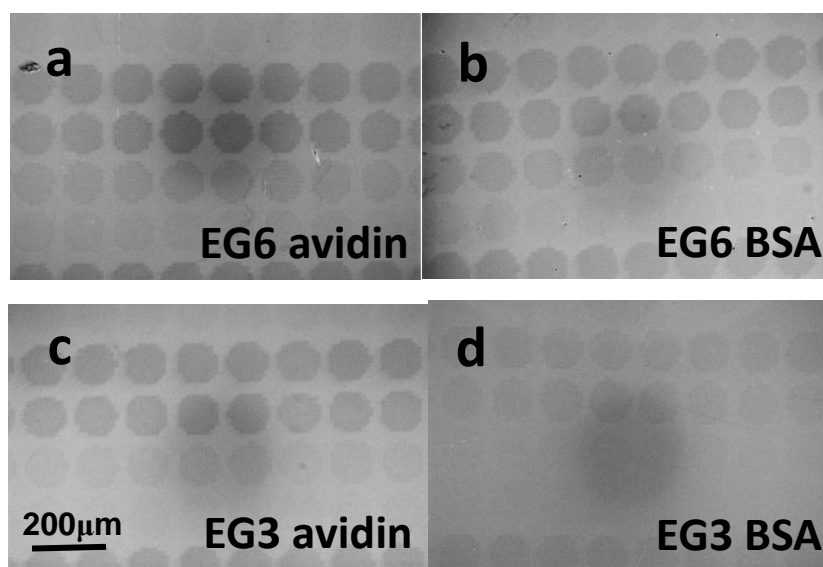


Figure 4.31 Protein patterns prepared by a combination of UVPER lithography and free-catalyst click reaction (series 2), a) EG6/C12N3-biotin template, exposure to avidin, b) EG6/C12N3-biotin template, exposure to BSA, c) EG3/C12N3-biotin template, exposure to avidin, d) EG3/C12N3-biotin template, exposure to BSA.

Maybe in BPA molecular, because of non-specific adsorption, the cyclo-alkynyl part with phenyl group can absorb more protein, and have more steric hindrance. For this reason, I used another molecular DBPB, with same alkynyl group as before. It can more easy to click, but need Cu^+ as catalyst.

4.3.3.4 Protein adsorption on catalyst clicked SAMs: XPS

In this part, I just compare catalyst clicked mixed $\text{EG}_n/\text{C12N3}$ SAMs immersing into BSA and avidin (0 J and 411 J/cm^2). In Figure 4.32, we can know that when the dose is 0 J/cm^2 , the intensity of N 1s peak of BSA and avidin are almost same and stay at a very low level; when the dose is 411 J/cm^2 , the sample in BSA do not have a obvious increase but the peak of sample in avidin increases much more than BSA.

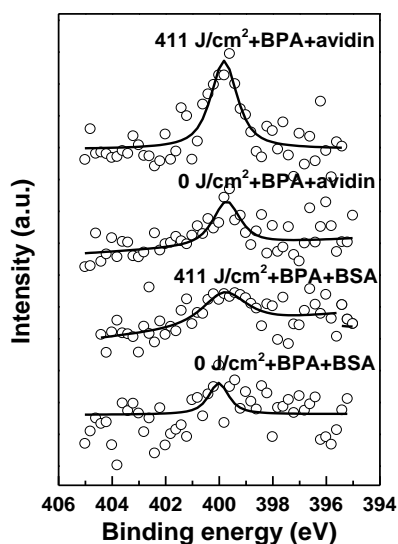


Figure 4.32 N 1s XPS spectra of the mixed EGn/C12N3 SAMs after the click reaction with BPA and exposure to BSA and avidin (UVPER with 0 J/cm² and 411 J/cm²).

4.3.3.5 Protein adsorption on catalyst clicked SAMs: lithography

Firstly, I use series 1 to do the research. Comparing a and b, we can see that avidin is much clearer than BSA, that is a good proof of specific protein adsorption; comparing a and c, we can see that EG6 is clearer than EG3, this is because EG3 at 0 J/cm² have more adsorption, which is maybe the main reason for clear pattern.

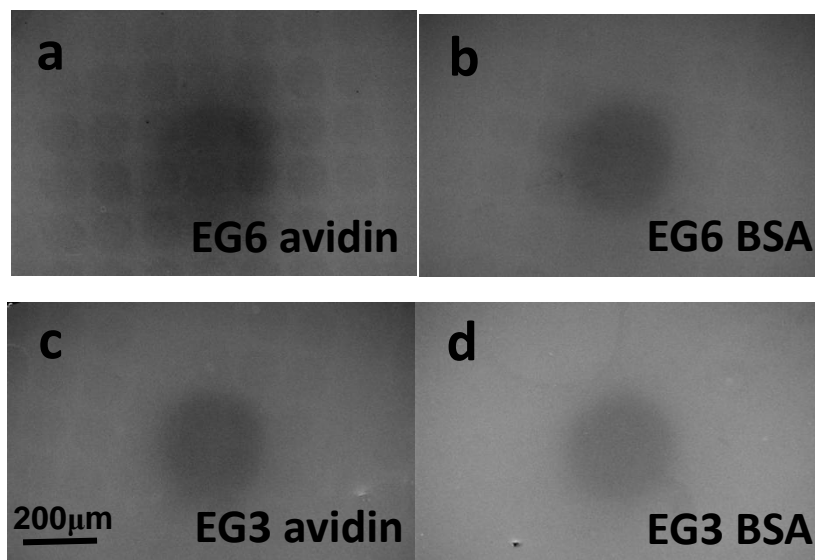


Figure 4.33 Protein patterns prepared by a combination of UVPER lithography and catalyst click reaction (series 1), a) EG6/C12N3-biotin template, exposure to avidin, b) EG6/C12N3-biotin template, exposure to BSA, c) EG3/C12N3-biotin template, exposure to avidin, d) EG3/C12N3-biotin template, exposure to BSA.

Comparing free-catalyst protein adsorption, the packing density of catalyst is more. For this reason, the specific protein adsorption can be conducted very well. Because the pattern is not clear enough, we use larger dose (series 2) to get new pattern.

In series 2, with higher dose, pattern are much more clearer but BSA also have much adsorption. Comparing e and g, we can see that EG6 is also clearer than EG3, this is because of the same reason that EG3 at 0 J/cm² have more adsorption.

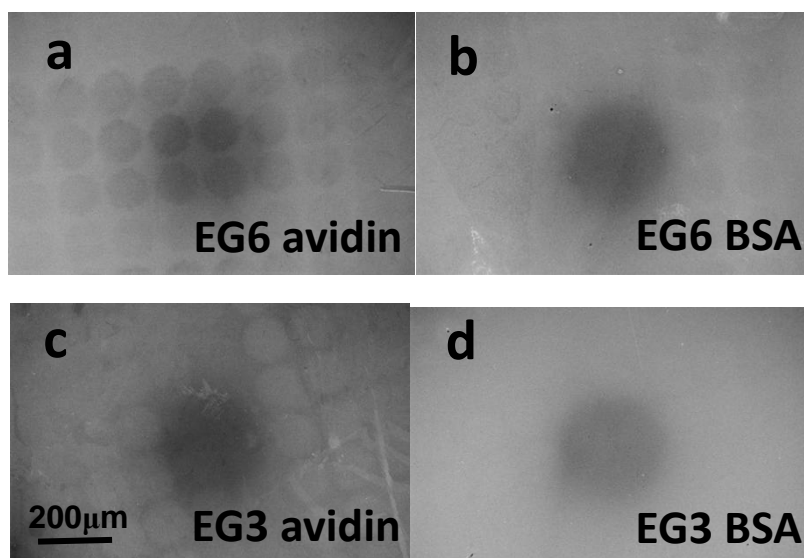


Figure 4.34 Protein patterns prepared by a combination of UVPER lithography and catalyst click reaction (series 2), a) EG6/C12N3-biotin template, exposure to avidin, b) EG6/C12N3-biotin template, exposure to BSA, c) EG3/C12N3-biotin template, exposure to avidin, d) EG3/C12N3-biotin template, exposure to BSA.

4.4 Modification of PEG nanomembranes by UV light

Specifically designed macromolecular membranes have potentials for biomedical and biological research as well as for various of practical applications such as medical diagnostics, sensor fabrication and therapy. Poly(ethylene glycols) (PEGs), which belong to biocompatible hydrogel membranes, have attracted more and more attention for the flexibility and many potentially properties^{106,122} including non-fouling behaviour, biocompatibility, non-toxicity, transparency and high optical quality. PEGs have various of possible applications, such as design of fabrication of model immunoprotective barriers for cell research,^{116,121} optical sensors,¹¹⁹ preparation of biofunctionalized microchannels for dynamic cell adhesion studies,¹²⁰ storage and controlled release of drugs, and protein affinity experiments.^{106,109,116,122}

Because of degree of cross-linking, PEG membranes can adsorb a significant amounts of water, which is mainly because of its spongy swelling.¹²⁰ Above all the biocompatibility, PEG membrane can be transferred to a particular object as far as it can be stably prepared. Such stably membrane can be fabricated by immobilizing PEG chains chemically on the substrate. On the other hand, one can use surface initiated polymerization (SIP) which regarded as “grafting-from” method to prepare reasonably dense PEG membranes of variable thickness.^{121,122} In this part, I present a relatively simple, novel and versatile method to prepare biocompatible PEG membranes on Au substrates. The main method is to mix two complementary components and polymerize spontaneously at a properly temperature. The functionalized STAR-branched PEGs I used are shown in Figure 7.1. This design can guarantee a high cross-linking degree, for this reason, the films remained stable on arbitrary, non-functionalized, substrates even after ultrasonication, and in future they have potential to process into free-standing membranes.¹²³

M. Zharnikov’s group have studied the modification of PEG membranes with electron irradiation and the effects on the wetting properties, chemical composition, the swelling behavior and protein-repelling properties of the PEG films are analyzed in detail. They demonstrated that electron irradiation can result in significant chemical modification and partial desorption of the PEG material. In our experiment, 254 nm UV light instead of electron irradiation is used as an irradiation method, chemical composition and swelling behavior are studied in our research.

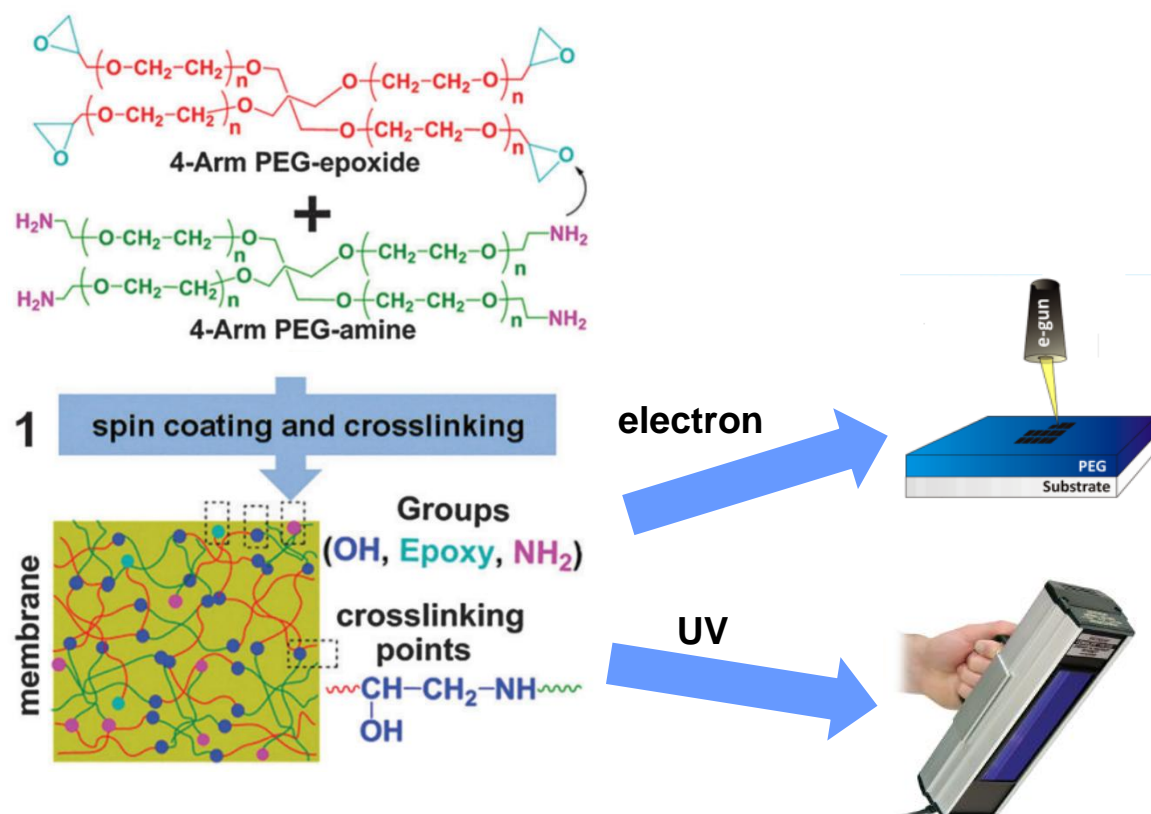


Figure 4.35 Fabrication of the PEG membranes and their subsequent modification.

4.4.1 UV irradiated membranes: XPS

Firstly, I use a lower flux of 0.5 mW/cm^2 , and irradiated the PEG membrane for various of time ranging from 0 h to 8 h. The results are shown below:

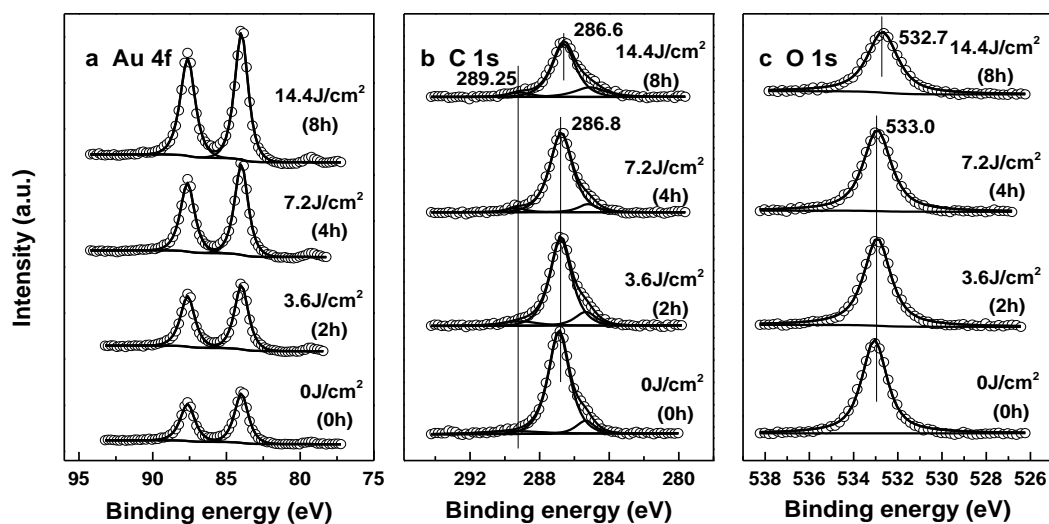


Figure 4.36 Au 4f (a), C 1s (b), O 1s (c) XPS spectra of pristine and UV irradiated PEG membranes. The UV doses are marked at the respective spectra. The UV flux was 0.5 mW/cm^2 .

In the Figure 4.36a, we can see that Au signal intensity increases with dose increasing, but the increase is not too rapid. That means there is material loss because of the UV irradiation. According to the equation:^{123,124}

$$I = I_{\infty} \exp\left(-\frac{d}{\lambda \cos\theta}\right), \quad (10)$$

when the thickness of membrane d decreased, the intensity of Au signal increased. For this reason, I can get a relationship between thickness and intensity. In Figure 4.36b, the C 1s spectra, from 0 J/cm^2 to 7.2 J/cm^2 , does not have obvious change and only at higher binding energy 289.25 eV , there is a very little peak appearing, which represents oxidized C atoms. But when the dose is 14.4 J/cm^2 , the peak at 289.25 eV become larger, and the peak at 286.6 eV which means C atoms in the EGN group decreased, so I can say that UV irradiation can damage the whole EGN parts. When the thickness is rather small, the gold substrate maybe have effect on the signal change. The results of oxygen can correspond to the C 1s results.

Next I increase the flux to 2 mW/cm^2 , and irradiated time also ranged from 0 h to 8 h . The results are shown in Figure 4.37:

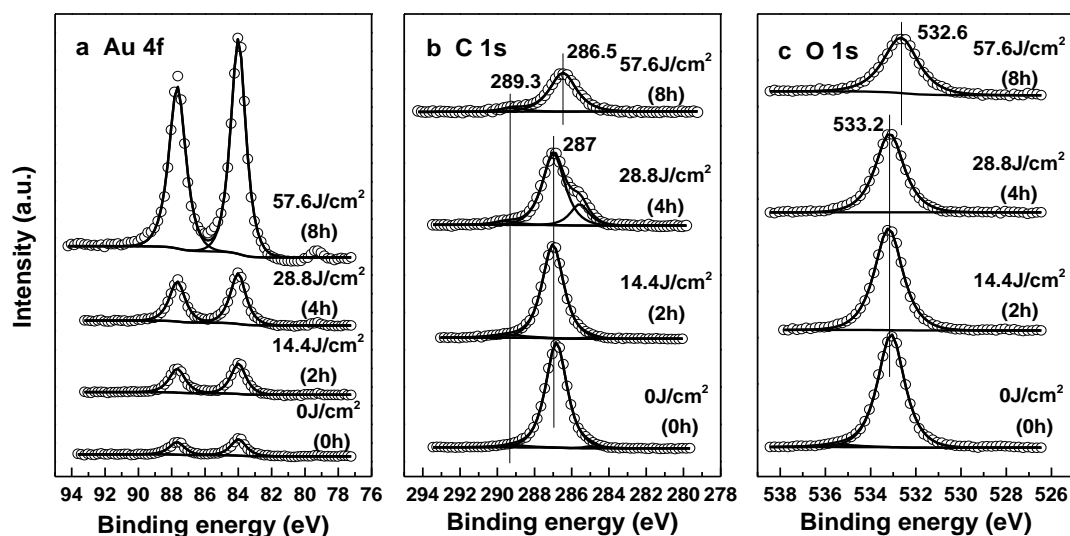


Figure 4.37 Au 4f (a), C 1s (b), O 1s (c) XPS spectra of pristine and UV irradiated PEG membranes. The UV doses are marked at the respective spectra. The UV flux was 2 mW/cm^2 .

In the Figure 4.37a, we can see that the dose range from 0 J/cm^2 to 57.6 J/cm^2 . Au signal intensity increases much more, which can well relate to the irradiation dose. When the total dose is more, the thickness decrease more. In Figure 4.37b, when the dose increase to 14.4 J/cm^2 , the C 1s does not have much difference, which is not same to before results, but when the dose increase to 57.6 J/cm^2 , the spectra have the

Results and discussion

similar situation as 14.4 J/cm^2 (0.5 mW/cm^2), which is also 8 h irradiation. This results can be explain that the change of component can be effect by either dose or irradiation time. The UV light can just damage the whole EGn part but can not reduce the -C-O- to -C-C- group, which is very different from the E-beam irradiation. The E-beam irradiation can reduce the C 1s peak at 286.5 eV to 284.6 eV, which represents the -C-C- group. The results of O 1s is also similar to before.¹²³

I use blank membrane intensity as a reference to plot C 1s, O 1s, Au 4f intensity shown in Figure 4.38.

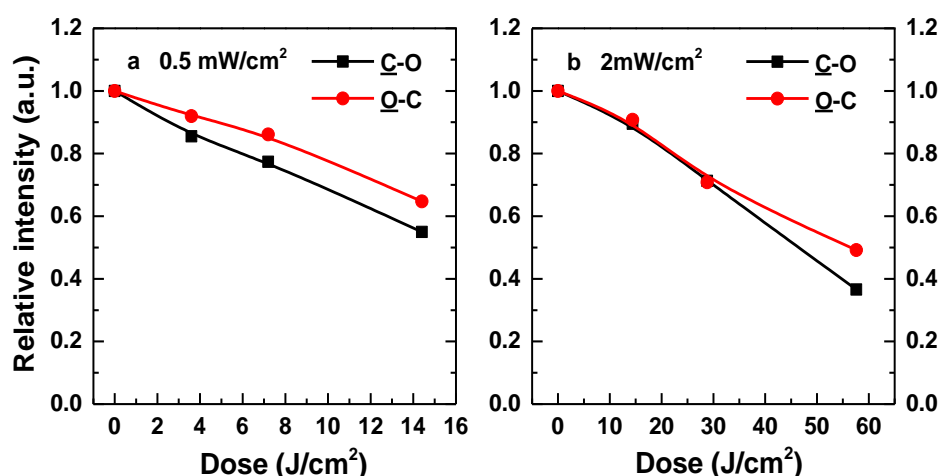


Figure 4.38 Intensities of the specific peaks in the C 1s and O 1s XPS spectra of irradiated PEG membranes as compared to the pristine ones. The flux of UV light was kept at either 0.5 mW/cm^2 (a) or 2 mW/cm^2 (b).

From Figure 4.38 we can see that in each flux the intensity of C 1s and O 1s decrease at a similar speed. Comparing the two kinds of flux, when the dose was 14.4 J/cm^2 , the portion of 0.5 mW/cm^2 was around 0.6, and the portion of 2 mW/cm^2 was about 0.88. When the irradiation time is 8 h, the portion of 0.5 mW/cm^2 is around 0.6, and the portion of 2 mW/cm^2 is about 0.4. From this result, I can conclude that both irradiation flux and irradiation time have effect on the damage.^{125,126}

From the Au XPS signal shown in Figure 4.39, we can see in the two kinds of flux, with the dose increasing, the intensity increase with a similar speed. The relationship between relatively ratio and dose is almost a exponential fitting.¹²⁷

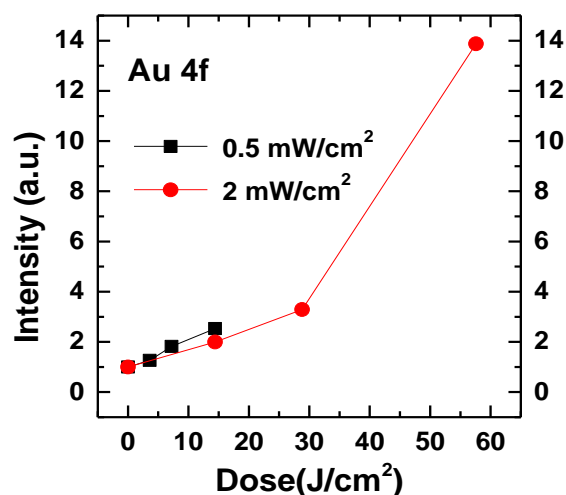


Figure 4.39 Intensity of the Au 4f XPS signal for UV irradiated PEG membranes comparing to the pristine membranes plotted as a function of UV dose. The flux of UV light was kept at either 0.5 mW/cm² (square, black line) or 2 mW/cm² (circle, red line), respectively.

In the end, I repeat this experiment with a higher flux, 3 mW/cm², the results are shown in Figure 4.40. With the dose increasing, the main peak representing the C atoms in EGN group, and there is no obvious increase of C atoms in C-C group, but peak of oxidized C atoms at 289.1 eV has a clearer increase. All of these results can fit our expect very well. I also plotted a curve of intensity against irradiation dose, the main peak intensity decrease gradually.

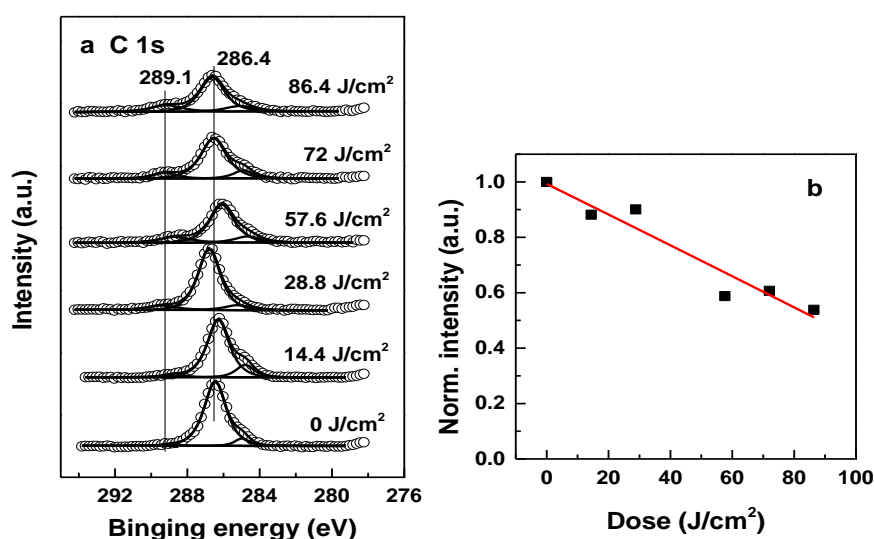


Figure 4.40 a) C1s XPS spectra of the pristine and UV irradiated PEG membranes at different doses, b) Normalized intensity of the C1s XPS peak at 286.4 eV as a function of UV dose.

4.4.2 Swelling properties of UV irradiated membranes: Ellipsometry

I used two kinds of methods to character the swelling properties. Firstly, I use a special holder with a cover, N₂ gas get trough water and blow into the holder from one side and out from the other side. By controlling the blowing speed of N₂, I can control the humidity on the PEG surface. Because of the limitation of the set up, the humidity can just range from 5% to 80%. For this reason, the swelling ratio equals thickness (80%)/thickness (5%), it is conducted in room temperature. Secondly, I put the substrate on a peltier plate without a cover, so I can control the swelling properties by controlling the temperature of the substrate. When the temperature decreased to 13 °C, there are many water drops appearing on the surface, so I can consider that at that time, the humidity on the surface is 100%, and when the temperature is above 30 °C, the thickness has almost no decrease. In this situation, the swelling ratio equals thickness (13 °C)/thickness (30 °C).

4.4.2.1 Swelling properties at humidity variation

When using the wetting N₂ to change the humidity on the surface, the thickness is measured by ellipsometry setup. The results are shown in Figure 4.41.

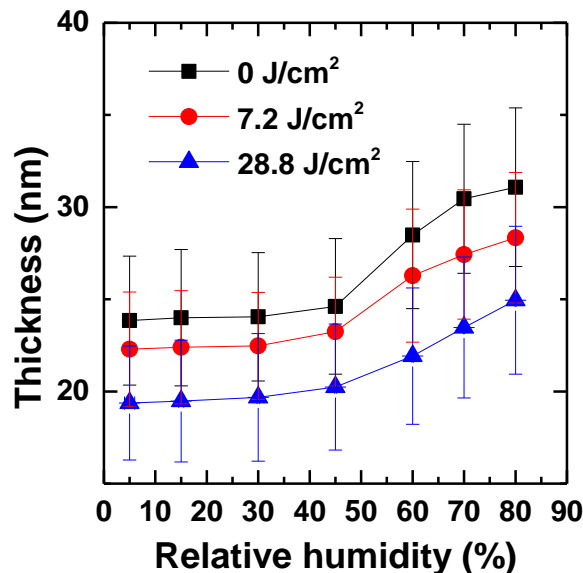


Figure 4.41 Thickness of the pristine and UV treated PEG membranes as a function of relative humidity.

Because of the limitation of the system, the error bar is a little bit larger, but the error is stable, so it can be used. When the humidity is below 40%, the thickness did not change very much; with the humidity increasing, the thickness have a rapid increase. For example, in the blank membrane, the thickness range from 24 nm to 31 nm. If the

humidity can reach 100%, the thickness can have a little increase, but from the tendency of the curve, the increase will be not large. Using the equation I showed before:

$$\text{Swelling ratio} = \frac{\text{thickness (80\%)}}{\text{thickness (5\%)}} \quad (11)$$

I got a curve of swelling ratio against UV dose, in this graph, we can see that when the dose is below 28.8 J/cm^2 , the swelling ratio stay almost at the same level, about 1.3, but this results is a little lower than other people's research. This is mainly because I can not make sure the humidity on the surface is same to the wetting N_2 and can not reach the 100% humidity, but it can be considered as a reference. In Figure 4.42b, I plotted at room humidity (45%), the thickness against UV dose. This curve looks like almost a straight line, which means there is just a degradation of PEG membrane but chemical change of the composition inside.

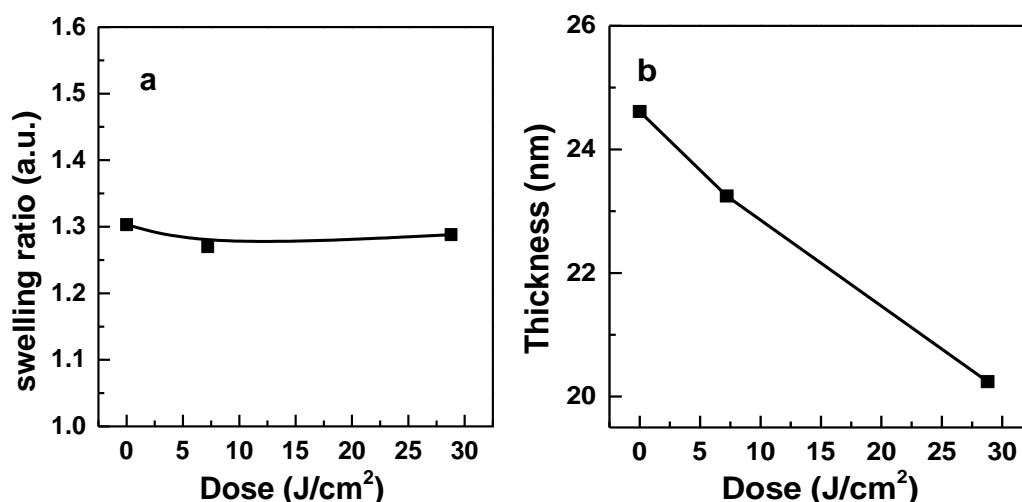


Figure 4.42 a) Swelling ratio of the membranes calculated from the data in Figure 4.41, b) thickness of irradiated membranes at the ambient humidity (45%) as a function of UV dose.

4.4.2.2 Swelling properties at temperature variation

Because of the limitation of last method, I use the second method to character the swelling properties. I used peltier plate to change the temperature. The data are presented below:

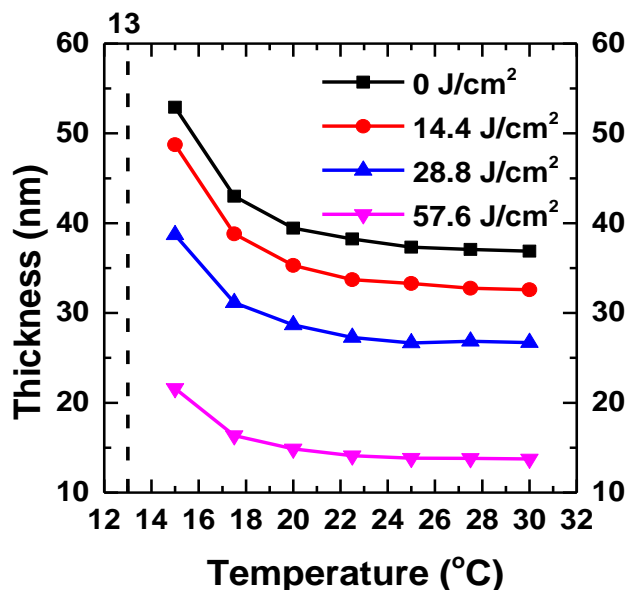


Figure 4.43 Thickness of the pristine and UV-treated (different doses) PEG membranes as a function of temperature.

When the temperature is above 25 °C, the thickness did not change significantly; with the temperature decreasing, the thickness has a rapid increase. For example, in the blank membrane, the thickness ranges from 37 nm (25 °C) to 31 nm (15 °C). When the temperature decreased to 13 °C, there is water appearing on the surface, that means the humidity is 100% on the surface but at that time, it is very hard to measure the thickness because of the effect of water. I can just measure thickness at 15 °C, and use the plots to linear an exponential curve, and then I can calculate the thickness at 13 °C. So I used this equation:

$$\text{Swelling ratio} = \frac{\text{thickness (13 °C)}}{\text{thickness (30 °C)}} \quad (12)$$

to get a curve of swelling ratio against UV dose, in this graph, we can see that when the dose is below 28.8 J/cm², the swelling ratio also stay at the same level, but this time the ratio is larger, ~2.0, which is better fit other people's research. When the dose is increasing to 57.6 J/cm², the ratio jumped to 2.3, which can be explained that when the thickness is small enough, the swelling properties should have some change not main because the structure and component inside the film but the huge change of thickness. In Figure 4.44b, I plotted the thickness against UV dose at room temperature (22.5 °C). This curve looks also like a straight line, which means there is just a degradation of PEG membrane but chemical change of the composition inside. The thickness have a significant decrease ranged from 38 nm to 14 nm.

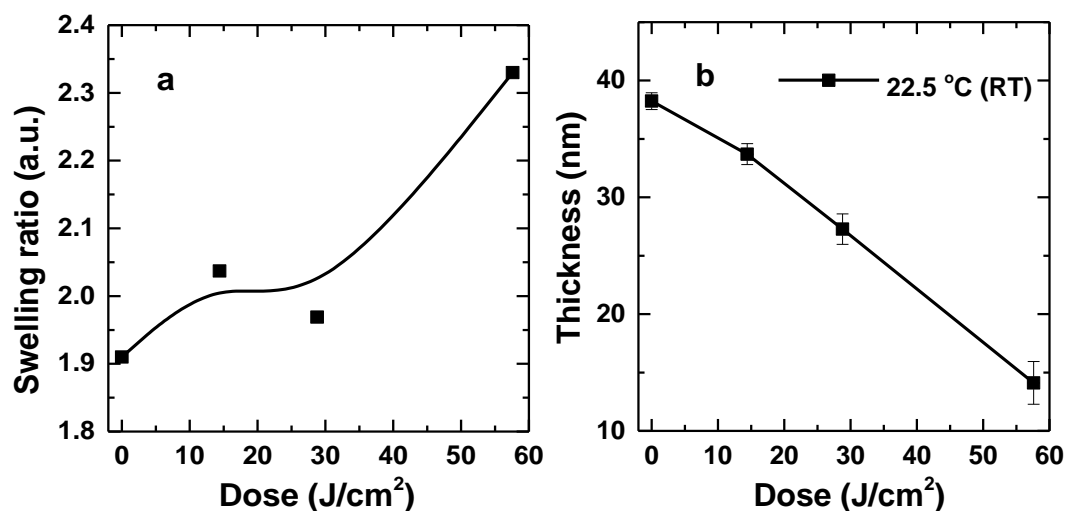


Figure 4.44 a) Swelling ratio of the PEG membranes calculated from the data in Figure 4.43, b) thickness of the UV irradiated membranes at room temperature as a function of UV dose.

The swelling experiments at humidity variation deliver partly different results in terms of the absolute value of the swelling ratio. I think however that the results of the temperatures experiment are more reliable since they agree better with the previous results of our group.^{61,128,129}

4.4.3 UV patterning of PEG membrane

In this part, I put a copper grid (grid size 1000 mesh \times 25 μ m pitch), which is shown as Figure 4.45, on the well-prepared PEG membrane. The flux is about 4 mW/cm² and the dose is 57.6 J/cm².

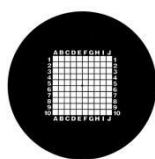


Figure 4.45 Copper grid used for UV patterning.

In the AFM setup, patterned surface under the camera is shown in Figure 4.46a. The pattern is big and clear enough to be seen with eyes. The horizontal line looks lighter and the vertical line is clearer. That maybe because there is a little difference in every copper grid but it will not have any effect on our results. Then the morphology of the surface are measured, which is shown in Figure 4.46b. We can see clearly there are several grid similar to observed with eyes. In Figure 4.46b, along the light line, I identify the height change of pattern and the result is shown in Figure 4.46. There is gap of about 17nm from the top to the bottom of the pattern, and this result can match

Results and discussion

well the results got from Figure 4.43.

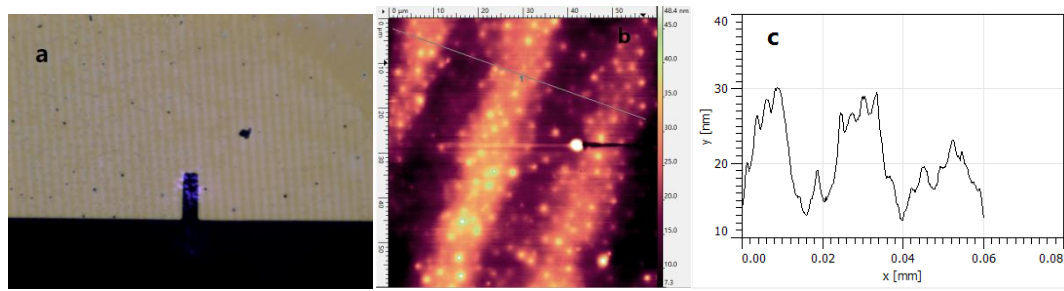


Figure 4.46 a) Optical image of a patterned membrane, b) AFM image of the pattern, c) the height profile along the white line in panel (b).

5. Conclusions and outlook

This thesis is devoted to use of UV light for controlled modification and patterning of organic and biological surfaces. First, I studied the effect of UV light irradiation at three different wavelengths (254, 312, and 375 nm) on non-substituted AT (C12) SAMs, which is of basic importance for the understanding of the respective processes. These experiments also helped me to optimize the parameters of the UV promoted exchange reaction (UVPER) in my subsequent studies. For this purpose, XPS and contact angle goniometry, in combination with UVPER (a COOH-bearing substituent), were applied. The cross-sections for both general impact of the UV light on the DDT SAMs and photooxidation of the SAM-substrate interface were estimated and found to decrease strongly with increasing wavelength of UV light.

Within the further studies, I investigated and demonstrated the possibility of UVPER between the primary AT SAM templates and an azide-bearing substituent (C12N3), capable of subsequent click reaction with ethynyl-bearing species. As primary matrix I used either the non-substituted (C12) or OEG-substituted (EG3 and EG6) AT SAMs, targeting mixed SAMs of chemical and biological significance. To demonstrate the flexibility of the approach I used UV light with two different wavelengths, viz. 254 nm and 375 nm, applying it to the non-substituted and OEG-substituted AT SAMs, respectively. Individual steps of the experimental procedure were monitored by contact angle goniometry, XPS, and NEXAFS spectroscopy.

In all cases, I was able to vary the portion of the C12N3 moieties in the mixed C12/C12N3 and EGn/C12N3 monolayers by selection of a suitable UV dose within the UVPER procedure. This portion could be varied from 10-20% to 90% in the case of the C12 template and from 0-10% to 40-70% in the cases of the EG3 and EG6 templates. The surface density of the chemically active azide groups embedded in the non-reactive primary matrix could be varied accordingly, as demonstrated by the subsequent click reaction between the C12/C12N3 templates and EFB as well as by the catalyst-mediated and catalyst-free click reactions between the EGn/C12N3 templates and BPA and DBPB, respectively. The latter reactions resulted in the preparation of templates for specific protein adsorption, comprising biotin-bearing moieties embedded in the protein-repelling EGn matrix. The density of the biotin receptors was varied according to the density of the C12N3 moieties in the EGn/C12N3 films, i.e. directly controlled by the UV dose within the UVPER procedure. The templates exhibited much higher affinity to the specific protein (avidin) as compared to a non-specific one (BSA). The surface density of the specifically

Conclusions and outlook

bound proteins could be varied in accordance with the density of the biotin receptors, i.e. could be directly controlled by the UV dose within the UVPER procedure. The entire approach was extended to lithography, relying on a commercial maskless UV lithography setup. Representative gradient patterns of specifically attached proteins in the protein-repelling EGN matrix were fabricated.

Note that the procedures described in this study are not limited to the representative moieties (EFB, DBPB and BPA) used for the click reaction in the given case but generally applicable to a broad variety of functional molecules bearing a suitable group for the click reaction with azide moiety. Also, the combination of these procedures with lithography can be performed in different fashions, relying on particular lithographic setups. Significantly, the fabrication of both mixed SAMs and the related lithographic patterns can be performed in a broad range of wavelengths, as demonstrated by utilizing UV light with wavelengths of 254 and 375 nm.

Within a further closely related subproject, UV light was applied to the modification of PEG films and membranes. These films and membranes were fabricated by thermoactivated, intermolecular cross-linking of epoxy and aminoterminated STAR-PEGs following a procedure developed earlier in our group. As shown by the experiments, UV irradiation on PEG films leads to significant material loss but no noticeable composition change, so that the UV-modified membranes maintain their hydrogel properties. This is in a drastic contrast to the case of electron irradiation where the hydrogel character of the membranes is strongly affected by electron irradiation. This opens new possibilities for nanoengineering and lithography, resulting in 3D patterned PEG films and membranes with the overall hydrogel character. It can be assumed that the biorepelling properties of the PEG films and membranes are still retained upon UV light treatment but this should be proved along with dedicated UV lithography experiments resulting in high quality patterns.

Bibliography

- 1 A. Ulman, Formation and Structure of Self-Assembled Monolayers. *Chem. Rev.* 1996, **96**, 1533-1554.
- 2 F. Schreiber, Self-Assembled Monolayers: From 'Simple' Model Systems to Biofunctionalized Interfaces. *J. Phys.: Condens. Matter* 2004, **16**, R881-R900.
- 3 J. C. Love; L. A. Estroff; J. K. Kriebel; R. G. Nuzzo; G. M. Whitesides, Self-Assembled Monolayers of Thiolates on Metals as a Form of Nanotechnology. *Chem. Rev.* 2005, **105**, 1103-1169.
- 4 N. Ballav; A. Shaporenko; A. Terfort; M. Zharnikov, A Flexible Approach to the Fabrication of Chemical Gradients. *Adv. Mat.* 2007, **19**, 998-1000.
- 5 N. Ballav; A. Shaporenko; S. Krakert; A. Terfort; M. Zharnikov, Tuning the Exchange Reaction Between a Self-Assembled Monolayer and Potential Substituents by Electron Irradiation. *J. Phys. Chem. C* 2007, **111**, 7772-7782.
- 6 Y. L. Jeyachandran; A. Terfort; M. Zharnikov, Controlled Modification of Protein-Repelling Self-Assembled Monolayers by Ultraviolet Light: The Effect of the Wavelength. *J. Phys. Chem. C* 2012, **116**, 9019-9028.
- 7 Y. L. Jeyachandran; M. Zharnikov, A Comprehensive Analysis of the Effect of Electron Irradiation on Oligo(Ethylene Glycol) Terminated Self-Assembled Monolayers Applicable for Specific and Non-Specific Patterning of Proteins. *J. Phys. Chem. C* 2012, **116**, 14950-14959.
- 8 N. Ballav; S. Schilp; M. Zharnikov, Electron Beam Chemical Lithography with Aliphatic Self-Assembled Monolayers. *Ang. Chem. Int. Ed.* 2008, **47**, 1421-1424.
- 9 M. N. Khan; V. Tjong; A. Chilkoti; M. Zharnikov, Fabrication of ssDNA/Oligo(Ethylene Glycol) Monolayers and Complex Nanostructures by an Irradiation-Promoted Exchange Reaction. *Angew. Chem. Int. Ed.* 2012, **51**, 10303-10306.
- 10 Y. L. Jeyachandran; T. Weber; A. Terfort; M. Zharnikov, Application of Long Wavelength Ultraviolet Radiation for Modification and Patterning of Protein-Repelling Monolayers. *J. Phys. Chem. C* 2013, **117**, 5824-5830.
- 11 Y. L. Jeyachandran; N. Meyerbröcker; A. Terfort; M. Zharnikov, Maskless Ultraviolet Projection Lithography with a Biorepelling Monomolecular Resist. *J. Phys. Chem. C* 2015, **119**, 494-501.

Bibliography

12 T. Weber; N. Meyerbröker; N. Khan Hira; M. Zharnikov; A. Terfort, UV-mediated Tuning of Surface Biorepulsivity in Aqueous Environment. *Chem. Comm.* 2014, **50**, 4325-4327.

13 V. V. Rostovtsev; L. G. Green; V. V. Fokin; K. B. Sharpless, A Stepwise Huisgen Cycloaddition Process: Copper(I)-Catalyzed Regioselective “Ligation” of Azides and Terminal Alkynes. *Angew. Chem. Int. Ed.* 2002, **41**, 2596-2599.

14 J. F. Lutz, 1,3-dipolar Cycloadditions of Azides and Alkynes: A Universal Ligation Tool in Polymer and Materials Science. *Angew. Chem. Int. Ed.* 2007, **46**, 1018-1025.

15 R. Chelmowski; D. Käfer; S.D. Köster; T. Klasen; T. Winkler; A. Terfort; N. Metzler-Nolte; C. Wöll, Postformation Modification of SAMs: Using Click Chemistry to Functionalize Organic Surfaces. *Langmuir* 2009, **25**, 11480–11485.

16 C. O. Kappe; E. Van der Eycken, Click Chemistry Under Non-Classical Reaction Conditions. *Chem. Soc. Rev.* 2010, **39**, 1280-1290.

17 C. P. Grodeman; E. S. Simon; K. L. Prime; G. M. Whitesides, Formation of self-assembled monolayers by chemisorption of derivatives of oligo(ethylene glycol) of structure HS(CH₂)₁₁(OCH₂CH₂)_mOH on gold. *J. Am. Chem. Soc.* 1991, **113**, 12-20.

18 K. L. Prime; G. M. Whitesides, Adsorption of Proteins onto Surfaces Containing End-Attached Oligo(Ethylene Oxide): a Model System Using Self-Assembled Monolayers. *J. Am. Chem. Soc.* 1993, **115**, 10714-10721.

19 P. Harder; M. Grunze; R. Dahint; G. M. Whitesides; P. E. Laibinis, Molecular Conformation in Oligo(ethylene glycol)-Terminated Self-Assembled Monolayers on Gold and Silver Surfaces Determines Their Ability To Resist Protein Adsorption. *J. Phys. Chem. B* 1998, **102**, 426-436.

20 J. Benesch; S. Svedhem; S. C. T. Svensson; R. Valiokas; B. Liedberg; P. Tengvall, Protein Adsorption to Oligo(Ethylene Glycol) Self-Assembled Monolayers: Experiments with Fibrinogen, Heparinized Plasma, and Serum. *J. Biomater. Sci. Polym. Ed.* 2001, **12**, 581.

21 S. Herrwerth; W. Eck; S. Reinhardt; M. Grunze, Factors that Determine the Protein Resistance of Oligoether Self-Assembled Monolayers—Internal Hydrophilicity, Terminal Hydrophilicity, and Lateral Packing Density. *J. Am. Chem. Soc.* 2003, **125**, 9359-9366.

22 A. Rosenhahn; S. Schilp; J. Kreuzer; M. Grunze, The Role of “Inert” Surface Chemistry in Marine Biofouling Prevention. *Phys. Chem. Chem. Phys.* 2010, **12**, 4275.

23 M. Montague; R. E. Ducker; K. S. L. Chong; R. J. Manning; F. J. M. Rutten; M. C. Davies; G. J. Leggett, Fabrication of Biomolecular Nanostructures by Scanning Near-Field

Photolithography of Oligo(ethylene glycol)-Terminated Self-Assembled Monolayers. *Langmuir* 2007, **23**, 7328-7337.

24 R. E. Ducker; S. Janusz; S. Sun; G. J. Leggett, One-Step Photochemical Introduction of Nanopatterned Protein-Binding Functionalities to Oligo(ethylene glycol)-Terminated Self-Assembled Monolayers. *J. Am. Chem. Soc.* 2007, **129**, 14842-14843.

25 N. Ballav; H. Thomas; T. Winkler; A. Terfort; M. Zharnikov, Making Protein Patterns by Writing in a Protein-Repelling Matrix. *Angew. Chem. Int. Ed.* 2009, **48**, 5833-5836.

26 J. Adams; G. Tizazu; S. Janusz; S. R. J. Brueck; G. P. Lopez; G. J. Leggett, Large-Area Nanopatterning of Self-Assembled Monolayers of Alkanethiolates by Interferometric Lithography. *Langmuir* 2010, **26**, 13600-13606.

27 L. M. Weber; C. G. Lopez; K. S. Anseth, Effects of PEG Hydrogel Crosslinking Density on Protein Diffusion and Encapsulated Islet Survival and Function. *J. Biomed. Res.* 2009, **90**, 720-729.

28 A. Mateescu; Y. Wang; J. Dostalek; U. Jonas, Thin Hydrogel Films for Optical Biosensor Applications. *Membranes* 2012, **2**, 40-69.

29 T. Hussain; N. M. Ranjha; Y. Shahzad, Swelling and Controlled Release of Tramadol Hydrochloride from a pH-Sensitive Hydrogel. *Des. Monomers Polym.* 2011, **14**, 233-249.

30 J. Park; A. N. Vo; D. Barriet; Y. Shon; T. Randall Lee, Systematic Control of the Packing Density of Self-Assembled Monolayers Using Bidentate and Tridentate Chelating Alkanethiols. *Langmuir* 2005, **21**, 2902-2911

31 M. N. Khan; M. Zharnikov, Irradiation Promoted Exchange Reaction with Disulfide Substituents. *J. Phys. Chem. C* 2013, **117**, 14534-14543.

32 S. Krakert; N. Ballav; M. Zharnikov; A. Terfort, Adjustment of the Bioresistivity by Electron Irradiation: Self-assembled Monolayers of Oligo (Ethylene Glycol)-Terminated Alkanethiols with Embedded Cleavable Group. *Phys. Chem. Chem. Phys.* 2010,**12**, 507-515.

33 G. E. Poirier; E. D. Pylant, The Self-Assembly Mechanism of Alkanethiols on Au(111). *Science (Washington, D.C.)* 1996, **272**, 1145.

34 L. H. Dubois; R. G. Nuzzo, Synthesis, Structure, and Properties of Model Organic-Surfaces. *Annu. Rev. Phys. Chem.* 1992, **43**, 437.

Bibliography

- 35 J. C. Love; D. B. Wolfe; R. Haasch; M. L. Chabiny; K. E. Paul; G. M. Whitesides; R. G., Nuzzo, Formation and Structure of Self-Assembled Monolayers of Alkanethiolates on Palladium. *J. Am. Chem. Soc.* 2003, **125**, 2597.
- 36 M. R. Shadnam; S. E. Kirkwood; R. Fedosejevs; A. Amirfazli, Direct Patterning of Self-Assembled Monolayers on Gold Using a Laser Beam. *Langmuir* 2004, **20**, 2667.
- 37 R. Klauser; I. H. Hong; S. C. Wang; M. Zharnikov; A. Paul; A. Goelzhaeuser; A. Terfort; T. J. Chuang, Imaging and Patterning of Monomolecular Resists by Zone-Plate-Focused X-ray Microprobe. *J. Phys. Chem. B* 2003, **107**, 13133.
- 38 W. Geyer; V. W. Stadler; Eck; A. Golzhauser; M. Grunze;. M. Sauer; T. Weimann; P. Hinze, *J. Vac. Sci. Technol. B* 2001,**19**, 2732.
- 39 T. Weimann; W. Geyer; P. Hinze; V. Stadler; W. Eck; A. Golzhauser, Nanoscale Patterning of Self-Assembled Monolayers Bye-Beam Lithography Microelectron. *Eng.* 2001, **903**, 57-58.
- 40 A. Golzhauser; W. Eck; W.Geyer; V. Stadler; T. Weimann; P. Hinze; M. Grunze, Chemical Nanolithography with Electron Beams. *Adv. Mater.* 2001, **13**, 806.
- 41 K. K. Berggren; A. Bard; J. L. Wilbur; J. D. Gillasp; A. G. Helg; J. J. McClelland; S. L. Rolston; W. D. Phillips; M. Prentiss; et al. Microlithography by Using Neutral Metastable Atoms and Self-Assembled Monolayers. *Science (Washington, D.C.)* 1995, **269**, 1255.
- 42 M. L. Chabiny; J. C. Love; J. H. Thywissen; F. Cervelli; M. G. Prentiss; G. M. Whitesides, Self-Assembled Monolayers Exposed to Metastable Argon Beams Undergo Thiol Exchange Reactions. *Langmuir* 2003, **19**, 2201.
- 43 The Ozone Layer Protects Humans From This. Lyman, T. (1914). "Victor Schumann". *Astrophysical Journal* 38: 1-4. Doi:10.1086/142050.
- 44 ISO 21348 Definitions of Solar Irradiance Spectral Categories
- 45 G. Korde; C. Vest. Stable Silicon Photodiodes for Absolute Intensity Measurements in the VUV and Soft X-ray Regions. *Jrnl of Elec. Spect. and Related Phenomena* 1996, **80**, 313-316.
- 46 F. Galeotti; A. Andicsova; F. Bertini; C. Botta, A Versatile Click-Grafting Approach to Surface Modification of Silk Fibroin Films. *J Mater Sci* 2013, **48**, 7004-7010.
- 47 S. Prakash; T. M. Long; J. C. Selby; J. S. Moore; M. A. Shannon, "Click" Modification of Silica Surfaces and Glass Microfluidic Channels. *Anal. Chem.* 2007, **79**, 1661-1667.

- 48 H. Qi; M. Li; R. Zhang; M. Dong; C. Ling, Double Electrochemical Covalent Coupling Method Based on Click Chemistry and Diazonium Chemistry for the Fabrication of Sensitive Amperometric Immunosensor. *Analytica Chimica Acta* 2013, **792**, 28-34.
- 49 D. Wasserberg; C. Nicosia; E. E. Tromp; V. Subramaniam; J. Huskens; P. Jonkheijm, Oriented Protein Immobilization Using Covalent and Noncovalent Chemistry on a Thiol-Reactive Self-Reporting Surface. *J. Am. Chem. Soc.* 2013, **135**, 3104-3111.
- 50 L. Hou; Y. Cui; M. Xu; Z. Gao; J. Huang; D. Tang, Graphene Oxide-Labeled Sandwich-Type Impedimetric Immunoassay with Sensitive Enhancement Based on Enzymatic 4-Chloro-1-Naphthol Oxidation. *Biosens. Bioelectron.* 2013, **47**, 149-156.
- 51 M. A. Seia; S.V. Pereira; C.A. Fontán; I.E.D. Vito; G.A. Messina; J. Raba, Laser-Induced Fluorescence Integrated in a Microfluidic Immunosensor for Quantification of Human Serum IgG Antibodies to Helicobacte Pylori. *Sens. Actuators B* 2012, **168**, 297-302.
- 52 N. Ballav; T. Weidner; M. Zharnikov, UV-Promoted Exchange Reaction as a Tool for Gradual Tuning the Composition of Binary Self-Assembled Monolayers and Chemical Lithography. *J. Phys. Chem. C* 2007, **111**, 12002-12010.
- 53 N. Ballav; T. Weidner; K. Rçfler; H. Lang; M. Zharnikov, A New Approach for the Fabrication of Strongly Heterogeneous Mixed Self-Assembled Monolayers. *ChemPhysChem* 2007, **8**, 819-822.
- 54 B. H. Clare; O. Guzman; J. J. de Pablo; N. L. Abbott, Measurement of the Azimuthal Anchoring Energy of Liquid Crystals in Contact with Oligo(ethylene glycol)-Terminated Self-Assembled Monolayers Supported on Obliquely Deposited Gold Films. *Langmuir* 2006, **22**, 4654-4659.
- 55 E. Darlatt; C. H.-H. Traulsen; J. Poppenberg; S. Richter; J. Kühn; C. A. Schalley; W. E.S. Unger, Evidence of Click and Coordination Reactions on a Self-Assembled Monolayer by Synchrotron Radiation Based XPS and NEXAFS. *Journal of Electron Spectroscopy and Related Phenomena* 2012, **185**, 85-89.
- 56 E. Darlatt; A. Nefedov; C. H.-H. Traulsen; J. Poppenberg; S. Richter; P. M. Dietrich; A. Lippitz; R. Illgen; J. Kühn; C. A. Schalley; C. Wödl; W. E.S. Unger, Interpretation of Experimental N K NEXAFS of Azide, 1,2,3-Triazole and Terpyridyl Groups by DFT Spectrum Simulations. *Journal of Electron Spectroscopy and Related Phenomena* 2012, **185**, 621-624.
- 57 S. Arumugam; V. V. Popik, Click Sequential “Click” – “Photo-Click” Cross-Linker for Catalyst-Free Ligation of Azide-Tagged Substrates. *J. Org. Chem.* 2014, **79**, 2702-2708.

Bibliography

- 58 J. M. Baskin; J. A. Prescher; S. T. Laughlin; N. J. Agard; P. V. Chang; I. A. Miller; A. Lo; J. A. Codelli; C. R. Bertozzi, Copper-Free Click Chemistry for Dynamic in Vivo Imaging. *National Academy of Sciences*, 2007, **104**, 16793-16797.
- 59 P. Kuhn; K. Eyer; T. Robinson; F. I. Schmidt; J. Mercerb; P. S. Dittrich, A Facile Protocol for the Immobilisation of Vesicles, Virus Particles, Bacteria, and Yeast Cells. *Integr. Biol.* 2012, **4**, 1550-1555.
- 60 N. Ballav; H. Thomas; T. Winkler; A. Terfort; M. Zharnikov, Making Protein Patterns by Writing in a Protein-Repelling Matrix. *Angew. Chem. Int. Ed.* 2009, **48**, 5833-5836.
- 61 N. Meyerbröcker; T. Kriesche; M. Zharnikov, Novel Ultrathin Poly(ethylene glycol) Films as Flexible Platform for Biological Applications and Plasmonics. *ACS Appl. Mater. Interfaces* 2013, **5**, 2641-2649.
- 62 N. Ballav; A. Terfort; M. Zharnikov, Fabrication of Mixed Self-Assembled Monolayers Designed for Avidin Immobilization by Irradiation Promoted Exchange Reaction. *Langmuir* 2009, **25**, 9189-9196.
- 63 Y. L. Jeyachandran; N. Meyerbroeker; A. Terfort; M. Zharnikov, Maskless Ultraviolet Projection Lithography with a Biorepelling Monomolecular Resist. *J. Phys. Chem. C.* 2015, **119**, 494-501.
- 64 D. Briggs; J. T. Grant, Surface Analysis by Auger and X-ray Photoelectron Spectroscopy. *IM Publications and Surface Spectra Limited* 2003.
- 65 D. Briggs; M. P. Seah. John Wiley and Sons Ltd, *Practical Surface Analysis (second edition)* 1990.
- 66 J. F. Moulder; W. F. Stickle; P. E. Sobol; K. D. Bomben, Handbook of X-ray Photoelectron Spectroscopy. *Physical Electronics Inc., Eden Prairie* 1995.
- 67 G. Beamson; D. Briggs; J. Wiley; S. Chichester, High Resolution XPS of Organic Polymers-The Scientia ESCA 300 Database 1992.
- 68 B. V. Crist, Handbooks of Monochromatic XPS Spectra, 5 Volume Series. *XPS International, Kawasaki* 1997.
- 69 C. R. Brundle; C. A. Evans; S. Wilson, Encyclopedia of Materials Characterization. *Butterworth-Heinemann* 1992.
- 70 N. Ideo; Y. Iijima; N. Niimura; M. Sigematsu; T. Tazawa; S. Matsumoto; K. Kojima; Y. Nagasawa, Handbook of X-ray Photoelectron Spectroscopy. *JEOL, Tokyo, Japan* 1991.

- 71 A. Bianconi, Surface X-ray Absorption Spectroscopy: Surface EXAFS and Surface XANES. *Appl. Surf. Sci.* 1980, **6**, 392-418.
- 72 A. Bianconi; M. Dell'Ariceia; P. J. Durham; J. B. Pendry, Multiple-Scattering Resonances and Structural Effects in the X-ray-Absorption Near-Edge Spectra of Fe II and Fe III Hexacyanide Complexes. *Phys. Rev. B* 1982, **26**, 6502-6508.
- 73 M. Benfatto; C. R. Natoli; A. Bianconi; J. Garcia; A. Marcelli; M. Fanfoni; I. Davoli, Multiple Scattering Regime and Higher Order Correlations in X-ray Absorption Spectra of Liquid Solutions. *Phys. Rev. B* 1986, **34**, 5774.
- 74 J. Stohr. Nexafs Spectroscopy (Springer Series in Surface Sciences).
- 75 H. Fujiwara; J. Wiley & Sons. Spectroscopic Ellipsometry: Principles and Applications, 2007.
- 76 H. Tompkins; E. A. Haber. Handbook of Ellipsometry. *William Andrew Publishing, NY*, 2005.
- 77 H. G. Tompkins; J. N. Hilfiker, Spectroscopic Ellipsometry: Practical Application to Thin Film Characterization. *Momentum Press* 2016.
- 78 M. Schubert, Infrared Ellipsometry on Semiconductor Layer Structures: Phonons, Plasmons, and Polaritons. *Springer Verlag* 2005.
- 79 J. Goldstein; Scanning Electron Microscopy and X-ray Microanalysis. *Kluwer Academic/Plenum Publishers* 2003, 689.
- 80 L. Reimer, Scanning Electron Microscopy : Physics of Image Formation and Microanalysis. *Springer* 1998, 527.
- 81 R. F. Egerton, Physical Principles of Electron Microscopy: an Introduction to TEM, SEM, and AEM. *Springer* 2005, 202.
- 82 A. R. Clarke, Microscopy Techniques for Materials Science. *CRC Press (electronic resource)* 2002.
- 83 Y. Yuan; T. R. Lee. Contact Angle and Wetting Properties.
- 84 A. Marmur, Thermodynamic Aspects of Contact Angle Hysteresis. *Advances in Colloid and Interface Science* 1994, **50**, 121.
- 85 I. Gao; T. J. McCarthy, Contact Angle Hysteresis Explained. *Langmuir* 2006, **22**, 6234.

Bibliography

86 A. Waldbaur; B. Waterkotte; K. Schmitz; B. E. Rapp, Maskless Projection Lithography for the Fast and Flexible Generation of Grayscale Protein Patterns. *Small* 2012, **8**, 1570-1578.

87 S. A. A. Ahmad; L.-S. Wong; E. ul-Haq; J. K. Hobbs; G. J. Leggett; J. Micklefield, Protein Micro- and Nanopatterning Using Aminosilanes with Protein-Resistant Photolabile Protecting Groups. *J. Am. Chem. Soc.* 2011, **133**, 2749-2759.

88 C. Olsen; P. A. Rowntree, Bond-Selective Dissociation of Alkanethiol Based Self-Assembled Monolayers Adsorbed on Gold Substrates, Using Low-Energy Electron Beams. *J. Chem. Phys.* 1998, **108**, 3750-3765.

89 M. Zharnikov; S. Frey; K. Heister; M. Grunze, Modification of Alkanethiolate Monolayers by Low Energy Electron Irradiation: Dependence on Substrate and on Length and Isotopic Composition of Alkyl Chains. *Langmuir* 2000, **16**, 2697-2705.

90 K. Heister; M. Zharnikov; M. Grunze; L. S. O. Johansson, Adsorption of Alkanethiols and Biphenylthiols on Au and Ag Substrates: A High-Resolution X-ray Photoelectron Spectroscopy Study. *J. Phys. Chem. B* 2001, **105**, 4058-4061.

91 A. Ulman, An Introduction to Ultrathin Organic Films: Langmuir-Blodgett to Self-Assembly. *Academic Press: New York* 1991.

92 N. Ballav; A. Shaporenko; S. Krakert; A. Terfort; M. Zharnikov, Tuning the Exchange Reaction Between a Self-Assembled Monolayer and Potential Substituents by Electron Irradiation. *J. Phys. Chem. C* 2007, **111**, 7772.

93 P. E., Laibinis; G. M. Whitesides, *J. Am. Chem. Soc.* 1992, **114**, 1990.

94 S. M. Flores; A. Shaporenko; C. Vavilala; H.-J. Butt; M. Schmittel; M. Zharnikov; R. Berger, Control of Surface Properties of Self-Assembled Monolayers by Tuning the Degree of Molecular Asymmetry. *Surf. Sci.* 2006, **600**, 2847.

95 A. B. D. Cassie, Contact Angles. Discuss. *Faraday Soc.* 1948, **3**, 11-16.

96 E.W. Wollman; D. Kang; C.D. Frisbie; I.M. Lorkovic; M.S. Wrighton, Photosensitive self-assembled monolayers on gold: Photochemistry of Surface-C Azide and Cyclopentadienylmanganese Tricarbonyl. *J. Am. Chem. Soc.* 1994, **116**, 4395-4404.

97 J. P. Collmann; N. K. Devaraj; T. P. A. Eberspacher; C. E. D. Chidsey, Mixed Azide-Terminated Monolayers: A Platform for Modifying Electrode Surface. *Langmuir* 2006, **22**, 2457-2464.

- 98 I. F. Gallardo; L. J. Webb, Tethering Hydrophobic Peptides to Functionalized Self-Assembled Monolayers on Gold through Two Chemical Linkers Using the Huisgen Cycloaddition. *Langmuir* 2010, **26**, 18959-18966.
- 99 E. Darlatt; C. H.-H. Traulsen; J. Poppenberg; S. Richter; J. Kühn; C. A. Schalley; W. E. S. Unger, Evidence of Click and Coordination Reactions on a Self-Assembled Monolayer by Synchrotron Radiation Based XPS and NEXAFS. *J. Electron Spectr. Relat. Phenom.* 2012, **185**, 85-89.
- 100 J. Stöhr, NEXAFS spectroscopy; *Springer-Verlag: Berlin*, 1992.
- 101 P. S. Bagus; K. Weiss; A. Schertel; Ch. Wöll; W. Braun; H. Hellwig; C. Jung, Identification of Transitions into Rydberg States in the X-ray Absorption Spectra of Condensed Long-Chain Alkanes. *Chem. Phys. Lett.* 1996, **248**, 129.
- 102 S. Frey; A. Shaporenko; M. Zharnikov; P. Harder; D. L. Allara, Self-Assembled Monolayers of Nitrile-Functionalized Alkanethiols on Gold and Silver Substrates. *J. Phys. Chem. B* 2003, **107**, 7716-7725.
- 103 Schreiber; F. Prog, Structure and Growth of Self-Assembling Monolayers. *Surf. Sci.* 2000, **65**, 151-256.
- 104 M. Zharnikov; M. Grunze, Spectroscopic Characterization of Thiol-Derived Self-Assembled Monolayers. *J. Phys. Condens. Matter.* 2001, **13**, 11333-11365.
- 105 E. Darlatt; A. Nefedov; C. H.-H. Traulsen; J. Poppenberg; S. Richter; P. M. Dietrich; A. Lippitz; R. Illgen; J. Kühn; C. A. Schalley; C. Wöll; W. E. S. Unger, Interpretation of Experimental N K NEXAFS of Azide, 1,2,3-Triazole and Terpyridyl Groups by DFT Spectrum Simulations. *J. Electron Spectr. Relat. Phenom.* 2012, **185**, 621-624.
- 106 J. Drelich; J. L. Wilbur; J. D. Miller; G. M. Whitesides, Contact Angles for Liquid Drops at a Model Heterogeneous Surface Consisting of Alternating and Parallel Hydrophobic/Hydrophilic Strips. *Langmuir* 1996, **12**, 1913-1922.
- 107 P. Harder; M. Grunze; R. Dahint; G. M. Whitesides; P. E. Laibinis, Molecular Conformation in Oligo(ethylene glycol)-Terminated Self-Assembled Monolayers on Gold and Silver Surfaces Determines Their Ability To Resist Protein Adsorption. *J. Phys. Chem. B* 1998, **102**, 426-436.
- 108 K. Feldman; G. Hähner; N. D. Spencer; P. Harder; M. Grunze, Probing Resistance to Protein Adsorption of Oligo(ethylene glycol)-Terminated Self-Assembled Monolayers by Scanning Force Microscopy. *J. Am. Chem. Soc.* 1999, **121**, 10134-10141

Bibliography

- 109 A. Larsson; T. Ekblad; O. Andersson; B. Liedberg, Photografted Poly(Ethylene Glycol) Matrix for Affinity Interaction Studies. *Biomacromolecules* 2007, **8**, 287-295.
- 110 A. Ulman; M. Ioffe; F. Patolsky; E. Haas; D. Reuvenov, Highly Active Engineered-Enzyme Oriented Monolayers: Formation, Characterization and Sensing Applications. *Journal of Nanobiotechnology* 2011, **9**, 26.
- 111 S. Krakert; N. Ballav; M. Zharnikov; A. Terfort, Adjustment of the Bioresistivity by Electron Irradiation: Self-Assembled Monolayers of Oligo(Ethylene Glycol)-Terminated Alkanethiols with Embedded Cleavable Group. *Phys. Chem. Chem. Phys.* 2010, **12**, 507–515.
- 112 P. Kuhn; K. Eyer; T. Robinson; F. I. Schmid; J. Mercerb; P. S. Dittrich, A Facile Protocol for the Immobilisation of Vesicles, Virus Particles, Bacteria, and Yeast Cells. *Integr. Biol.* 2012, **4**, 1550–1555.
- 113 N. Y. Wong; H. Xing; L. H. Tan; Y. Lu, Nano-Encrypted Morse Code: A Versatile Approach to Programmable and Reversible Nanoscale Assembly and Disassembly. *J. Am. Chem. Soc.* 2013, **135**, 2931–2934.
- 114 J. M. Baskin; J. A. Prescher; S. T. Laughlin; N. J. Agard; P. V. Chang; I. A. Miller; A. Lo; J. A. Codelli; C. R. Bertozzi, Copper-Free Click Chemistry for Dynamic in Vivo Imaging. *PNAS* 2007, **104**, 16793–16797.
- 115 P. T. Charles; V. R. Stubbs; C. M. Soto; B. D. Martin; B. J. White; C. R. Taitt, Reduction of Non-Specific Protein Adsorption Using Poly(Ethylene Glycol) (PEG) Modified Polyacrylate Hydrogels in Immunoassays for Staphylococcal Enterotoxin B detection. *Sensors* 2009, **9**, 645-655.
- 116 L. M. Weber; C. G. Lopez; K. S. Anseth, Effects of PEG Hydrogel Crosslinking Density on Protein Diffusion and Encapsulated Islet Survival and Function. *J. Biomed. Res.* 2009, **90**, 720-729.
- 117 F. Pippig; A. Holländer, Hydrogel Nanofilms for Biomedical Applications: Synthesis via Polycondensation Reactions. *Macromol. Biosci.* 2010, **10**, 1093-1105.
- 118 A. Mateescu; Y. Wang; J. Dostalek; U. Jonas, Thin Hydrogel Films for Optical Biosensor Applications. *Membranes* 2012, **2**, 40-69.
- 119 S. Kruss; L. Erpenbeck; M. P. Schön; J. P. Spatz, Circular Nanostructured and Biofunctionalized Hydrogel Microchannels for Dynamic Cell Adhesion Studies. *Lab Chip* 2012, **12**, 3285-3289.

- 120 E. Cambria; K. Renggli; C. C. Ahrens; C. D. Cook; C. Kroll; A. T. Krueger; B. Imperiali; L. G. Griffith; *Biomacromolecules* 2015, **16**, 2316 – 2326.
- 121 P. Krsko; M. Libera, Biointeractive Hydrogels. *Mater. Today* 2005, **8**, 36-44.
- 122 C. G. Götzlander; J. N. Herron; K. Lim; P. Claesson; P. Stenius; J. D. Andrade, In Poly(ethylene glycol) Chemistry: Biotechnical and Biomedical Applications, 2nd ed.; Harris, J. M., Ed.; *Plenum Press: New York* 1992, 221–245.
- 123 S. Sharma; K. C. Popat; T. A. Desai, Controlling Nonspecific Protein Interactions in Silicon Biomicrosystems with Nanostructured Poly (Ethylene Glycol) Films. *Langmuir* 2002, **18**, 8728-8731.
- 124 H. W. Ma; D. J. Li; X. Sheng; B. Zhao; A. Chilkoti, Protein-Resistant Polymer Coatings on Silicon Oxide by Surface-Initiated Atom Transfer Radical Polymerization. *Langmuir* 2006, **22**, 3751-3756.
- 125 H. W. Ma; M. Wells; T. P. Beebe; A. Chilkoti, Surface-Initiated Atom Transfer Radical Polymerization of Oligo(ethylene glycol) Methyl Methacrylate from a Mixed Self-Assembled Monolayer on Gold. *Adv. Funct. Mater.* 2006, **16**, 640-648.
- 126 A. Nefedov; C. Wölfl, Advanced Applications of NEXAFS Spectroscopy for Functionalized Surfaces, in Surface Science Techniques, Bracco, G.; Holst, B. Eds.; *Springer Series in Surface Science* 2013, **51**, 277-306; Springer-Verlag, Berlin, Heidelberg, New York, Tokyo.
- 127 P. E. Batson, Carbon-1s Near-Edge-Absorption Fine-Structure in Graphite. *Phys. Rev. B* 1993, **48**, 2608-2610.
- 128 M. Khan; S. Schuster; M. Zharnikov, Chemical Derivatization and Biofunctionalization of Hydrogel Nanomembranes for Potential Biomedical and Biosensor Applications. *Phys. Chem. Chem. Phys.* 2016, **18**, 12035--12042.
- 129 N. Meyerbröcker; M. Zharnikov, Modification and Patterning of Nanometer-Thin Poly(ethylene glycol) Films by Electron Irradiation. *ACS Appl. Mater. Interfaces* 2013, **5**, 5129–5138.

Acknowledgements

First of all, I am glad to express my thanks to the China Scholarship Council (CSC), who offered scholarship to me so that I could perform and complete the research projects within my PhD thesis.

I would also like to express my deep gratitude to all those who helped me during the PhD work. I gratefully acknowledge the help and advices of my supervisor, Prof. (apl.) Dr. Michael Zharnikov, who has offered me valuable suggestions in the academic studies. When my research had problems, he spent necessary time analyzing the situation and provided me with inspiring advice. Without his patient instruction, insightful criticism and expert guidance, the completion of my experiments would not have been possible.

I would like to thank our partners at the Department of Chemistry of the University of Basel, viz. Prof. Marcel Mayor and Dr. Loïc Le Pleux, for the synthesis of the C₁₂N₃ compound.

I would like to thank the technical staff of APC, viz. Mr. Reinhold Jehle, Mr. Günther Meinus, and Mr. Peter Jeschka, for their help with experimental setups and computers.

I would also like to thank our group members and office mates for their support and productive scientific discussions, in particular Can Yildirim, Musammir Khan, Eric Sauter, Tobias Wächter, André Brink, and Mustafa Sayin.

My thanks also go to Prof. (apl.) Dr. Reiner Dahint for agreeing to be the second reviewer of my thesis.

I should finally like to express my gratitude to my beloved parents who have always been helping me out of difficulties and supporting me without a word of complaint.

**Eidesstattliche Versicherung gemäß § 8 der Promotionsordnung
der Naturwissenschaftlich-Mathematischen Gesamtfakultät
der Universität Heidelberg**

1. Bei der eingereichten Dissertation zu dem Thema

Modification of self-Assembled Monolayers
and Hydrogel Nanomembranes by Ultraviolet Light

handelt es sich um meine eigenständig erbrachte Leistung.

2. Ich habe nur die angegebenen Quellen und Hilfsmittel benutzt und mich keiner unzulässigen Hilfe Dritter bedient. Insbesondere habe ich wörtlich oder sinngemäß aus anderen Werken übernommene Inhalte als solche kenntlich gemacht.

3. Die Arbeit oder Teile davon habe ich wie folgt/bislang nicht¹⁾ an einer Hochschule des In- oder Auslands als Bestandteil einer Prüfungs- oder Qualifikationsleistung vorgelegt.

Titel der Arbeit: _____

Hochschule und Jahr: _____

Art der Prüfungs- oder Qualifikationsleistung: _____

4. Die Richtigkeit der vorstehenden Erklärungen bestätige ich.

5. Die Bedeutung der eidesstattlichen Versicherung und die strafrechtlichen Folgen einer unrichtigen oder unvollständigen eidesstattlichen Versicherung sind mir bekannt.

Ich versichere an Eides statt, dass ich nach bestem Wissen die reine Wahrheit erklärt und nichts verschwiegen habe.

Heidelberg 06.09.2016
Ort und Datum

Yan, Rin
Unterschrift

¹⁾ Nicht Zutreffendes streichen. Bei Bejahung sind anzugeben: der Titel der andernorts vorgelegten Arbeit, die Hochschule, das Jahr der Vorlage und die Art der Prüfungs- oder Qualifikationsleistung.